Battelle
The Business of Innovation

Interim Report for Phase II – Task 2 of the Comprehensive Study to Understand Longitudinal ERW Seam Failures

"Pipe Inventory, Inspection by In-The-Ditch Methods and In-Line Inspection, and Hydrostatic Tests - a Continuation of Phase 1, Task 2"

Jennifer M. O'Brian, Author
Bruce A. Young, Project Manager

Battelle Memorial Institute
505 King Avenue
Columbus, OH 43201

Prepared for

U.S. Department of Transportation
Pipeline and Hazardous Materials Safety Administration
1200 New Jersey Ave., SE
Washington DC 20590

Contract No. DTPH56-11-T-000003
Battelle Contract No. G006084
Battelle Project No. 100004552

August 2017

Battelle does not engage in research for advertising, sales promotion, or endorsement of our clients' interests including raising investment capital or recommending investments decisions, or other publicity purposes, or for any use in litigation.

Battelle endeavors at all times to produce work of the highest quality, consistent with our contract commitments. However, because of the research and/or experimental nature of this work the client undertakes the sole responsibility for the consequence of any use or misuse of, or inability to use, any information, apparatus, process or result obtained from Battelle, and Battelle, its employees, officers, or Directors have no legal liability for the accuracy, adequacy, or efficacy thereof.

Acknowledgments

This project would not have been possible without the numerous pipeline operators and mill manufacturers who contributed line pipe pulled from the field and harboring longitudinal seam anomalies. Although donated anonymously, a big Thank You is extended to those companies and individuals who supported this program in its pursuit to increase knowledge and safety of Low Frequency ERW (LF-ERW) pipe and pipelines.

With the lengthy quest for ERW pipeline joints with crack-like anomalies in the seam, a big thank you is also extended to those individuals who reached out to pipeline operators on behalf of this program. To the Department of Transportation staff including Mr. Steve Nanney and Mr. Jim Merritt, and to Dr. John Kiefner, and Dr. Brian Leis – thank you. This report is also indebted to the laboratory support of Mr. Robert Gertler and Mr. Jacob Markiewicz.

Appreciation is also extended to the participating non-destructive evaluation (NDE) service providers ApplusRTD and JENTEK as well as In-Line Inspection (ILI) service providers ROSEN and TDW for partaking in this study, representing today's technologies, and contributing text on their respective systems. Technical expertise and important report contributions were also provided by Dr. Bruce Nestleroth and Mr. Pushpendra Tomar of Kiefner and Associates, Inc.

Acronyms

ASTM	American Society of Testing and Materials
ABI	Automated Ball Indentation
API	American Petroleum Institute
C-MFL	Circumferential Magnetic Flux Leakage
COD	Crack Opening Displacement
CVN	Charpy V-Notch Impact Energy
CW	Cold Weld
DOT	Department of Transportation
EMAT	Electromagnetic Acoustic Transducer
ERW	Electric Resistance Welded
FMC	Full Matrix Capture
FW	Flash Welded
HAZ	Heat Affected Zone
HC	Hook Crack
HC/UFI	Hook Crack or Upturned-Fiber Imperfection
HF	High Frequency
ID	Inner Diameter
ITDM	In the Ditch Method(s)
IWEX	Inverse Wave Field Extrapolation
LF	Low Frequency
MDS	Multiple Dataset Platform (i.e. a TDW ILI product)
MFL	Magnetic Flux Leakage
MPI	Magnetic Penetrant Inspection
MT	Magnetic Penetrant Inspection (Certification Acronym)
MWM	Meandering Winding Magnetometer
N/A	No Correlated Anomaly Reported
NACE	National Association of Corrosion Engineers

NDE	Non-Destructive Evaluation
NPS	Nominal Pipe Size
NWT	Nominal Wall Thickness
OD	Outer Diameter
OES	Optical Emission Spectrometer
PAUT	Phased Array Ultrasonic
PCB	Polychlorinated Biphenyls
PHMSA	Pipeline and Hazardous Material Safety Administration
PMI	Positive Material Identification
POD	Probability of Detection
POI	Probability of Identification
$RoCD^2$	Rosen's Crack Detection and Coating Disbondment (i.e. a Rosen ILI product)
S-MFL	Spiral Magnetic Flux Leakage
SMYS	Specified Minimum Yield Strength
SWA	Seam Weld Anomaly
TDW	T.D.Williamson, Inc.
TFM	Total Focusing Method
TOFD	Time of Fight Diffraction
UT	Ultrasonic
WT	Wall Thickness

Table of Contents

List of Figures

List of Tables

Introduction

The DOT PHMSA comprehensive study to understand longitudinal electric resistance welded (ERW) seam failures (DTPH56-11-T-000003) was conducted to address characteristics of ERW seams that make them susceptible to failure and identify factors that pipeline operators should consider in order to increase their assurance that their ERW pipelines are safe. This program is subdivided into five different tasks. The objectives of Task 2, the subject of this report, were to collect representative seam anomalies from the field, understand current capability of inspection methodologies for these anomalies, conduct hydrostatic burst tests to validate failure prediction modeling, and improve in-line inspection (ILI) and in-the-ditch methods (ITDM) by providing access to these naturally occurring anomalies.

In total over 2,500 feet of pipe was collected, which contained nearly 90 crack-like anomalies 25% deep with respect to wall thickness or greater. A wide range of crack geometries was collected including cold welds, hook cracks, stress corrosion cracking (SCC) and laminations. A total of five different inspection technologies were used between inline inspection (ILI) and in-the-ditch non-destructive methods. All inspection technologies were then given the opportunity to improve their tool and/or technique and re-inspect before the crack-like anomalies were destructively evaluated. Upon completion of the inspections, nineteen (19) anomaly sets were selected for validation; two were hydrostatically tested to failure, two were later deemed false positives, and the remaining underwent metallographic examination.

Background

This task is an extension of the 2013 Phase I, Task 2 task, in which the executive summary is reported in reference [1], as the long seam anomalies collected at that time lacked variety (i.e., vast majority were cold welds or mill anomalies), and they were later found to lack the necessary severity as all but one burst test failed above SMYS. This limited variety and lack of failure below SMYS stagnated the progress of the project's assessment model development, evaluation of inspection technologies, and experimental

verification. Therefore, a second collection of field anomalies was initiated in late 2013 and was more successful as a variety of seam weld anomalies (i.e., cold weld, hook cracks, stress corrosion cracking, laminations) were acquired, some with significant size. These anomalies are the focus of this task report and subject of ILI, ITDM, and destructive inspection.

Testing and validating ILI and ITDM inspection tools provide a unique challenge, which was recognized and mitigated early in the task. First, the inspection methods under test were also the means of identifying anomalies for validation. Therefore, if a crack was present but was not reported by any inspection technique, its existence and therefore the false negative reporting went undocumented. This limitation was recognized and mitigated in the test plan; many different inspection techniques were tested and the program primarily focused on the larger indications collected. It was therefore assumed that a consequential crack-like anomaly in the seam was seen by at least one of the five inspection technologies employed. The second challenge revolved around the objective to collect representative seam anomalies from the field. The dilemma is the sequence of events: one cannot ensure the anomaly population is representative until the pipe collection period is closed and testing complete, at which point it is typically too late to search for additional anomalies if deemed necessary. This was a natural limitation of the Phase I work and was improved upon in this Phase II effort. After due diligence a broad range of crack types and depths ranging all the way to 99% through-wall cold welds to the onset of stress corrosion cracking were successfully collected. In total over 2,500 feet of pipe was acquired, and the pipe contained nearly 90 crack-like anomalies 25% deep or greater. Of those features nineteen (19) anomaly sets were then selected for validation. Two of the anomalies were discovered to be false positives, which is when a crack detected with a non-destructive technique is subsequently found not to exist. Shear wave originally reported these two flaws' depths as near through wall, but the remaining inspection technologies were in overwhelming consensus that no seam crack existed in these locations. This included both EMAT and MFL ILI as well as PAUT, TOFD, and IWEX. These false positives left seventeen (17) to undergo full destructive evaluation via a pressure test and/or standard metallography. This validation subset included both cold

welds and hook cracks as well as isolated features and those within close proximity to one another and/or directly adjoined to a lamination. While all features were pulled from pipe once in-service, two of the cold welds were found to be particularly uncommon; they appeared to be mill repairs of leaking cold welds detected by the mill hydrotest, which is no longer acceptable post the 1940s war era. Regardless, this task successfully acquired a broad range of seam anomalies that were representative of the field in varying sizes and geometries.

One of the key benefits of this research was providing inspection technologies and service providers the opportunity to improve their analytical analyses and/or hardware if desired. This was done by providing each technology multiple rounds to inspect and also access to truth data via destructive testing, which is rarely available in the field. Knowledge gained and immediate improvements were quickly observed in this program. For example, one ITDM technology showcased noticeable improvements among their different inspection rounds, and one ILI technology was able to re-review their data and locate three anomalies not previously reported. It is expected that the inspection service providers will use these results for further advancement of their technology, each of which is anticipated to be proprietary.

As technologies are continually evolving, this report should be considered a snapshot in time of their performance. The inspections themselves and their reporting took place between 2014 and early 2016. Also note the assessment of available technologies was not exhaustive in this program, as many more ILI and ITDM technologies are available than were tested. Furthermore, analysis of the data provided by ILI and ITDM technologies is a manual process; the differences in interpretation of results were not part of this study.

Overview of Pipe Collected in Phase 1

For background, a brief overview of the first pipe collection and subsequent Task 2 report [1] are provided.

In total, 70 pipe sections totaling 2,560 feet were collected, but only 32 of the 70 pipes had detectable weld anomalies. Burst testing were conducted on three pipes with

some of the largest anomalies, and the results showed that these anomalies would not fail during a typical hydrostatic test (hydrotest) as they failed under extreme loading at and up to 133% of SMYS. These anomalies and joints' failure pressures are summarized in Table 1. Based on these results all of the anomalies detected could be classified as small and would not fail under typical operating conditions. These anomalies would most likely survive all but the most aggressive hydrotest procedures unless a growth mechanism such as fatigue was occurring, in which case additional analysis would be required.

Table 1: Overview of Burst Tests Conducted from LF-ERW Pipe Collected in Phase 1

Test #	**Joint ID**	**Nominal Pipe Diameter (in)**	**Actual Wall Thickness (in)**	**Grade**	**Fabrication (year/manufacturer)**	**Anomaly(ies) Size per Traditional ITDM (length, % max depth)**	**Testing Temp.**	**Failure Pressure**
1	16-16	16	0.260	X52	~1956 / Lonestar	(3", 24%), (4", 15%), (6.25", mill anomaly)*[ILI] (7", mill anomaly)[ILI]	70 °F	94% SMYS
2	10-07	10	0.231	X52	Pre 1970 / unknown	(3.3", 30%), (1.2", 19.1%) Note: Pipe failed in seam at neither detected anomaly above. Failure initiated near previously undetected black oxide.	70 °F	133% SMYS
3	22-11	22	0.290	X52	1956 / YS&T	(83", 16%)[ILI] Note: Pipe failed in seam but not at detected anomaly above. Failure initiated near previously undetected black oxide.	70 °F	133% SMYS

* Site of burst initiation

[ILI] Previously detected by ILI

While the burst-tests were intended to develop comparisons between inspection data to failure predictions, the ERW seam anomalies gathered during Phase 1 were not

very instructive. For the development of ILI and ITDM and the assessment of performance, it was anticipated that many of the pipes would be burst tested, exposing the anomalies and enabling the full quantification of the type and geometry of the anomaly. However, two pipe sections were subjected to stresses in excess of 130 percent of yield and did not fail at the detected anomalies, rather at others. (See the asterisks (*) in Table 1 for failure location.) In addition, anomaly geometry could not be objectively quantified by destructive measures, and neither the ILI nor the ITDM could be used as the basis for comparison, so that performance results of the inspection technologies could not be established from the pipe collected during Phase 1.

The time-trending report in Phase 1 [2] showed that many ERW processes can make mechanically sound welds that are still robust today; however upsets can produce anomalies with some processes producing more anomalies than others. With mill hydrotests and inspections, most of the pipe that was used to fabricate pipelines did not have service limiting anomalies.

At the end of Phase 1, the in-line inspection tools and in-the-ditch methods were able to detect anomalies in the pipe samples collected. However, the ability to objectively assess the capabilities and limitations of these technologies was limited by the lack a full range of types and sizes. To fully assess and improve these technologies, additional representative samples were required, which was the subject of a second pipe collection effort in Phase 2 and is the subject of this report.

Pipe Collected in Phase 2

In continuation of Phase 1, additional ERW pipe specimens with seam anomalies were collected from the field and mills. As before, all samples were contributed as donations from either operators or pipe manufacturers and were absolutely critical for this program's completion.

The objective was to acquire seam anomalies in ERW or FW pipe that vary in geometry and size, including severe cracks that threaten safe pipe operations below SMYS. This second call for pipe varied from the first in two ways. For example, in attempt to increase response rate the pipe request was expanded to a broader audience,

including mills for comparison purposes, and more pipe diameters were deemed acceptable. Increased project awareness from the previous phase completion also assisted.

A total of 92 additional joints of pipe, over 2,500 feet, were collected as part of the Phase 2 effort. Out of the hundreds of seam anomalies present, nearly 90 of them had depths 25% or deeper as determined by ITDM completed during this project. IWEX was able to differentiate the various crack-like geometries and report each feature as a suspected cold welds, hook cracks, or lamination for example. A breakdown of the anomalies and pipe pedigrees collected throughout both phases are summarized in Table 2 and Table 3. Note that ITDM characterization was completed to the best of technology ability at the time. Phase 1 relied on MPI, PAUT, and TOFD for sizing and identification. IWEX was available in Phase II and subsequently was also relied upon for anomaly sizing. MPI, TOFD and PAUT were used mainly as screening methodologies to detect as many cracks as possible in Phase 2.

Table 2: Summary of Seam Anomalies Reported Deeper than 25% NWT per Best-Available ITDM Characterization at the Time of Each Phase

	Phase I		Phase II	
Seam Anomalies	**Qty**	**Deepest Flaw (depth , length)**	**Qty**	**Deepest Flaw (depth , length)**
Cold Weld	35	(53.9%, 0.87")	23	(100%, 1")
				(91%, 3")
Significant Stitching	-	-	1	(39%, 1.279")
Hook Crack	-	-	41	(65% , 0.9")
SSWC	-	-	-	-
SCC	-	-	2	(27.44%, 0.925")
Lamination	-	-	8	(52%, 1.8")
Upturned Lamination	-	-	14	(67%, 3.582")
TOTAL	35	-	89	-

Table 3: Summary of Pipe Pedigree Collected over Both Phases

Nominal Diameter	Qty	Lots	Confirmed Grades	Anomalies*	Frequency Type
10"	18	5	Not Documented	CW, SCC, HC	Low
12"	35	6	X46	CW, Mill, Mch, Corr	Low
14"	2	1	Grade B	CW, HC	Low
16"	37	6	Grade B, X46, X52	CW, HC, Lam, Mill	Low
18"	6	3	Not Documented	Not Documented	Low
20"	37	5	X46	CW	Low and High
22"	18	3	X52	CW, Lam, HC, Mill	Low
24"	9	3	X45	SSWC, Corr, Lam	Low and High

Preparation for ITDM Inspection

Upon the pipes' arrival to Battelle's laboratory, specimens were assigned unique identification numbers, had their physical dimensions and condition documented, and any previous inspection markings were photographed. The electronic database included additional information when known, such as vintage, manufacturer, anomaly history, hydrotesting history, operation history, flow direction, and previous inspection reports.

Prior to furthering handling of the pipe and coating, asbestos and PCBs levels were tested. Coatings were then removed in compliance with asbestos abatement restrictions per the Ohio Department of Health and the Ohio EPA. The surface finish was then sandblasted to NACE 2 finish to complete the pipe preparation for ITDM inspection.

ITDM inspection included commercial magnetic particle inspection (MPI), phased array ultrasonics (PAUT), and time-of-flight diffraction (TOFD), provided by ApplusRTD. ApplusRTD's developing IWEX was also ran to provide additional crack geometry and sizing insight. Differences in PAUT, TOFD, and IWEX signals are pictorially displayed in Figure 1 for a sample location on joint 14-03. When sizing the features, TOFD offers length and depth to the bottom of the indication only. PAUT and IWEX offers length, depth, and height insight. However, discrepancies can arise in the final crack type call. For example, PAUT in Figure 1 suggests the crack is a cold weld while the IWEX signal shows an angled indication, a capability beyond PAUT and

TOFD, which suggests the flaw is a hook crack. As such, IWEX calls were used to differentiate crack geometry throughout Phase II as well as general detection and sizing.

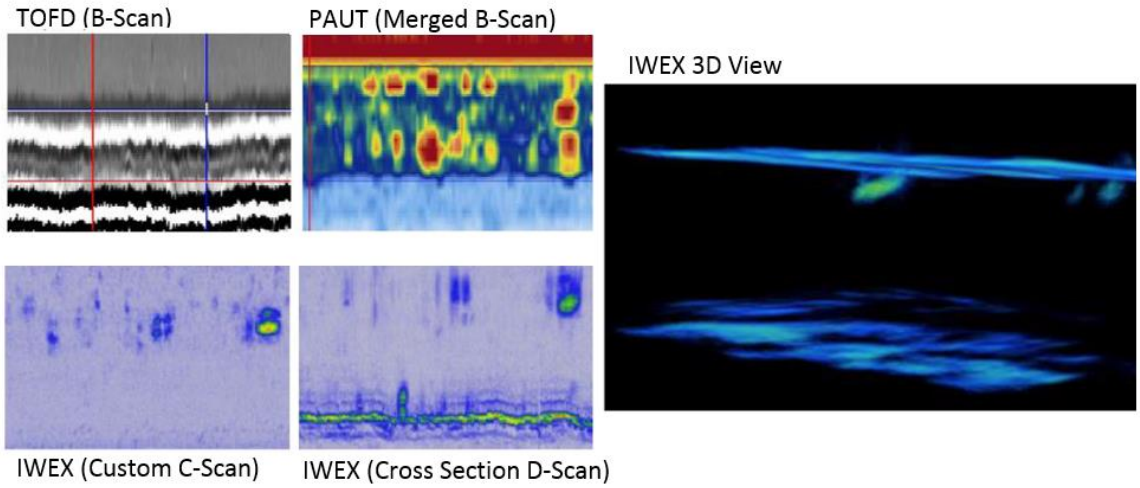

Figure 1: Pictorial Comparison of ITDM Signals Taken from Joint 14-03 [3]

The main objective of the ITDM inspection was to identify pipes with seam anomalies for burst testing and destructive analysis after ILI and ITDM data were collected. A secondary objective of the ITDM inspection was to understand the seam anomalies as best as one can non-destructively for subsequent ILI comparisons. This was accommodated by inspecting the same cracks with multiple techniques (MPI, PAUT, TOFD, IWEX) and setting them up beforehand with calibration blocks. These calibration blocks were specified by the ITDM service providers and consisted of known internal and external EDM notches and a machined midwall anomaly. The calibration blocks had similar wall thickness, pipe diameter, and pedigree as those inspected.

To expedite the process of identifying pipes with anomalies for the development of assessment methods and destructive testing, MPI, PAUT, TOFD, and IWEX sizing were reported together by the NDE service provider. That is, *one* crack size and location were reported despite using multiple NDE techniques. IWEX sizing was considered the most accurate and therefore was depended on for any ITDM discrepancies, as deemed by the service provider. This aligned with the task's objective to quickly characterize

hundreds of cracks within the best of NDE ability before down-selecting cracks for ILI and destructive characterization.

Preparation for ILI Inspection

The majority of the anomalies found by ITDM existed in 16-inch nominal diameter pipe. The most severe flaws of these were then used to construct a 300ft long simulated pipeline for multiple ILI assessments at Battelle's pull rig facility. Figure 2 provides a sketch of this pipe assembly and Table 4 provides each joint's mill manufacturer and year it was installed in the field.

Prior to ILI assessments the pipes were tarped to mask ITDM markings previously written on the pipe exterior. No information on the pipe was shared with the ILI service providers prior to pulling other than nominal diameter, wall thickness range, and suspect anomalies (i.e., ERW seam cracks). This was structured to mimic what a typical operator may or may not know of their line prior to running ILI.

The interior of the pipes were also cleaned prior to pull testing with multiple mechanical cleaning pigs until layers of scale and debris were sufficiently removed per visual inspection.

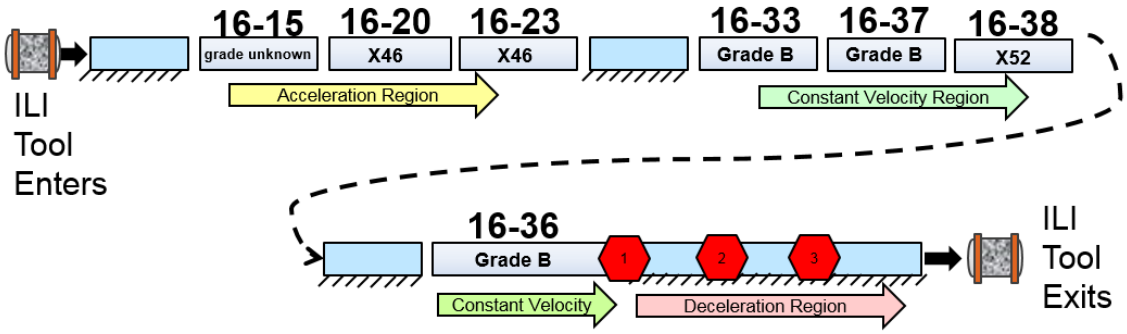

Figure 2: Layout of Simulated Pipeline for ILI Assessments at Battelle's Pull Rig

Table 4: Mill Manufacturer and Install Date for Each Joint Pull Tested

	Manufacturer	Install Year
16-15	Lonestar	1956-57
16-20	Lonestar or CalMetal	1956
16-23	Lonestar or CalMetal	1956
16-33	Republic Steel	1941
16-37	Republic Steel	1941
16-38	A.O.Smith	~1949
16-36	Republic Steel	1941

Inspection Technologies Employed

A total of five different ITDM technologies and two different ILI technologies were employed. All examined joints were subjected to MPI with shear wave sizing, PAUT, and TOFD inspections conducted by ApplusRTD. ApplusRTD also employed their IWEX ITDM. At that time, the scanner used for collecting IWEX readings was also able to collect PAUT and TOFD readings in the same pass along the pipe. The fifth and final ITDM technology employed was MWM Array by Jentek, which can size and detect surface breaking cracks. This was only conducted on the joints installed in the pull rig as sketched in Figure 2. Unless otherwise noted, references to "ITDM" herein include the first four technologies. MWM array technology is included intermittently in ITDM references, but is indicated when such, as it was only completed on a subset of pipe and limited to OD surface breaking flaws. The term "traditional ITDM" is in reference to MPI, PAUT, and TOFD only, which are routine techniques widely used in field inspections today.

A minimum sizing threshold was imposed to maximize the number of pipe joints screened by ITDM in a cost effective manner. As a result, hundreds of small seam anomalies were not reported by ITDM despite being detected, and the saved time was better utilized on more joints of pipe with potentially larger features. In Phase I this reporting threshold required only anomalies greater than one inch in length and greater than 30% nominal wall thickness (NWT), or all anomalies greater than 40% NWT be

reported. This was later expanded to anomalies with depths 25% NWT and greater. Phase II held the 25% NWT minimum for full imaging and was able to drop the minimum length threshold with no time penalty. This threshold was set at sizes to be cost effective for maximum screening while still capturing features that could potentially exceed the minimum detection threshold provided in the ILI specifications and provide useful burst test data for the new integrity assessment model.

The largest number of anomalies above the reporting threshold were identified by the ITDM in the donated 16 inch diameter pipe, which became the focus for ILI inspection capability assessment phase of the this project. At the time of the pull testing, two commercially available EMAT tools were available for 16-inch diameter pipe, ROSEN's RoCD^2 and TDW's SpirALL®EMAT. Their respective MFL tools that target axial anomalies are typically run in parallel to improve identification of seam anomalies while dismissing innocuous seam features such as trim variation. ROSEN supplied their RoCorr-CMFL tool and TDW supplied their MDS tool including SpiraALL®MFL). Together these technologies are reported herein as "EMAT" and "MFL" regardless of the service provider differences and any other technical variations that may be present.

Each individual ILI tool was pull tested at four speeds that spanned that individual tool's specification. Each speed was then re-pulled for consistency verification. Per a service provider's request and their desire to learn more, an ILI tool was also tested above its maximum specified tool speed. They were not required to report results for this run.

As part of Task 2, selected inspection results were provided to service providers with a brief time window so that they could enact any improvements such as better anomaly detection or more accurate sizing algorithms. The two ILI providers and the MWM Array method provider received the IWEX data. The IWEX provider received both sets of ILI results. Inspection providers faced a dilemma modifying technology based on inspection results, as the data may errors that would not be quantified until the anomalies were destructively assessed.

ApplusRTD opted to re-run their full matrix capture (FMC) technology, which is discussed later in the "Performance Capability" section. While no ILI technique was re-tested at the pull through facility, in-house improvements and learnings were acquired

when they reviewed and re-reviewed their original data. One EMAT vendor shared partial insight on this in section "ILI Subsequent Review of Results", as they learned they were able to detect and size anomalies they originally did not reported.

Service provider specific details regarding tool calibration, ability to identify crack location with respect to the seam (i.e., in bondline, HAZ, or pipe body), and future improvements are discussed below. A brief technology overview is also included for IWEX only as it is an emerging technique that is less understood by industry than the other ITDM and ILI methods.

ROSEN EMAT-C and C-MFL*

ROSEN provided electromagnetic acoustic transducer (EMAT), based technologies to detect and characterize linear anomalies. The magnetic flux leakage method (MFL) applied in circumferential direction is also provided by ROSEN for the characterization of axial anomalies. In this context, the technology supports the discrimination of cracking from volumetric anomalies in the pipe body and the long seam.

Each EMAT sensor is embedded in a permanent magnetic field and consists of pairs of sender and receiver coils as shown in Figure 3. The sender coils (P), are used to induce the horizontal polarized shear wave into the pipe wall, whereas the receiver coils (T, E) measuring the reflected (E) and transmitted signal (T). The special setup on each EMAT sensor carrier generates two (2) sensitive areas, which are defined as pixels. Within each pixel a crack-like anomaly can be detected and sized. The total number of channels is depending on the number of sensors carried for each tool. The 16 inch inspection tool has 36 channels.

Text courtesy of ROSEN with minor edits made by the author.

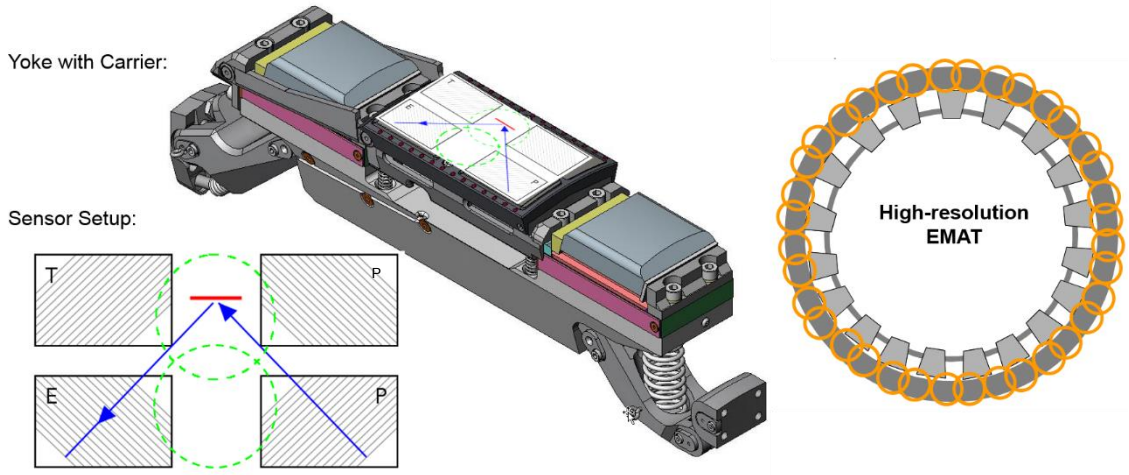

Figure 3: Illustration of the ROSEN Sensor Configuration (left), the Sensor Position in the Magnetizer Yoke (center) and the Distribution of Yokes for Pipe Inspection (right)

After each EMAT tool is assembled, pull tests are performed on pipe joints with well-known natural and artificial anomalies to prove and establish the detection, identification and sizing capabilities based on the data recorded. It is crucial to have natural features to weight the artificial anomalies, but the amount in the pull test inventory is limited. To generally qualify the EMAT technology on natural features NDE results gained in the ditch using accepted procedures are compared with the reported dimensions. All field verification results are stored in a database in order to train the algorithms used during the data analysis process. The service provider's database currently contains more than 4,900 verified crack-like anomalies.

ROSEN is combining the two technologies EMAT and MFL to support an optimal differentiation between linear anomalies and other volumetric anomalies. The use of MFL-C is not mandatory but has been proven to be effective in those cases where a high probability of identification for cracking is required from an abundance various types of anomalies. Recent developments at ROSEN will further improve the probability of identification (POI) and allow a better determination of the exact position of an anomaly on the long seam. It is anticipated that the granularity will be sufficient to differentiate between center-line and toe-line cracking. This will help in differentiating

between environmental-assisted cracking (e.g. SCC) and mill-related cracking (e.g. cold weld) in the weld area.

TDW SpirALL® EMAT and MDS with SpirALL® MFL[†]

The majority of magnetic flux leakage (MFL) surveys performed to date have used axially oriented magnetizers, capable of detection and quantification of most classes of volumetric metal loss features. In certain cases, metal loss and other types of manufacturing anomalies exist with extreme length to width aspect ratios. When these are combined with alignment parallel to the applied magnetic field direction, the difficulty of detection and sizing is increased when using the MFL technique. In the case of elongated, axially oriented features, detection and accurate quantification may become difficult for MFL tools using axially oriented magnetizers. In order to provide consistent detection and sizing, magnetizers using circumferentially or obliquely oriented fields have been placed into service. While MFL-based tools are not comprehensive crack detection tools, they are capable of detecting and quantifying certain classes of planar or crack-like features; and in the case of ERW long seams, additional anomaly classes that have been shown to be detrimental to in-service pipelines. Axially oriented long seam features having either a small gap or magnetic discontinuity are capable of being detected and quantified using the MFL technique, with the field applied in a circumferential or oblique direction to the pipe axis.

In addition to MFL, electromagnetic acoustic transducer (EMAT) guided wave and ultrasonic (UT) piezoelectric shear wave techniques are being further developed by TDW to provide detection and sizing capabilities for these feature classes. The UT piezo electric method requires a liquid coupling medium to achieve optimum performance, while EMATs will function in either an air or liquid environment. EMAT based tools currently developed by TDW were made available for this project. Tool specifications and design specifications were provided.

[†]T*ext courtesy of TDW with minor edits made by the author*.

A cross-sectional schematic with sensor coverage of the EMAT tool is shown below in Figure 4. A total of eight receivers (Rx) and four transmitters (Tx) are used on the 16" EMAT tool. This unique sensor configuration provides a significant amount of redundancy (~4x or quadruple) that allows for multiple receivers to detect and size the same crack-like anomaly. The total number of receivers and transmitters employed on each tool will vary depending on pipe diameter.

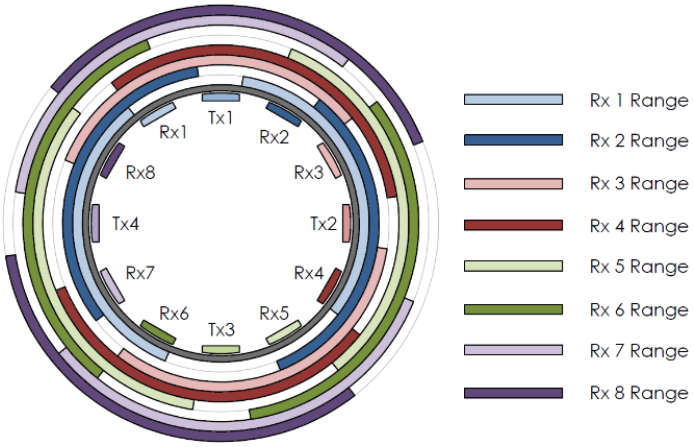

Figure 4: Pictorial Cross-sectional of TDW EMAT

EMAT tools are run subsequent to an MDS survey which includes deformation (DEF), high field MFL (MFL), helical/spiral MFL (S-MFL), low field MFL (LFM), internal/external discrimination (ID/OD), and mapping (XYZ coordinates) on the same inspection platform. MDS allows for comprehensive MFL-based inspection of a pipeline including metal loss, mechanical damage, seam features, hard spots, and pipeline attributes for discrepancy analysis and material documentation.

When attempting to identify crack location with respect to seam, HAZ, and bondline, detailed assessment of the weld position is needed.

For seam position assessment with EMAT, acoustic energy reflections may result due to thickness and long seam trim variations. Reflections may also be present due to bond line regions, in addition to attenuation of the acoustic energy as the seam is traversed, allowing identification of the seam region. Quite often, seam regions will be relatively smooth, absent significant thickness variation or bond line acoustic reflections, resulting in an absence of either reflected energy or attenuation of the acoustic wave. For

these instances, the long seam may not be identified in EMAT data. Additionally, for EMAT data, a determination of the exact location of the bond line relative to the edge of the long seam trim region may be difficult. In the MFL data, localized differences due to seam trim may be identified in the axial MFL data, however, the primary MFL data set for seam identification and assessment is the helical/spiral field (SMFL). The helically applied field encounters the seam in an oblique circumferential direction, allowing for detection of the seam region. Leakage fields may be generated by each of several conditions: over trim, under trim, can/edge upset and the HAZ. Bond lines with zones creating magnetic discontinuities may be detected and identified as being near the center of the seam, while other discontinuities may be identified as immediately adjacent to the seam, within the HAZ.

Continued SMFL data analysis/comparison to the EMAT data results, with the potential to discriminate the location of features as being either within (center) or immediately adjacent to the seam are potential future improvements.

ApplusRTD IWEX[‡]

UT imaging using inverse wave field extrapolation (IWEX) is an emerging NDE technique that is being applied to improve discrimination and sizing of anomalies in pipelines. IWEX finds its origin in the application field of seismic exploration, where acoustic wave fields are used to reconstruct structures and layers in the subsurface in the search for oil and natural gas deposits. With the introduction of ultrasonic array technology, and advancements in computing technology the principles to reconstruct images from measured wave fields became applicable for other applications such as girth and seam weld inspection. A goal of IWEX imaging is to produce images capable of detecting, discriminating, and sizing crack-like features such as cold welds, surface breaking hook cracks, and fatigue cracks and discrimination these from non-surface breaking upturned fiber indications, poor trim, offset plate edges, laminations and

[‡]*Text courtesy of ApplusRTD with minor edits made by the author*

inclusions. In mapping these anomalies the sizing needs to be sufficiently accurate to qualify in-line inspection tools used for crack inspection.

Approaches for ultrasonic imaging using arrays such as IWEX are based on capturing the full waveform of data received at the individual array elements, often called full matrix capture (FMC) data. An image is produced from this data by assembling a collection of A-scans, using all pairs of array elements as sources and receivers. In contrast to beam forming as used by phased array inspection, imaging approaches enable focusing at every point in a region of interest. Common methods for imaging in non-destructive testing are the Total Focusing Method (TFM) [4] and IWEX [5]. Although IWEX is applied to obtain UT imaging results for this project, a similar approach could be used for imaging with TFM.

The first application of the IWEX technique was for the inspection of pipeline girth welds during new pipeline construction. Application for seam weld is more recent and is currently under development with DOT PHMSA funding [6]; although the work is not yet complete. The variations in the seam geometry (ERW, EFW), trim variation, and pipe diameters make inspection much more challenging than girth weld inspection. The various crack-like flaw orientations and morphologies that can be formed in the welding process are also challenging to detect and size.

To overcome the geometry variable, various scanning techniques were used during the progression of the project varying from hand scanning, a band scanner, a magnetic wheel scanner, and most recently a linear screw scanner where the probes were held is a fixed orientation to follow a pipe seam. We found the band scanner difficult to use on some of the smaller ERW diameter pipe commonly used in service. The magnetic wheel scanner was susceptible to drift especially in the 3:00 and 9:00 o'clock positions leading to seam scans that appears to show a meandering seam. The linear screw scanner is much better at holding the probes in a constant circumferential orientation while axially scanning down the pipe. Although this latter design is not a unique solution to scanning the long seam, the results were satisfactory for effective data analysis.

In-the-Ditch-Methods and ILI Findings

ILI reporting iterations were executed in a similar fashion to their field pipeline inspections. That is, both ILI service provider's supplied a preliminary report of anomaly calls and then Battelle provided in the ditch results for a few selected features for calibration. This ITDM feedback loop was to mimic ILI calibration and verification digs in the field. Afterwards ILI service provider's supplied a final report. Upon review, little to no change was made to those anomaly calls first issued in the preliminary report.

Assessing Performance Capability

Assessing the performance of ITDM and ILI tools requires representative naturally occurring anomalies. In the 16 inch diameter pipe, 19 anomaly locations in the seam weld were identified for comparison. This is not nearly enough to perform a meaningful statistical evaluation. However, the results do provide insight into the performance potential of ITDM and ILI. This also provided valuable data for crack assessment algorithm development and improvement to inspection technology.

The 19 features selected for inspection technology validation are outlined in Table 5. Two of these features, #11 and #12, were included as they were considered to be deep, nearly through wall flaws previously identified by magnetic penetrant inspection (MPI) and shear wave even though neither were reported by ILI nor IWEX. These two features were later confirmed false positives upon further NDE investigation, reducing the anomaly subset count to 17. Human error and trim tool markings are the suspect cause of the false calls. This remaining anomaly set was less than ideal but still quite instructive.

Actual flaw lengths and depths were taken from metallographic and fractographic examinations. These are reported in detail in Appendix A and summarized in Table 5. Often the fracture surfaces revealed multiple cracks in close proximity, in which case the reported length in Table 5 is the overall length, which is also known as the overall footprint. This composite length was used for more appropriate comparisons of fracture results to ILI, as ILI observes closely aligned cracks as one feature due to sensor aperture limitations. The exact rule followed for closely aligned cracks was:

For individual anomalies that were within 1.5 inches of a neighboring crack AND shorter than the detection threshold for length (which was most of them), multiple cracks were tabulated as one feature. 1.5 inches is a general (non-tool specific) specification for the minimum anomaly length detectable. The largest depth among the multiple cracks was reported as the depth of the composite anomaly.

Table 5 summarizes the crack length, depth, and type reported by various inspection methods as well the true, absolute dimensions as determined destructively. The tabulated ILI sizing is the average of the two slowest pull tests for each tool. Typically this was 1.5 mph, with the exception of one MFL system where the slowest pull was 2 mph. IWEX sizing reported in this table is from their later generation tool tested in this program. Fracture surface depths reported were the deepest observed for each crack, or in the case of multiple cracks combined, the deepest of the set. Metallographic images used for sizing are documented in Appendix A. This appendix also documents when multiple cracks in close proximity were reported herein as one.

Note that five features are denoted with a single asterisk (*) in Table 5. This denotes features which were later discovered adjoined to a long running lamination. They are not included in the subsequent ILI unity plots (Figure 9, Figure 12, and Figure 15) as laminations are generally outside the detection and sizing specifications of MFL and EMAT. In addition, this unique anomaly set may not be representative of the bulk line pipe in service. Due to the IWEX's ability to identify and characterize laminations, though, these features were included in their unity plots (Figure 15, Figure 16).

The available ITDM data in Phase 2 of this study was primarily focused on IWEX. In most cases MPI, PAUT, TOFD, and IWEX sizing were reported together by the NDE service provider. That is, *one* crack size and location were reported despite using multiple NDE techniques. IWEX sizing was considered the most accurate and thereby was depended on for any ITDM discrepancies, as deemed by the service provider. This aligned with the task's objective to quickly characterize hundreds of cracks within the best of NDE ability before down-selecting cracks for ILI and destructive characterization.

Table 5: Flaw Characterization per IWEX, ILI, and Metallography

Anomaly #	Joint #	Length (Inch)						Depth (% Wall Thickness***)							Defect Type
		IWEX	EMAT M Avg.	MFL O Avg.	EMAT N Avg.	MFL P Avg.	Actual (from Fracture Surface°)	IWEX (mils)	IWEX	EMAT M Avg.	MFL O Avg.	EMAT N Avg.	MFL P Avg.	Fracture Surface°	Actual (from Fracture Surface)
1	16-37	2.8	3.4	2.0	3.4	1.7	**3.0**	0.3	92	84	27	62	32	**99**	CW
2	16-33	2.5	2.8	2.3	3.2	2.0	**2.0**	0.3	100	70	32	46	35	**92**	CW
3*	16-36	3.1	2.6	4.7	12.8	1.4	**3.8**	0.3	94	46	12	17	20	**60**	HC (due to Lamination)
4*	16-36	0.6	#4 and #7 Reported as one anomaly	1.1	#4 and #7 Reported as one anomaly	1.6	**1.2**	0.181	68	#4 and #7 Reported as one anomaly	15	#4 and #7 Reported as one anomaly	28	**63**	HC (due to Lamination)
5	16-20	1.4	1.9	< Spec; Length < 1.5inches & Depth < 25% wt			**1.0**	0.181	56	50	< Spec; Length < 1.5inches & Depth < 25% wt			**68**	CW
		0.1	< Spec				**0.2**	0.051	16	< Spec				**12**	CW
6	16-20	0.2	1.7	< Spec; Length < 1.5inches & Depth < 25% wt			**0.3**	0.157	49	38	< Spec; Length < 1.5inches & Depth < 25% wt			**50**	CW
		0.1	< Spec				**0.1**	0.102	32	< Spec				**31**	CW
7*	16-36	5.4	4.5	5.4	22.4	Lamination; Multiple Calls	**5.7**	0.197	74	38	11	27	Lamination; Multiple Calls	**63**	HC (due to Lamination)
8	16-38	2.6	2.1	-	2.5	-	**1.7**	0.114	45	32	-	39	-	**56**	HC
9	16-38	2.7	3.1	2.2	-	1.5	**2.6**	0.201	80	32	18	-	18	**34**	HC
10	16-38	1.3	< Spec; Length < 1.5inches & Depth < 25% wt				**1.1**	0.114	45.2	< Spec; Length < 1.5inches & Depth < 25% wt				**32**	HC
		0.4	< Spec; Length < 1.5inches & Depth < 25% wt				**0.5**	0.122	48	< Spec; Length < 1.5inches & Depth < 25% wt				**16**	HC
		1.7	1.7	1.1	4.0	1.1	**1.8**	0.114	45	38	24	26	18	**44**	HC
11	16-36	No Calls reported by ILI or IWEX													
12	16-33	No Calls reported by ILI or IWEX													
13	16-38	0.1	6.3	6.3	5.5	-	**1.6**	0.102	40	10	10	38	-	**24**	Stringer
14	16-38	0.3	< Spec; Length < 1.5inches & Depth < 25% wt				**0.6**	0.185	73	< Spec; Length < 1.5inches & Depth < 25% wt				**18**	Stringer
15	16-38	1.9	1.7	1.2	3.4	0.7	**3.7**	0.114	45	21	13	25	10	**32**	HC
16*	16-36	6.6	5.1	7.2	5.7	4.8	**7.4**	0.252	94	61	10	27	10	**75**	HC (due to Lamination)
17	16-38	1.8	2.5	-	3.6	-	**1.5**	0.110	44	32	-	35	-	**52**	HC
18*	16-36	23.9	Start of Lamination, No Call	Start of Lamination, Multiple Calls	Start of Lamination, No Call	3.4	**56.0**	0.000	0	Start of Lamination, No Call	Start of Lamination, Multiple Calls	Start of Lamination, No Call	10	**7**	Lamination
19	16-38	2.2	3.0	-	3.9	8.7	**2.3**	0.091	36	32	-	26	No Depth Listed; "Seam Variation"	**48**	HC
		0.4						0.000	0						Lamination

* 3, 4, 7, 16 & 18 orginate from one lamination with 3 surface breaking hook cracks

** Further analysis required to determine defect type.

*** Nominal Wall thickness used for ILI data and Actual Wall thickness used for IWEX data and fracture surface

° Fracture length is overall footprint when multiple cracks tightly spaced. Frature depth is reported here as max depth among the multiple cracks. See text above and Appendix A for more details.

ILI Testing

The objective of the ILI testing was to conduct tests on pull test thru pipe with representative anomalies in order to demonstrate the effectiveness of ILI assessment methodologies. Another objective was to improve inspection technologies by providing access to natural seam weld anomalies that were fully characterized by destructive analysis. Most often, ILI vendors get feedback from pipeline companies in the form of ITD measurements. This approach worked well for MFL assessment of corrosion as the depth and shape of corrosion is visible and easier to quantify than crack geometry. To improve their technology, inspection vendors need to see the full profile and shape of many cracks. Also, in addition to crack geometry, crack type (cold weld, hook crack, SCC etc.) need to be provided. This project starts to provide data to aid in the development of algorithms to fully assess crack in pipe seams.

Pull testing limited the types of tools that could be tested, as the testing of liquid coupled ultrasonic tools was not practical. The following sections provide a description the tool performance the ILI tools tested.

ILI Detection of Seam Cracks

The common method to quantify seam crack detection capability is the probability of detection (POD). Though often given as a number, a more complete assessment would be a three dimensional surface with POD given for every combination of depth and length. The number of cracks necessary to determine a complete POD surface requires many in a wide variety of sizes that have been characterized by ITDM. As a place to start, a simple measure of POD defined here can be useful:

$$simplePOD = \frac{\#\ by\ ILI}{\#\ by\ ITDM} \quad (1)$$

where

 # by ILI is the number of confirmed cracks identified by ILI

 # by ITDM is the number of cracks found by ITDM that have sufficient size to be detected by the ILI tool

This simple measure is useful in assessing relative ILI tool performance.

Observations on EMAT Crack Detection

Within this limited dataset, both EMAT tools preformed nominally to their respective seam crack detection specifications:

EMAT A Observed POD: 88%
EMAT B Observed POD: 92%
EMAT A & B Reported POD: 90% for their specified minimum crack size (length and depth)[§]

Therefore, both service providers are on target with their reported PODs, especially when considering this limited sample set that contains less than 15 cracks that should be detectable per EMAT specifications. It should be noted that for accuracy the observed PODs reported above are tool specific. PODs were evaluated against each tool's specified minimum crack size, not the generic specification used elsewhere in this report. Each EMAT tool missed one crack that was larger than their specified minimum crack depth and length. In both cases they were hook cracks approximately 30% through nominal wall thickness (NWT) and between 1" and 2.6" long (i.e., anomaly #9 and #10-1, shown in Figure 5). All other seam cracks within tool specifications were detected. It is important to note that both of these undetected anomalies were hook cracks and existed in varying A.O.Smith flash thicknesses, which adds unique complexity to ILI data interpretation.

§ Depending on the EMAT tool, the minimum crack length for 90% POD confidence varied from 1-inch to 1.97-inches. Minimum depth varied from 0.04-inch to 20% of wall thickness.

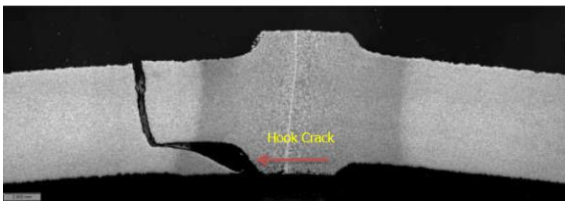

Anomaly #9
(2.64” long, 33.7% NWT deep)

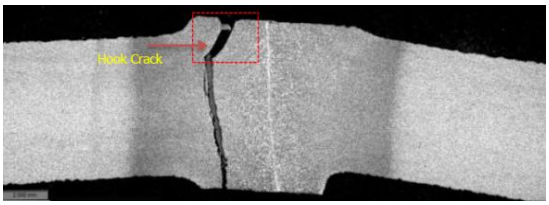

Anomaly #10-1
(1.14” long, 31.8% NWT deep)

Figure 5: The Two Seam Cracks That Went Undetected by at Least One EMAT Tool Despite being within Tool Detection Specifications (Notice heavy and uneven flash, which adds unusual complexity for ILI.)

Despite the complication of varying flash thickness, EMAT technologies today are still capable of finding seam cracks when large enough. This is exemplified when comparing detected hook cracks #15 and #19 to undetected hook cracks #9 and #10-1, which were in the same uneven trim but were slightly smaller. Anomaly #19 was 14% deeper and actually slightly shorter than #9, yet was successfully detected. Anomaly #15 was the same depth as #10-1 but was 2.54” longer, which made the difference between being detected and not. Cross sections of these anomalies are shown in Figure 5 and Figure 6 for comparison. In order to conclude a minimum crack depth and length for ILI to reliably detect within uneven flash thicknesses, substantially more samples would be required than these four. In the interim it is recommended to work with the ILI providers directly as they may have past case studies with equivalent flash thicknesses, ID/OD misalignment, and indication types as the pipeline in question.

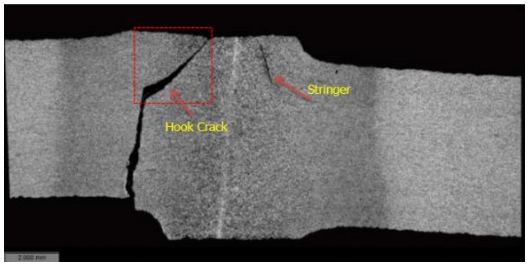

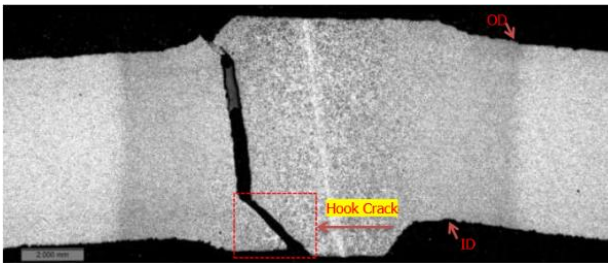

Figure 6: Two Example Seam Cracks That Were Detected by Both EMAT Tools

Anomaly #19
(2.30” long, 47.6% NWT deep)

Anomaly #15
(3.68” long, 31.8% NWT deep)

Observations on MFL Crack-Like Anomaly Detection[**]

Within this limited dataset, both MFL tools' seam crack detection performance were on target to meet or exceeded a typical MFL POD specification[††]:

MFL A Observed POD: 88%

MFL B Observed POD: 100%

MFL A & B Reported POD: 90% for a typical MFL specification[††]

Results here are reported against a *typical* MFL POD for crack-like anomalies in the seam as opposed to *tool-specific* because the crack opening width was not verified, which is part of the minimum crack size per a service provider. This generalization allowed cracks that "should be detectable" to be flagged as such per their length and depth only, not crack opening. Upon evaluating the dataset, this was a valid assumption as all but one of these flagged anomalies appeared to be sufficiently opened as all were detected by both MFL but one hook crack. This may not be the case for all crack-like seam anomalies in the field, but it did hold true for this set tested.

Sample size is important to take into consideration especially as this set was very small at only eight seam cracks above this typical MFL detection threshold. The cracks included in this analysis were #1, #2, #3, #7, #9, #15, #16, and #19. Six of the eight were hook cracks, some of which originated from laminations. The other two were near-through wall cold welds. All eight were successfully detected by one MFL ILI; the other MFL ILI detected all but #19. All the hook cracks were ID connected except #19. Crack #1 and #2 were -connected cold welds that were repaired by welding. One service provider reported a magnetic permeability feature in the low field axial MFL data before the weld repair was discovered by metallography.

[¨] While it is generally accepted that MFL technology is not well suited for detection and sizing of all cracks types, MFL still has a suitable role in crack inspection as discussed later in this report and in the conclusions (e.g. differentiating innocuous features such as trim variation from potentially injurious anomalies, locating hook cracks with large crack openings, etc)

[††] 90% POD for a minimum crack size of 2" long, 30% deep. Sufficient crack opening was assumed for all cracks in this sample set larger than this non-tool specific size threshold.

While it is a small sample set, this observed success demonstrates that MFL may be useful in screening crack-like seam anomalies especially when paired with EMAT sizing. This is a common approach as MFL tools which target axial anomalies are often run in parallel with EMAT to improve identification of seam anomalies while dismissing innocuous features such as trim variation.

One may be tempted to quickly match these reported PODs of MFL[‡‡] against EMAT[§§], however each tool type is held to different minimum crack sizes and therefore are not directly comparable. Regardless, the overall takeaway is that both EMAT and MFL technologies targeted at axial cracks performed within their product specification in this program.

ILI Sizing of Seam Cracks

EMAT and MFL sizing as compared to actual metallographic results are shown in unity plots Figure 9 and Figure 10.

Observations on EMAT Crack Sizing

In general, seam cracks tend to be called slightly longer and shallower than reality.

- Length calls were generally conservative as 17 of 21 EMAT calls were overstated +0.4" to +4.7". The remaining four seam calls were undersized in length:
  - Anomaly #9: an EMAT reported no crack while actual length 2.6 inches
  - Anomaly #10: an EMAT reported 1.7 inches while actually 1.8 inches long
  - Anomaly #15: an EMAT reported 1.7 inches while actually 3.7 inches long
  - Anomaly #15: a different EMAT tool reported 3.4 inches length while actually 3.7 inches

‡‡ Non-tool specific (i.e. generic) crack size threshold for MFL = 90% POD confidence for a minimum crack size of 2" long, 30% deep, and sufficient crack opening.

§§ Crack size threshold for EMAT = 90% POD confidence for either 1-inch or 1.97-inches, depending on the vendor specification. Minimum depth at 90% POD varied from 0.04-inch to 20% of wall thickness in a similar, vendor specific, manner.

- "Short" Cracks (< 1.75" long actual): tendency to overstate length by at least 1 inch if detected at all.
- Depth calls were typically within +/- 25% of actual depth *if* the seam crack was detected and shallower than 70% through-wall.
- Depth calls were typically 15 to 40% shallower than reality *if* the seam crack was detected and near through-wall (90%+ deep). In these scenarios, a notable depth (50% or more) was still reported by EMAT and the length was overstated.
- Depth call accuracy appeared to be independent of crack length for these features less than 4 inches long (Figure 10).
- Length call accuracy generally improved as cracks became deeper (Figure 10).
- EMAT ILI has the capability to size even complex features relatively well despite other anomalies in the same region. In the case of joint 16-36 with long laminations overlapping hook cracks, both service providers successfully detected and sized these anomalies above expectation especially with lamination detection excluded from tool specifications for pipe seams. Refer to Figure 7 for an example cross section and Figure 8 for a depth profile. Sizing details for these cracks are provided in Table 5 and are denoted with an asterisk (*). Discussions around Figure 5 and Figure 6 showcase the limitations of this capability.

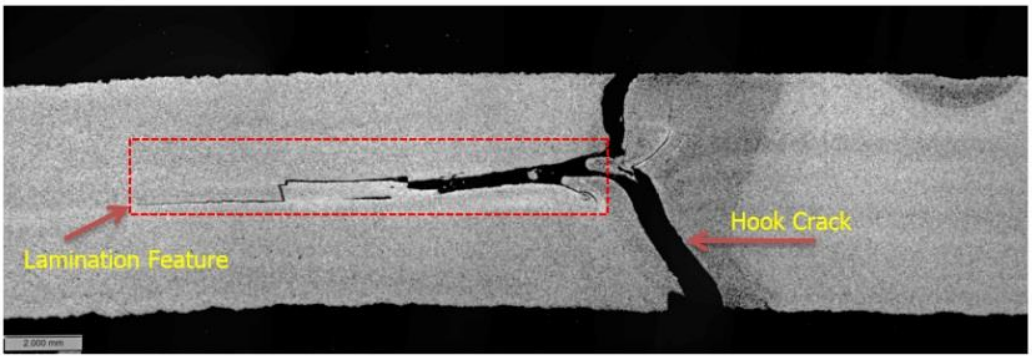

Figure 7: Anomaly #3 in Joint 16-36, Which Showcases the Complex Lamination/Hook Crack Combination (EMAT was Still Capable of Sizing the Hook Crack.)

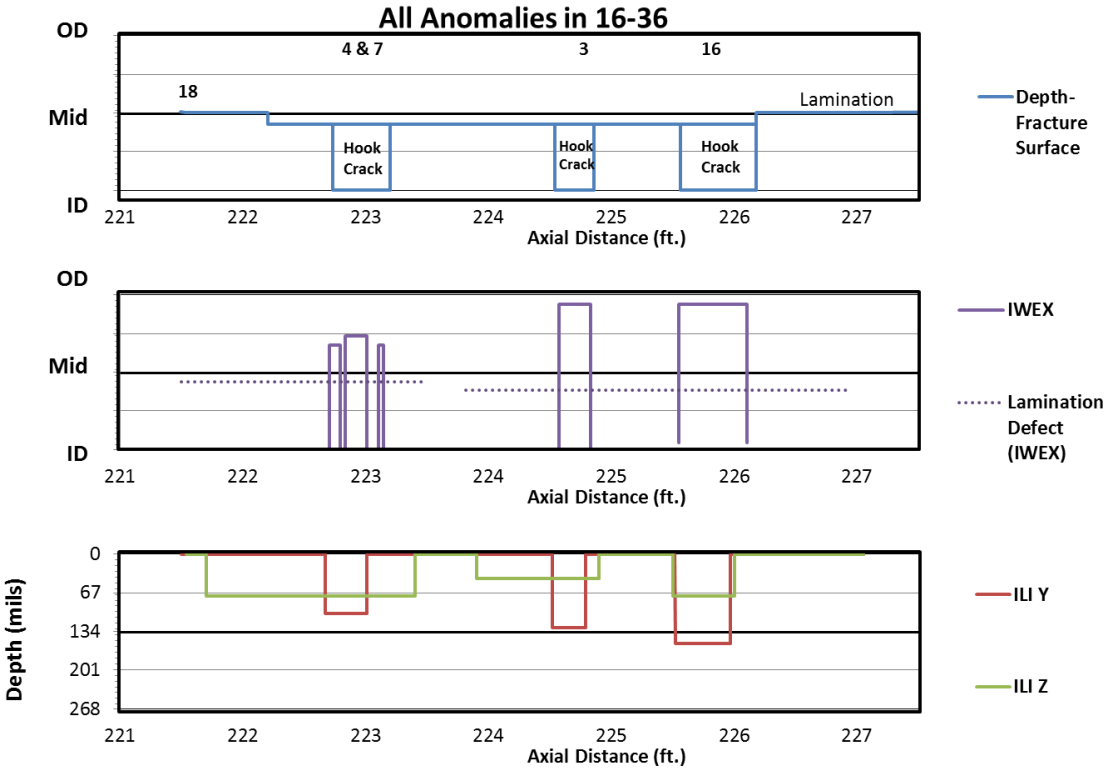

Figure 8: Depth Profile and Inspection Results of Complex Anomalies in Joint 16-36, Including Anomaly #3 Shown in Previous Image

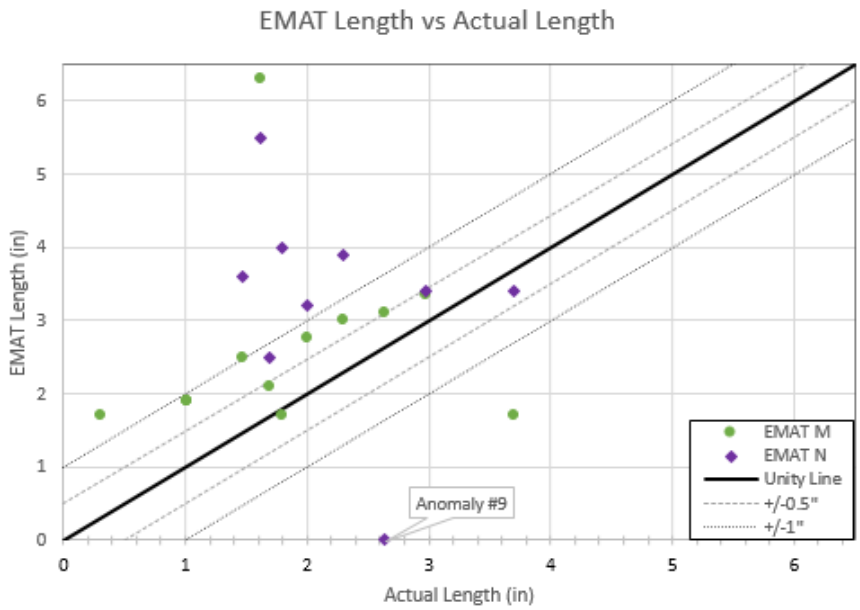

(a)

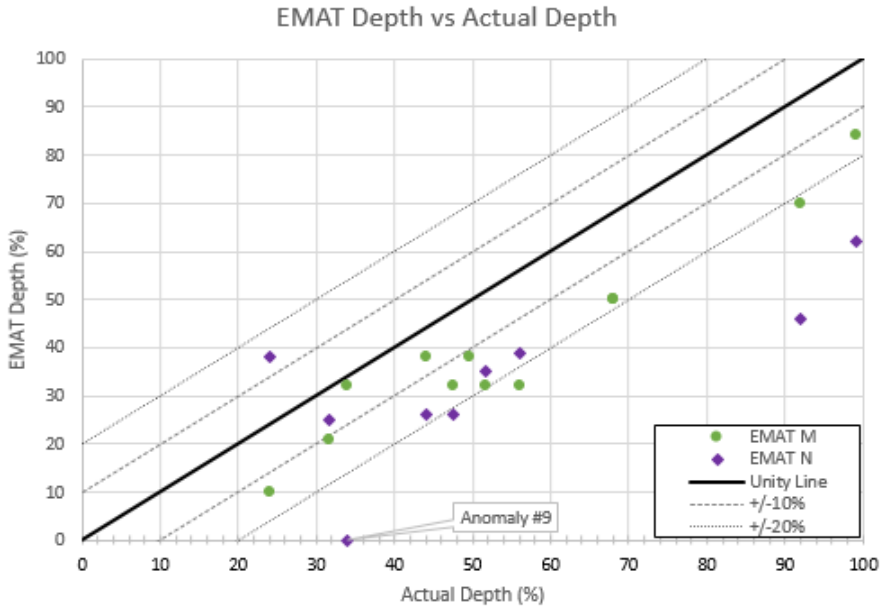

(b)

Figure 9: Unity Plots of EMAT versus Actual Crack Sizing from Fracture Surface Length-to-Length (a) and Depth-to-Depth (b)

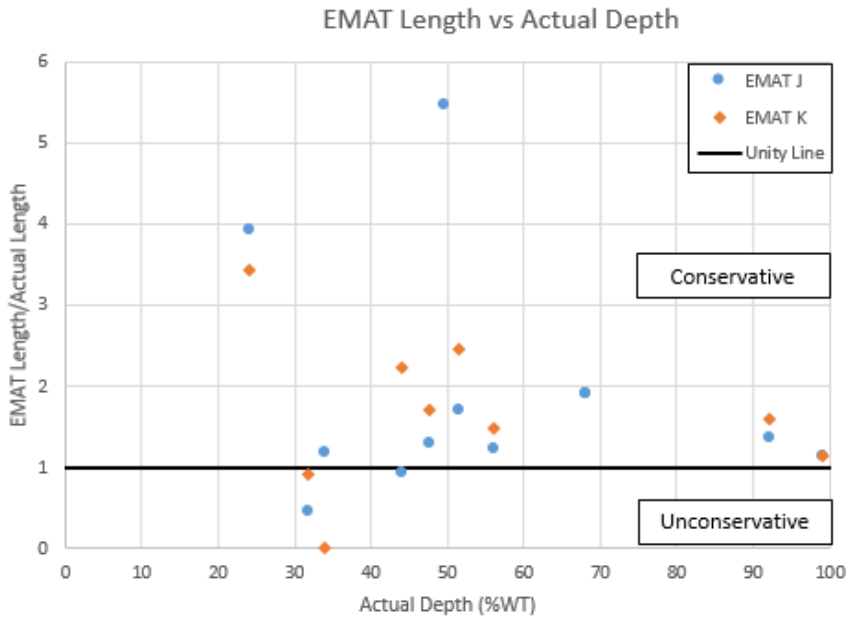

(a)

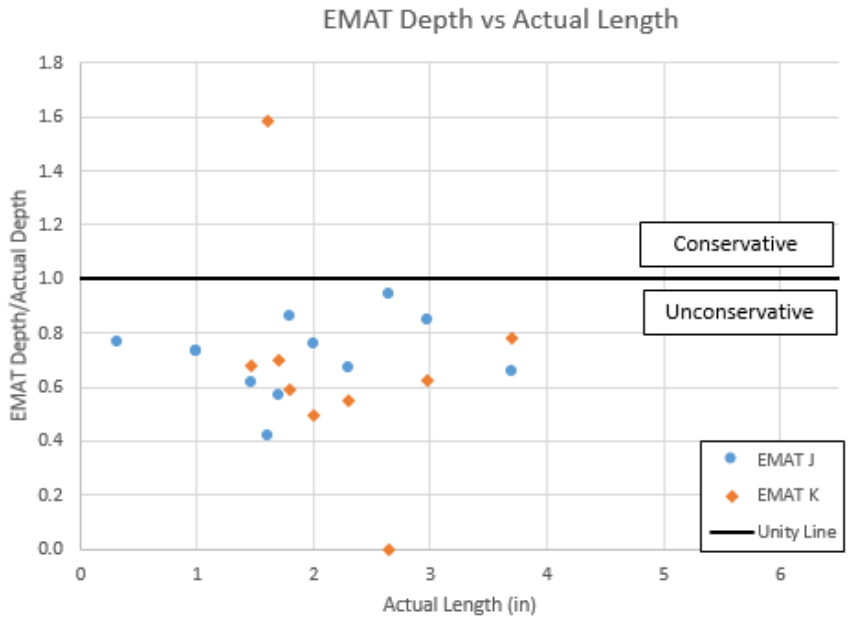

(b)

Figure 10: Unity Plots of EMAT versus Actual Fracture Sizing of Perpendicular Dimension
Length-to-Depth (a) and Depth-to-Length (b)

Observations on Failure Predictions Using EMAT Crack Sizing

The impact of EMAT's crack sizing on failure pressure predictions is illustrated in Figure 11. The majority of the predictions were slightly unconservative (i.e. predicted failure pressure was higher than what would be anticipated in reality). This is driven by the EMAT depth calls. While the crack lengths were reported longer than reality and the depths slightly shorter, the combination of length and depth generally resulted in an unconservative burst pressure. This is because the failure pressure is more dependent on crack depth than length, although both certainly play a role.

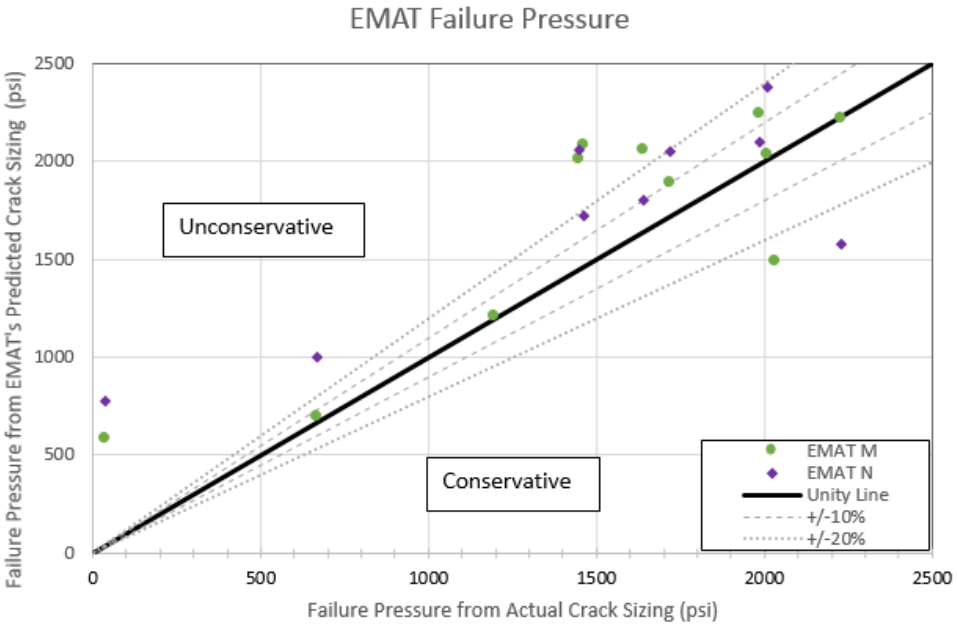

Figure 11: Battelle's PipeAssess PI^{TM} (Version 1.03) Failure Predictions When Using EMAT Crack Sizes Versus Actual Fracture Crack Sizes

All failure predictions in Figure 11 and subsequently Figure 14 and Figure 17 were modeled with actual seam properties when available and assumed properties when unknown.

Despite the non-conservative failure pressure predictions in Figure 11, it is important to acknowledge that these predictions are improving with time as EMAT technology advancements are constantly developing. Later in the report, Figure 22 and Figure 26,

contest to this ILI advancement over time as sizing from historic MFL and EMAT tools are compared to today's fleet and also actual flaw sizing uncovered in metallography.

Observations on MFL Crack Sizing

It is generally accepted that MFL technology is not well suited for detection and sizing of all seam anomaly crack types. However, MFL still has a suitable role in crack inspection; when paired with EMAT, it commonly is used as a screening tool for identifying the long seam, pipe fabrication type, and aides in discriminating crack-like anomalies from seam variations such as excess trim. MFL can also be used independently for "crack-like" anomalies that are sufficiently open and resemble a metal loss volume, which is not uncommon for certain hook cracks for example. Transverse MFL is meant for long, narrow, axially oriented metal loss or these crack-like anomalies with volume.

In general, MFL undersized the long-seam anomalies in this study. In the case of near-through wall cracks, MFL severely undersized them, reporting 30% NWT depths when in reality they exist at 90%+. Therefore, additional conservatism may be required for dig criteria and fatigue analysis when using this method.

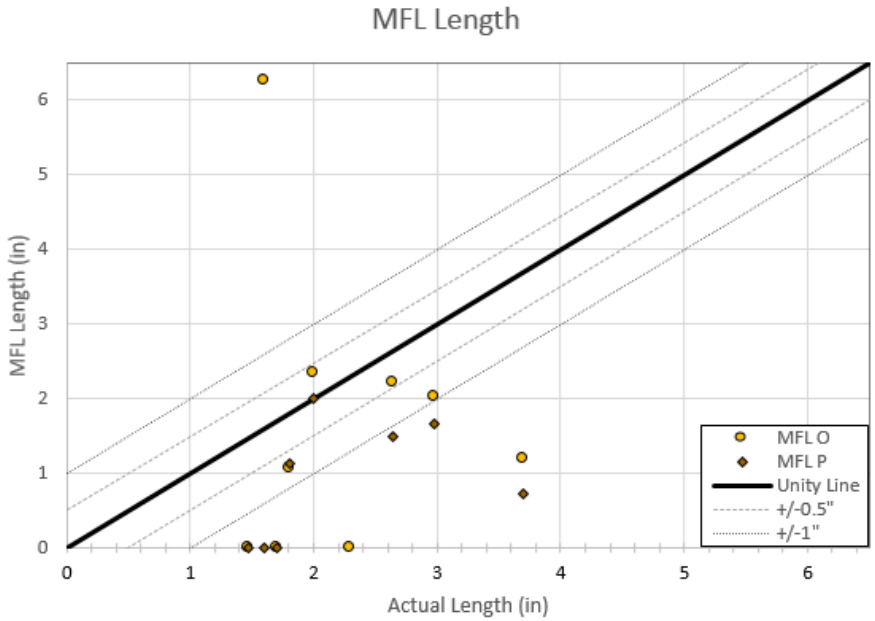

(a)

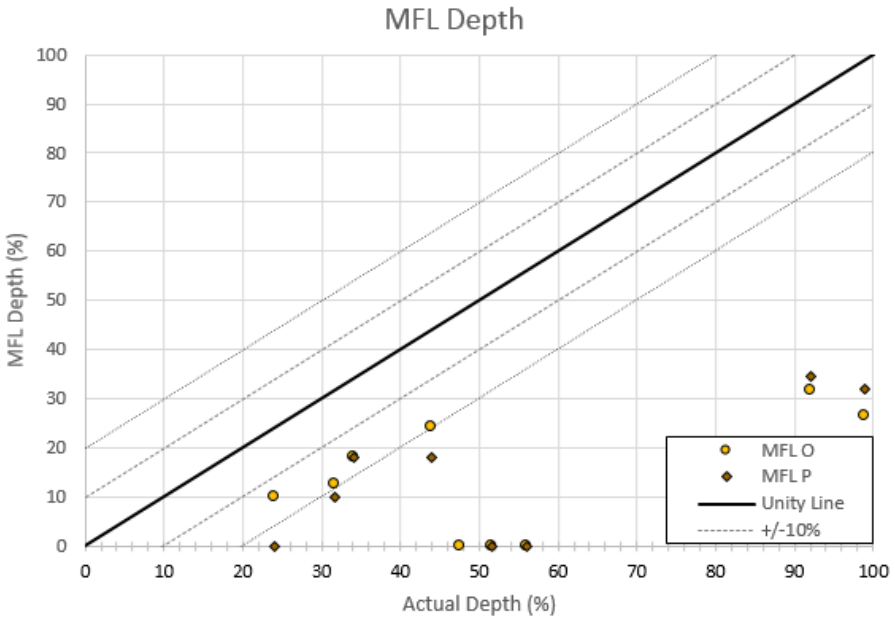

(b)

Figure 12: Unity Plots of MFL versus Actual Fracture Surface Crack Sizing
Length-to-Length (a) and Depth-to-Depth (b)

The crack-like anomalies in this study were generally undersized by MFL, most likely due to minimal crack opening (width), which is critical for proper MFL performance. Although secondary, another contributing factor is the depth which ILI first detects a crack length. The physical principles naturally limit ILI to a minimum measurement threshold. If an anomaly extends out to the surface beyond perpendicular, the length beyond the measurement threshold is not detected. Therefore, the ILI measured length is typically shorter than actual, as shown in Figure 13.

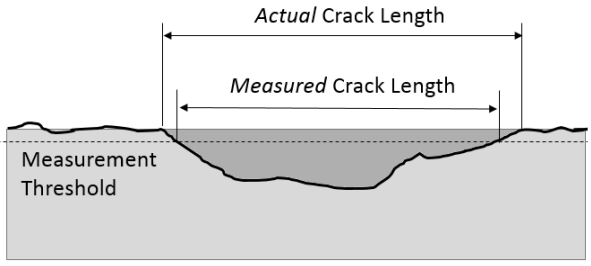

Figure 13: Illustration of ILI Measured Crack Length before Any Predictive Algorithms for Reported Length

The measurement threshold is different per joint and depends on signal noise. Upon special request, some ILI vendors are able to quantify this noise and put it into perspective when considering sizing tolerance unique to the joint. Overall this concept is important to understand as general background when interpreting ILI results, and it could be investigated further on a one-off basis for particularly heavy scrutiny of anomaly sizing.

ILI Subsequent Review of Results

Upon review of Table 4 and Appendix A, ILI vendor N reported that anomalies 5-1, 6-1, and 9 could be detected and sized within their original EMAT data. The initial pull test report for ILI vendor N did not include these anomalies for two reasons: 1) The shorter lengths of anomalies 5-1 and 6-1 reduced detection capabilities, therefore data normalization adjustments were necessary to properly identify the anomalies and 2) Excessive long seam trim of joint 16-38 masked anomaly 9 and made identification more difficult for the analyst. Data normalization adjustments were also used to help identify this anomaly.

By adjusting data normalization within the standard analysis process and utilization of the same sizing methods, the three anomaly lengths and depths were calculated for these locations. These three locations are shown in Table 6 with EMAT lengths and depths.

Table 6: Anomalies that Went Previously Undetected by EMAT Vendor N but Upon Subsequent Evaluation was Discovered to be Detectable

Anomaly #	Joint #	Fracture Length (in)	Fracture Depth (% wt)	EMAT Length (in)	EMAT Depth (% wt)	Anomaly Type (fracture surface)
5-1	16-20	1	68	1.4	15	CW
6-1	16-20	0.3	50	0.77	8	CW
9	16-38	2.6	34	1.96	17	HC

Observations on Failure Predictions Using MFL Crack Sizing

The impact of MFL's crack sizing on failure pressure predictions is illustrated in Figure 14. No new conclusions are drawn. As previously stated, it is generally accepted that MFL technology is not well suited for detection and sizing of all seam anomaly crack types. This comparison is simply included for report completeness.

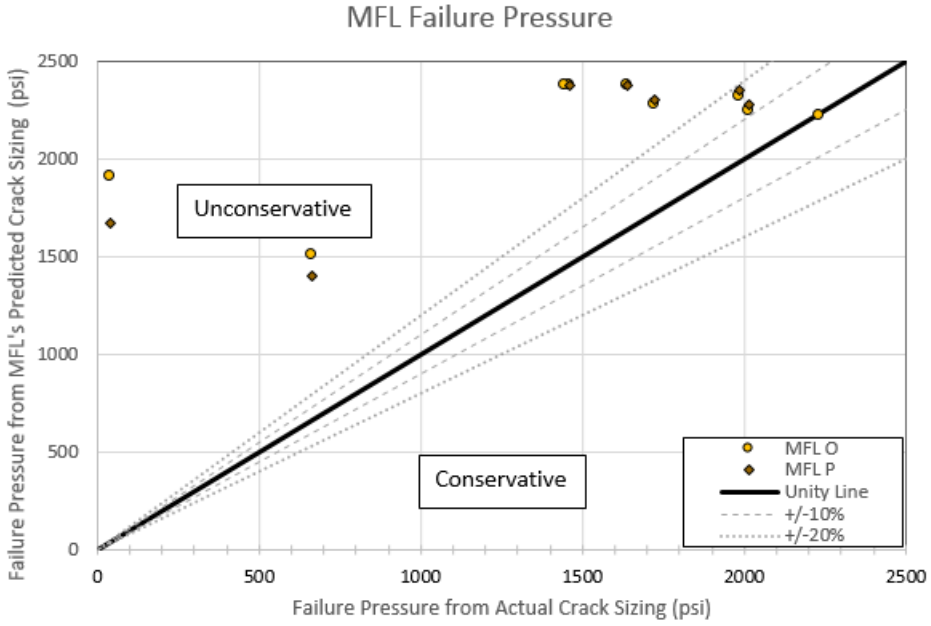

Figure 14: Battelle's PipeAssess PI™ (Version 1.03) Failure Predictions When Using MFL Crack Sizes Versus Actual Fracture Crack Sizes

ITDM

The objective of the ITDM inspection was to identify as many seam cracks as possible and understand the geometry as best as one can non-destructively for subsequent ILI comparisons and burst testing. These objectives are somewhat contradictory as ITDM testing was time limited; examination of more pipe was valued over complete ITDM measurements. There was an understanding that all significant cracks would be destructively examined. An elevated quality of detection was accommodated by inspecting the same pipes with multiple techniques (MPI and shear wave UT, PAUT, TOFD, IWEX), using qualified and accomplished inspectors, providing calibration blocks of similar pipe material and geometry, and inspecting in a controlled indoor

environment when able. Crack sizing evaluated under these conditioned circumstances were reported by ITDM and are discussed in the following section.

MPI and Shear Wave

The process of identifying significant seam cracks using MPI for detection and shear wave UT for sizing proved to be unreliable. There were two cracks that exceeded the threshold for length and depth only to be dismissed as false calls after further investigation by other methods. These two supposed anomalies were sized as nearly-through wall cracks (i.e., feature #12 and #11). Feature #12 coincided with a minor OD trim tool marking, which is the suspect cause of the false crack call. Human error is suspected in Feature #11.

In the same light, there was a severe false negatives per MPI as well. A very short but nearly through-wall feature went undetected by a qualified Level II UT/MT inspector. This occurred even in the controlled environment of a lab where ambient lighting, temperature, and positioning of the pipe was optimum compared to most field settings. This anomaly was identified post MPI via other ITDMs. ILI confirmed the presence of this seam crack as well. Once the inspector received feedback on the false negative, they applied additional diligence and personal pressure on himself, which actually negatively impacted the inspection accuracy as the level of false positives drastically increased. At this point trivial or simply non-existent cracks were being increasingly reported by the MPI and shear wave UT approach. This may also help explain the false positive MPI call of feature #11 and #12, but it fails to explain the false shear wave sizing which reported nearly-through wall cracks that were later found to be non-existent. Overall these false calls, both negative and positive, prove that MPI calls can be highly subjective and can be severely unreliable for detecting seam cracks even with a qualified inspector. It is strongly recommended that MPI and shear wave UT approach not be used alone to locate and size significant longitudinal ERW seam cracks. It is also recommended to take caution when sizing seam anomalies only with single beam shear wave and complex seam geometry is suspect.

Full Matrix Capture Ultrasonic Imaging

Two generations of IWEX tools were ran and significant changes were observed between the 2015 and 2016 calls on the same pipe as a direct result of this project. The largest improvement between the two generations was the scanning technique to overcome geometry variances and better tracking of the pipe seam.

Of the latter IWEX generation, the depth and length of many anomalies were accurately detected and sized while a few were misinterpreted when the flaw was revealed by destructive testing. There is no published specification yet, but data presented in the paper [6] from the PHMSA project [7] provides initial estimates of tool accuracy. The goal of the current phase of the PHMSA IWEX project is to cut the depth or height tolerance by over half to +/-0.2 mm (0.008-in). In theory this is possible if all sources of error in producing an image can be accounted. This will be tested on a practical basis during the PHMSA R&D project [7].

Within this project, IWEX sized all 16 simple anomalies (i.e., not overlapped with a lamination). The length accuracy was typically within +/- 0.5" with two outliers. The two outliers (#13 and #15) were under called by 1.5" and 1.8", respectively. The first was a stringer, the latter a hook crack. Overall IWEX's tendency was to call anomalies shorter than actuality for features shallower than approximately 50% through-wall and over state feature length for deeper anomalies (Figure 16, left).

The depth accuracy was typically within +/-16%, with three outliers (#9, #14, #15). Overall the depth calls increased in accuracy as the anomaly length increased and approached 4 inches long (Figure 16, right). The three outliers were oversized up to 55% deeper and were either stringers or hook cracks. While significantly overcalled, it is interesting to note that one feature (#14) was below EMAT detection thresholds and another feature (#9) was a false negative for one EMAT tool. Therefore, despite wider sizing accuracy on these two cracks, the ability to even detect and approximately size them exceeds usefulness for ILI verification in the field. ITDM and ILI are complementary inspections and are optimized when ITDM verifies ILI calls. Therefore, if there is no ILI call, there is no anomaly to verify with ITDM in the field. This would

have been the case for anomaly #9 and #14 in this study had they still been in an underground pipeline and not a laboratory. Unity plots for comparison to all validated cracks are shown in Figure 15 and Figure 16.

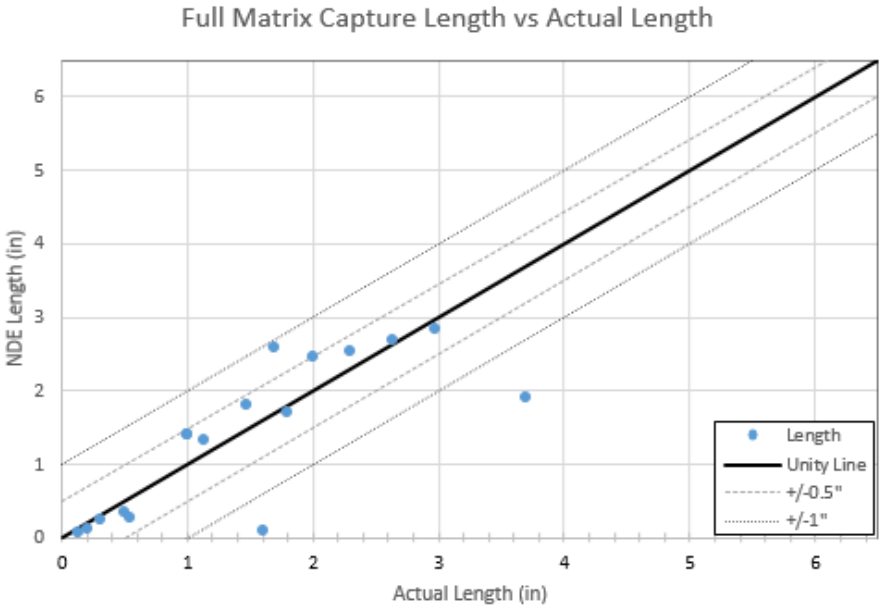

(a)

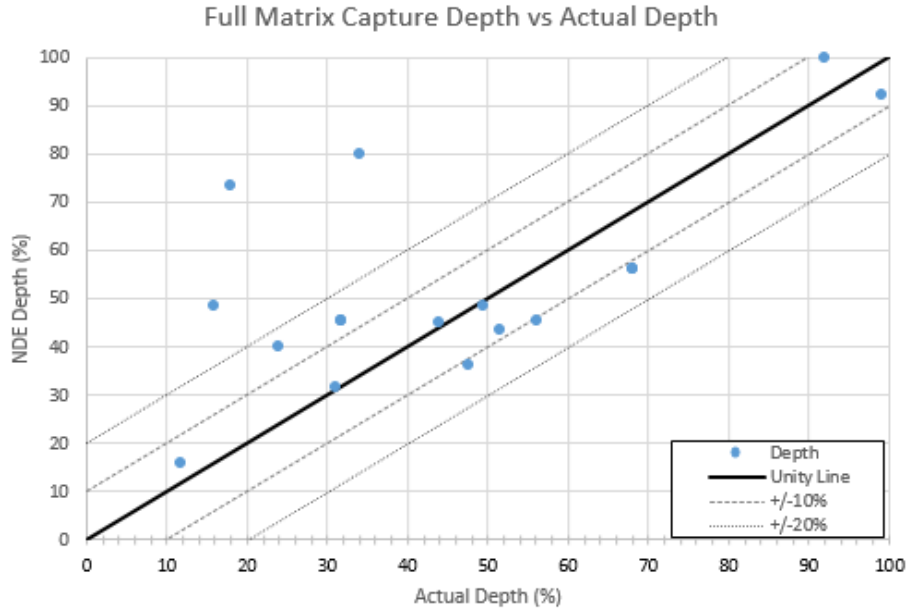

(b)

Figure 15: Unity Plots of FMC versus Actual Crack Sizing from Fracture Surface of Same Dimension

Length-to-Length (a) and Depth-to-Depth (b)

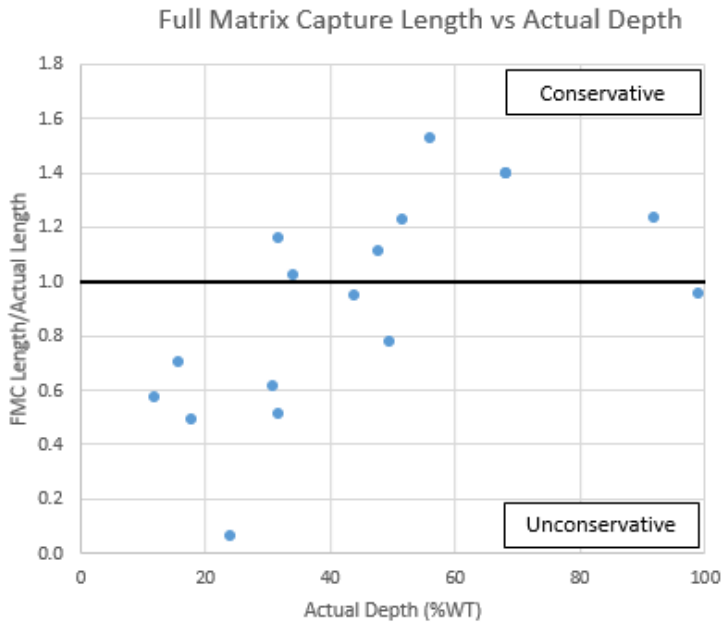

(a)

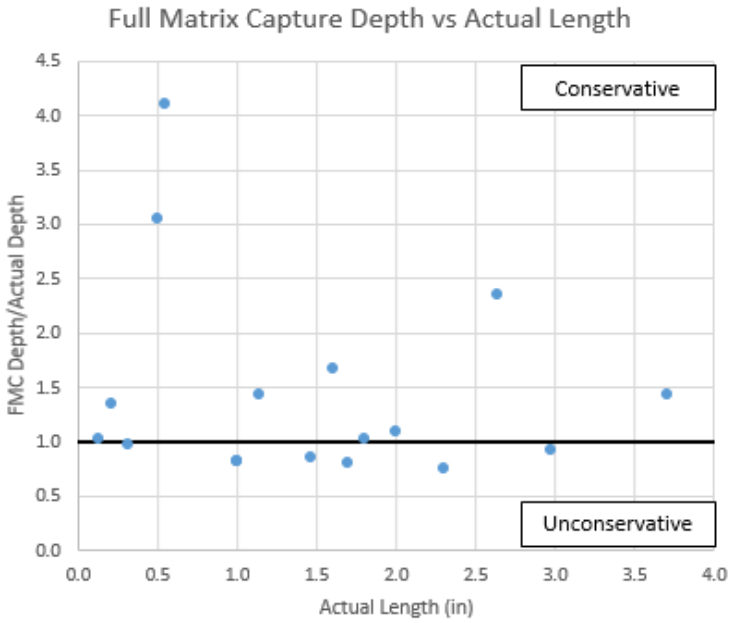

(b)

Figure 16: Unity Plots of FMC versus Actual Crack Sizing of Fracture Surface of Perpendicular Dimension
Length-to-Depth (a) and Depth-to-Length (b)

Observations on Failure Predictions Using Full Matrix Capture Crack Sizing

The impact of Full Matrix Capture crack sizing on failure pressure predictions is illustrated in Figure 17. Eight of twelve predictions were within +/- 10% error. The remaining four produced both conservative and unconservative predicted failure pressures, some of which wavered from actual predictions considerably. Conservative failure pressure predictions are those that yield lower failure pressures than reality; unconservative predictions yielding higher failure pressures than actuality.

The three shortest cracks detected and reported in Figure 15 were beyond cold weld stress intensity factor solutions currently available in PipeAssess PI™ and thus were unable to be modeled.

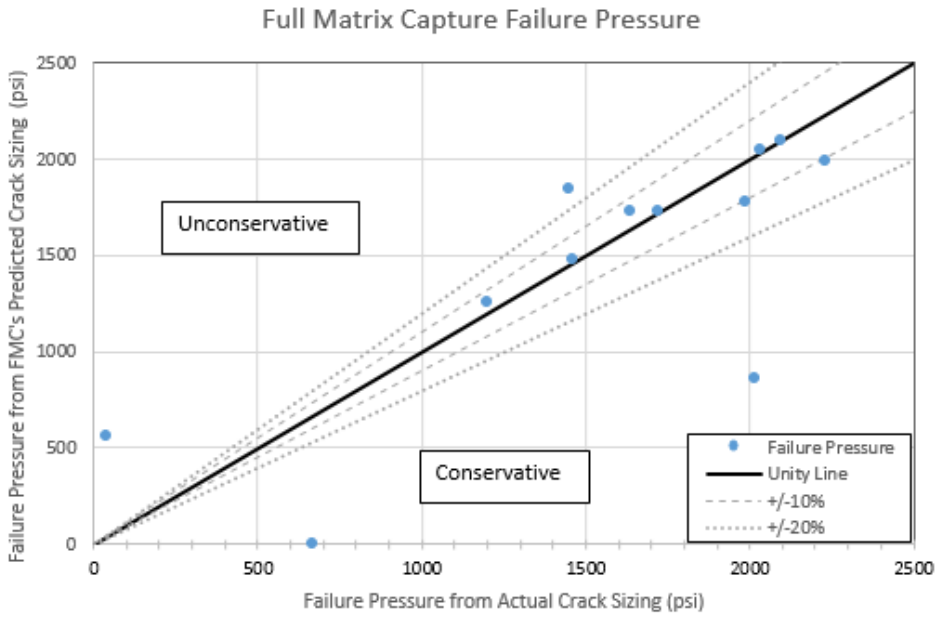

Figure 17: Battelle's PipeAssess PI™ (Version 1.03) Failure Predictions When Using FMC Crack Sizes Versus Actual Fracture Crack Sizes

Ability to Classify Seam Crack Type via ITDM and ILI

The vast majority of the seam anomalies collected in this project were also the three most common weld seam anomalies: cold weld, hook crack, and lamination. Many ITDM inspectors in MPI, PAUT, and TOFD are not always successful at delineating between single linear cracks such as a cold weld and those with inclination such as a hook crack. In this scenario the returning signals and signal strength that reflect from both crack geometries may appear the same to the inspector, and as such they often are characterized as the same crack type. To add to the confusion, some hook cracks are fairly straight while cold welds can have a slight angle due to uneven pressures during seam manufacturing. This causes additional difficulty for these traditional ITDM, which are signal amplitude based inspections.

Seam laminations were the third examined crack type. While not all pipe with lamination have hook cracks, hook cracks are rarely seen in pipe that does not have laminations. Of the six joints found to have laminations via ITDM, all reportedly had hook cracks too. These six joints represented three different pipe pedigrees. The reverse statement held less confidence within the small sample size; that is, hook cracks were not strong indicators of laminations. Of the twelve joints with hook cracks, half had seam laminations as well. Regardless, the majority of the hook cracks and seam laminations reported by traditional ITDM were not reported by ILI as they fell outside of the tools' specification. These noted features were smaller than ILI's minimum sizing threshold or in the case of laminations, were not classified as a detectable geometry in the seam region.

The results of this study show that traditional ITDM (MPI, PAUT, TOFD), MFL, or EMAT ILI cannot routinely differentiate between linear seam cracks and inclined seam cracks, such as hook cracks, that were part of this examination. **All of these technologies are capable of routinely identifying seam cracks to some level, but *routinely characterizing* the actual crack geometry remains unseen at this time.** The traditional ITDM are limited fundamentally when used as is. However, upcoming ITDM such as full matrix capture methods have demonstrated some ability to differentiate crack

geometry successfully. This technology has the advantage over traditional UT ITDM inspection techniques in that it is not an amplitude-based inspection and instead uses full waveform capture and inversion to provide an ultrasound image of anomalies. This helps in improved characterization of anomalies. In fact, IWEX performed very well in regards to anomaly characterization: 17 of 24 anomaly type calls were correct. This was the best defect characterization of tools employed in this study. All the miss-interpreted crack geometries per IWEX were inclined features such as hook cracks or stringers (also known as "embedded hook cracks" or "inclusions"). In those calls IWEX occasionally reported them as cold welds. Refer to Table 7 for a complete listing.

Table 7: Anomaly Type Characterized per IWEX versus Actual

Anomaly #	Joint #	Defect Type	
		IWEX	Fracture Surface
1	16-37	CW	CW
2	16-33	CW	CW
3*	16-36	HC	HC (due to Lamination)
4*	16-36	HC/UFI	HC (due to Lamination)
5	16-20	CW	CW
		CW	CW
		CW	CW
6	16-20	CW	CW
		CW	CW
7*	16-36	Unknown**	HC (due to Lamination)
		Unknown**	
8	16-38	HC/UFI	HC
9	16-38	HC	HC
10	16-38	CW	HC
		HC	HC
		HC	HC
11	16-36	No Calls reported by ILI or IWEX	
12	16-33	No Calls reported by ILI or IWEX	
13	16-38	CW	Stringer
14	16-38	CW	Stringer
15	16-38	CW	HC
16*	16-36	HC	HC (due to Lamination)
17	16-38	CW	HC
18*	16-36	Lamination	Lamination
19	16-38	HC	HC
		Lamination	

Note that technology improvements are possible. Certain EMAT ILI developers are examining this challenge to further differentiate flaw types themselves. **In the few pull tests completed, characterizing seam crack geometry (cold weld vs. hook crack) via ILI proved to be more difficult than anticipated and development is continuing.**

Ability to Classify Seam Crack Location via ITDM and ILI

Previous reports [1] within this program have discussed the importance of using accurate material properties local to the crack. Knowing whether the crack was in the base metal, in the heat affected zone or on the bond line can be critical for properly applying assessment criteria. For instance, charpy v-notch (CVN) energy can vary significantly within the same pipe joint depending if the material body, heat affected zone (HAZ), or seam bondline are in question. This can have a direct impact on failure pressure predictions if a large variation exists. Table 8 shows a sample range of CVN energies Battelle has witnessed within their repository. More conservative lower bounds for CVN energy which were back-calculated with a brittle-fracture model (i.e., Raju/Newman equation) from a large 600+ case set within Battelle and Kiefner and Associates Inc. databases are also included in Table 8. These were originally reported in Phase 1 of this program in References [1] and [8] . This information is provided as general guidance and is not intended to cover absolute maximum and minimum values. Table 8 shows sample cracks in various seam locations, which could thereby be associated with different CVN energy values.

Table 8: CVN Impact Energy Values for Various Locations with Respect to the Longitudinal Pipe Seam

Location	CVN Energy Range per Testing[A]	# of Samples Evaluated[A]	CVN Energy, Lower Bound per Brittle Fracture Calculation[B]
Body	2.8 - 65 ft-lbs	137	--
ERW Seam	4.5 - 17.4 ft-lbs	8	4 ft-lbs for cold welds and hook cracks 0.4 ft-lbs for SSWC
ERW HAZ	5.4 - 36 ft-lbs	5	--

[A] Data from Battelle Repository Sample of Full-Size CVN Impact Energy Values Tested at 45°F or 50°F for Circa 1970s and Earlier Pipe, Grade B Through X65

[B] These lower bound values determined after evaluating over 600 cases between Battelle and Kiefner database. When using a brittle fracture model (i.e., the Raju/Newman equation), these fracture toughness values were back calculated [1] and [8].

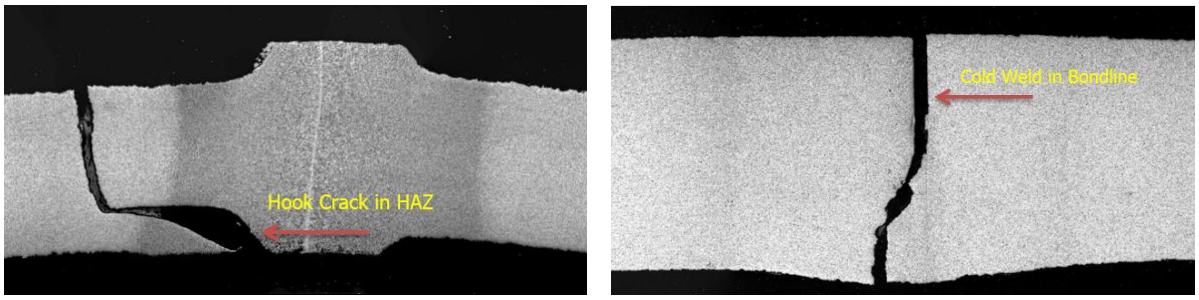

Figure 18: Example of Different Crack Position with Respect to Seam Geometry

While understanding a seam crack's precise location is ideal, gathering that insight from ILI is not fully developed at this time. Current EMAT ILI resolution restricts this ability, with sensor size and frequency of operation being the major driving factors. A certain EMAT service provider is able to provide guidance if a seam crack is "on" or "near" seam, but differentiating between HAZ and bondline remains undemonstrated. Most of the ITDM rely on the trim to determine the location of the bond line, but this is not a reliable measure. The Full Matrix Capture Ultrasonic Imaging technique employed, however, can characterize crack type, which can then be used to infer most likely location. That is, a true cold weld will be located in the bondline. Hook cracks generally lie in the HAZ, although they can extend to the bondline and pipe body.

Non-Destructive Positive Material Identification (PMI) via ITDM and ILI

As part of Task 2, pipe material was well characterized. Mechanical properties of the bondline, heat affected zone, and base metal were evaluated with a subset of Vickers microhardness per ASTM E-384, T-L charpy tests per ASTM A-370, and metallographic cross sections per ASTM E-3 where performed, as well as grain sizing per ASTM E-112. Elemental composition was also evaluated per ASTM A-751 and flattened tensile tests per ASTM A-370 for base metal only. Detailed results are provided in Appendix B.

Per PHMSA's request, these well-characterized pipe samples were also made available to NDE PMI technique developers seeking additional validation, an endeavor outside the scope of this program but within other DOT PHMSA initiatives. Samples

were made available to multiple developers that sought interest: TDW's optical emission spectrometer (OES), ball indenter, and ILI permeability feature as well as an Iowa State University technique involving UT [9]. PMI results and evaluation are not included as it is outside this project's scope.

The Effect of Velocity on ILI Results

While pulls were made at speeds ranging from 1.5 to 4 miles per hour, the results were not conclusive on the effect of speed. Two of the more significant anomalies, #17 (52% deep, 1.5 inch long hook crack) and 19 (48% deep, 2.3 inch long hook crack) were studied in detail. For depth, one vendor reported the same depth (±2% for all speeds while the other vendor results increased for the one higher speed pull. For length, both vendors reported variation over an inch, but measurement variation did not correlate with speed. It is difficult to conduct this type of analysis in a blind manner using repeated pulls through the same set of anomalies. Therefore, no conclusion could be drawn on the effect of velocity on the ILI results.

Burst Testing and Anomaly Metallography

Two additional burst tests were completed in Phase II, with the previous three tests completed in Phase I [1]. Testing temperature was intentionally lowered from that 70^{o}F used in Phase I to 50^{o}F to better represent ground temperature that a buried pipe would experience. As before, the pipes were filled with water and pressurized to failure. A summary table of burst tests completed in this phase is provided in Table 9.

Table 9: Overview of Burst Tests Conducted from LF-ERW Pipe Collected in Phase 2

Test #	Joint ID	Nominal Pipe Diameter (in)	Actual Wall Thickness (in)	Grade	Fabrication (year/manufacturer)	Anomaly Size per Fracture Surface (length, % max depth)	Testing Temp.	Failure Pressure
4	16-37	16	0.266	Grade B	1941 install / Republic Steel	2.97", 99% cold weld[ILI*]	50°F	820 psi (70%SMYS)
5	16-33	16	0.266	Grade B	1941 install / Republic Steel	2.00", 92% OD cold weld[ILI*]	50°F	1450 psi (125%SMYS)

* Site of burst or leak initiation

[ILI] Previously detected by ILI

Burst Test 4

Feature #1 in joint 16-37 was pressurized to failure. The nominal pipe diameter is 16-inch and average wall thickness is 0.266". This Grade B pipe was manufactured by Republic Steel and installed in 1941. This line was hydrotested in 1969, at which point the line experienced multiple leaks and ruptures: It was first pressurized to 800 psi where it experienced a rupture. After repairs, the line was re-tested to 865 psi before a leak was detected and pressure began to drop. After additional repairs the line was pressurized to 795 psi and experienced a rupture. After repairs the line was brought to 855 psi where it experienced another rupture. After repairs the line was then taken to 865 psi and then decreased to 835 psi, with the difference attributed to entrained air. The line was then held at 835 psi for 20 hours.

The 2016 hydrotest of this one joint, 16-37, began to leak at 820 psi at the previously identified feature #1. The initial leak was minimal; at the initiation the pressure immediately decreased 8 psi before the next pump's stroke increased pressure. It was only by visual observation moments afterwards was the leak recognized, as shown in Figure 19.

While leaking, pressure was then increased to 1420 psi (125% SMYS). The joint continued to leak but remained otherwise intact. At this point the test was terminated as

the leak rate met the pump's capacity and vessel pressure could no longer be increased. Crack opening displacement and pipe pressure measurements indicated that the crack began to reseal around 550 psi. Figure 20 shows the resealed crack in comparison to moments before at the maximum test pressure. Pressure-volume plots suggest the joint did not yield leading up to the leak.

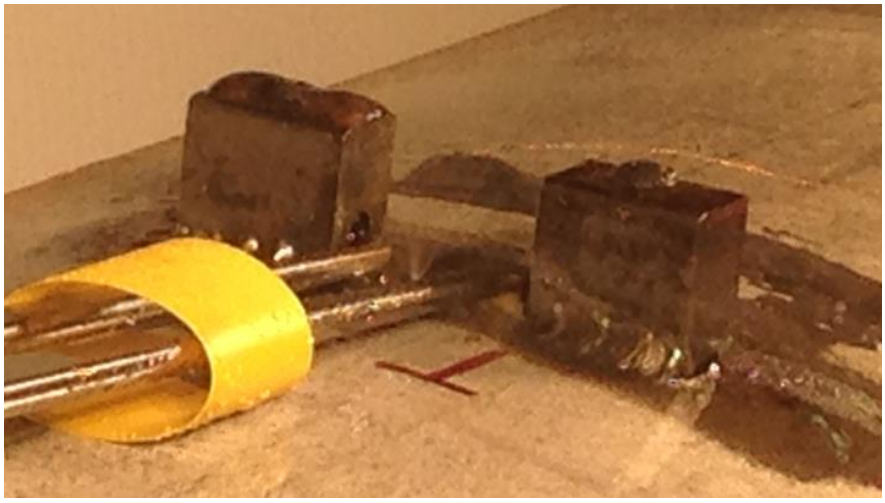

Figure 19: Feature #1 Shortly after Leak Initiation at 125%SMYS

Figure 20: Feature #1 Leaking While Pipe at Approximately 1420 psi (left) and Then Shown after De-pressurized (right)

Per the latest in-the-ditch-methods this flaw was characterized as a 2.83” long, 92% deep cold weld before the burst test. Post testing the specimen underwent metallography (Figure 21) to determine actual size of the initial crack, and it exposed a 2.97” long, 99% deep cold weld. The metallurgical section (Figure 21-b) also revealed indications of a repair weld and no subsequent heat treatment. Historic records suggest this repair weld may have been conducted at the mill as nothing was found that may indicate post-construction repair in the ditch. The operator’s inspection records have no notations of coating repair, and photos of the pipe prior to the coating removal appeared to show coal tar coating consistent with the original coating. Interestingly, one EMAT service provider also noted a permeability change co-incident with this anomaly.

(a) (b)

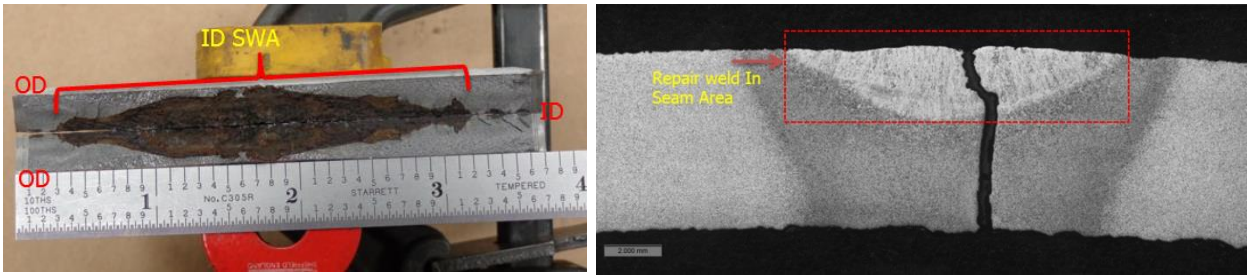

Figure 21: Anomaly 1 Fracture Surface (a) and Cross Section at the Deepest Point (b)

Table 10 displays flaw sizes as reported by various inspection methods over time, including the ILI calls in 2013 that originally flagged this feature in the field and the 2014 ITDM validation calls. Figure 22 is a pictorial representation of these calls with respect to the actual crack size and show how technologies have improved over two years.

Predicted failure pressures were calculated with actual material properties and flaw size. PipeAssess PI^{TM} predicted failure pressure to be less than 100psi when utilizing API 579 K solutions, legacy K solutions derived by Battelle and Computation Mechanics, Inc. in the early 1990s [10], and also new cold weld K solutions developed under this contract by Engineering Mechanics Corporation of Columbus and Battelle. Recall that the actual failure pressure of 820 psi was far higher than the predicted, which was less than 100 psi. The residual stress observed via the pipe re-sealing after depressurization is suspect for the large difference in predicted versus actual failure pressure. Recall that the metallurgical section suggested no post weld heat treatment was performed after a repair

weld, which is not the norm and is also suspect. Further analysis beyond this program would be necessary for more conclusive results.

Table 10: Various NDE Sizing of Feature #1 over the Years

	Year	Sizing Method	Length (in)	Depth (%)	Comments
	2016	Actual Size per Metallography	2.97	99%	ID cold weld
ITDM	2016	ITDM, IWEX Cycle 2	2.83	98%	Midwall cold weld
ITDM	2015	ITDM, IWEX Cycle 1	2.93	83%	Crack type not clear per IWEX
ITDM	2015	ITDM, MWM Array*	0.7	42%	Although not an OD anomaly, close enough to surface that this technique is able to detect
ITDM	2014	ITDM, field MPI	3	N/A	
ITDM	2014	ITDM, field Shear Wave	1.5	52%	
EMAT	2015	EMAT 1	3.4	84%	
EMAT	2015	EMAT 2	3.4	62%	
MFL	2015	MFL 1	2.0	27%	
MFL	2015	MFL 2	1.7	32%	
MFL	2013	MFL 3	2.41	26%	

* Recall the MWM array technology employed is only able to detect OD surface breaking flaws. ID or midwall surface breaking flaws are not detectable.

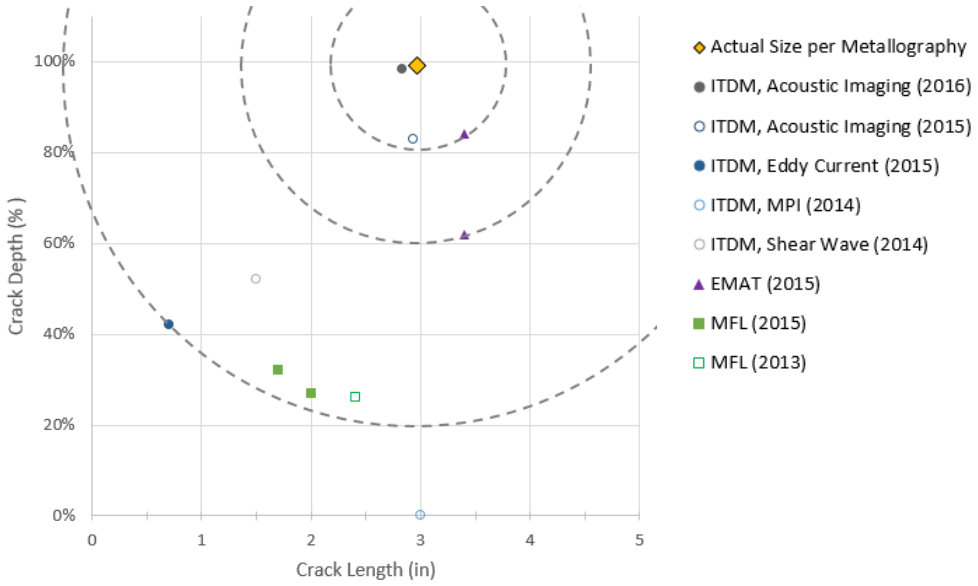

Figure 22: Various NDE Sizing of Feature #1 over the Years

Burst Test 5

Feature #2 in joint 16-33 was pressurized to failure. The nominal pipe diameter is 16-inch and average wall thickness is 0.266". This Grade B pipe was manufactured by Republic Steel and installed in 1941. This joint is from the same lot as joint 16-37 and subsequently underwent the same hydrotest in 1961, which is detailed in "Burst Test 4."

This joint began to leak at 125% SMYS. After the leak, initiated the pressure was slowly increased to 133% SMYS before it was de-pressurized. Reviewing video and pressure vessel measurements revealed the crack resealed at approximately 390 psi. Figure 23 shows the resealed crack and moments earlier when it was at maximum test pressure. Pressure-volume plots suggest the joint began yielding shortly before the leak initiated.

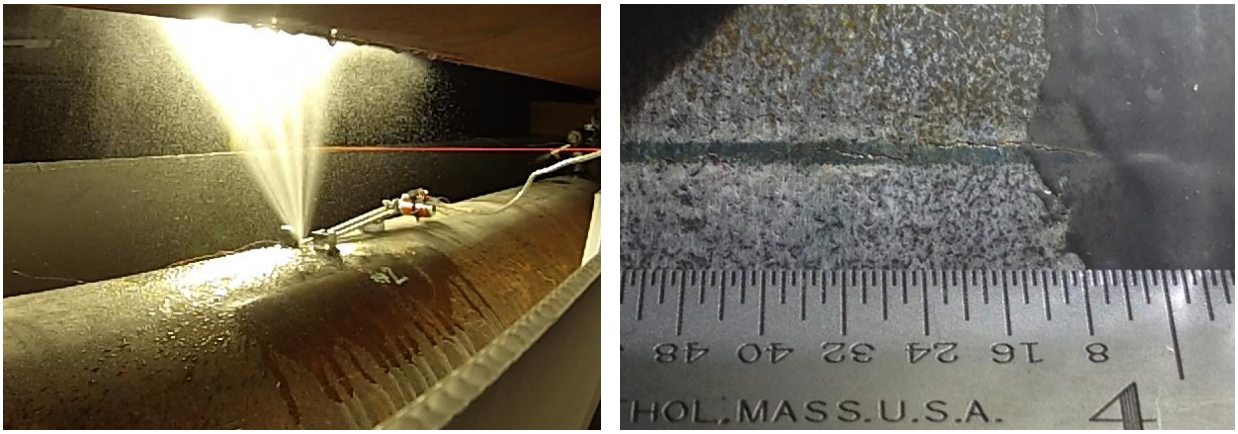

Figure 23: Feature #2 Leaking While Pipe at Approximately 1500 psi (left) and Then Shown after De-pressurized (right)

Per the latest ITDM this flaw was characterized as a 1.2" long, 81% deep OD cold weld before burst testing. Post testing the specimen underwent metallography to determine actual size of the initial crack. Freeze and break methods revealed a cold weld 2.00" long, 92% deep as shown in Figure 24 and Figure 25. Similar to Anomaly #1, a repair weld with no post weld heat treatment was observed. Again, one EMAT service provider also noted a permeability change co-incident with this anomaly.

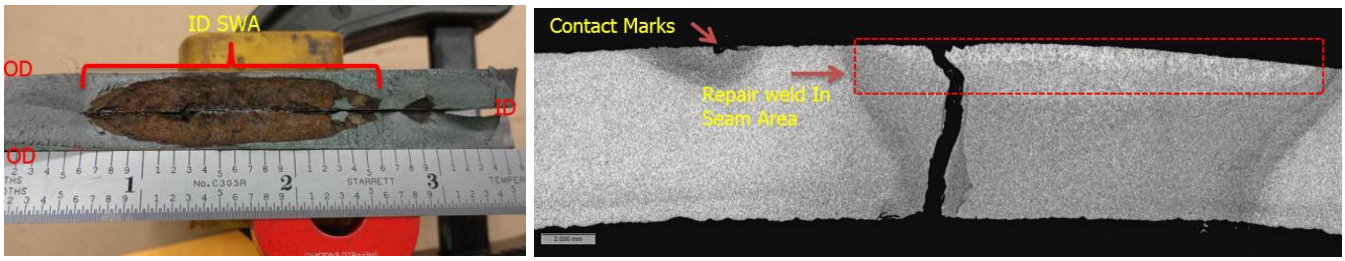

(a) (b)

Figure 24: Anomaly 2 Fracture Surface (a) and Cross Section at the Deepest Point (b)

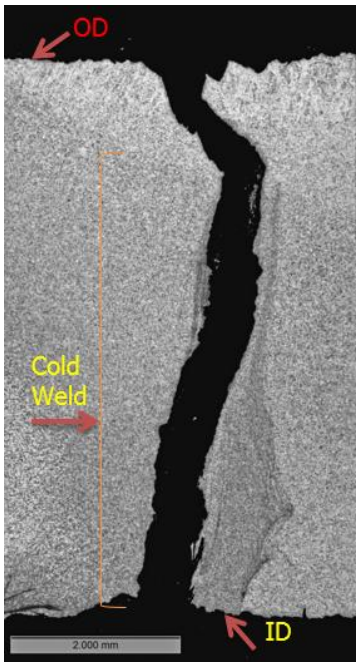

Figure 25: Cross Section at Deepest Point of #2 at 25X Magnification

Table 11 displays the flaw sizes as reported by various inspection methods over time, including the original ILI calls in 2013 that originally flagged this feature in the field and the 2014 ITDM validation calls. Figure 26 is pictorial representation of these calls with respect to the actual crack size and show how technologies have improved over two years.

Predicted failure pressures were calculated with actual material properties and flaw size. The PipeAssess PI^{TM} predicted failure pressure was less than 100 psi when utilizing API 579 K solutions, legacy K solutions, and also new cold weld K solutions developed under this contract. Recall that actual failure pressure of 1,450 psi was far higher than the predicted failure pressure, which was less than 100 psi. The residual stress

observed via the pipe re-sealing after depressurization is suspect for the large difference in predicted versus actual failure pressure. Recall that the metallography cross section suggested no post weld heat treatment was performed after a repair weld, which is not the norm and is also suspect. Further analysis beyond this program would be necessary for more conclusive results.

Table 11: Various NDE Sizing of Feature #2 over the Years

	Year		Length (in)	Depth (%)	Comments
	2016	Actual Size per Metallography	2.00	92%	ID cold weld
ITDM	2016	ITDM, IWEX Cycle 2	2.41	100%	Through wall cold weld
ITDM	2015	ITDM, IWEX Cycle 1	1.2	81%	OD cold weld
ITDM	2015	ITDM, MWM Array*	--	--	No anomaly detected
ITDM	2014	ITDM, field MPI	19	n/a	"minor surface linear indication/possible SCC"
ITDM	2014	ITDM, field Shear Wave	--	--	No anomaly detected
EMAT	2015	EMAT A	2.8	70%	
EMAT	2015	EMAT B	3.2	46%	
MFL	2015	MFL A	2.3	32%	
MFL	2015	MFL B	2.0	35%	
MFL	2013	MFL C	2.87	25%	

* Recall the MWM array technology employed is only able to detect OD surface breaking flaws. ID or midwall surface breaking flaws are not detectable.

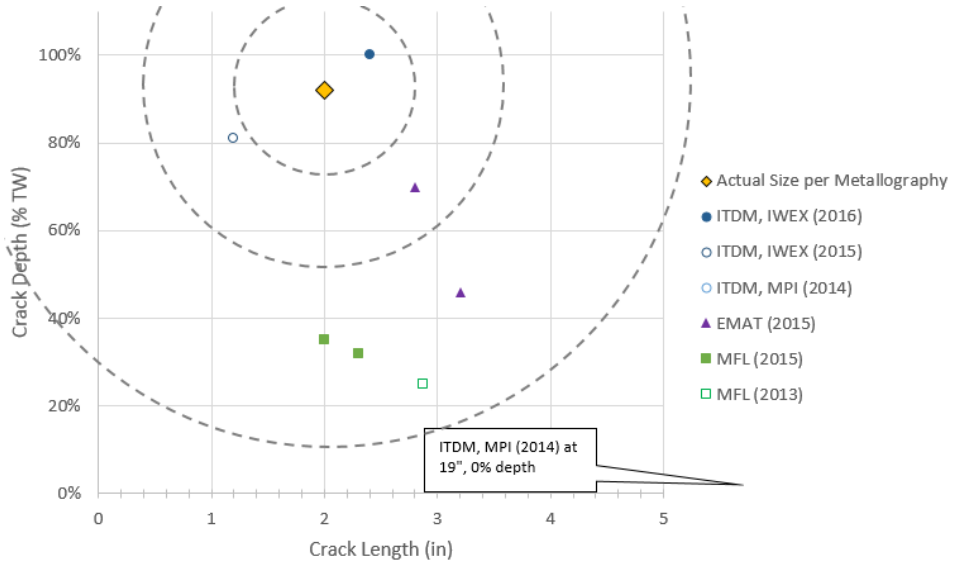

Figure 26: Various NDE Sizing of Feature #2 over the Years

Conclusions and Recommendations

Locating sizable seam cracks pulled from field LF-ERW pipe for R&D proved to be a challenge, but after several years of collecting pipe, nearly 90 seam cracks deeper than 25% NWT were acquired. They represent a broad spectrum of crack geometries including cold welds, hook cracks, stress corrosion cracking, and laminations. The largest number of the flaws existed in 16-inch nominal diameter pipe and those that were the most severe flaws were installed into a 300ft long simulated pipeline for multiple ILI assessments. A total of five different ITDM technologies and two different ILI technologies were employed. ITDM were supplied by ApplusRTD and JENTEK, which included MPI with shear wave sizing, PAUT, TOFD, MWM Array, and Full Matrix Capture Ultrasonic Imaging. ILI technologies were supplied by ROSEN and TDW and included EMAT and MFL with flux lines that cross the seam weld. FMC technology was supplied by ApplusRTD with IWEX.

Among all the ITDM technologies tested, the primary focus was on IWEX, a Full Matrix Capture method. In most cases MPI, PAUT, TOFD, and IWEX sizing were reported together by the NDE service provider. That is, *one* crack size and location were reported despite using multiple NDE techniques. IWEX sizing was considered the most accurate and thereby was depended on for any ITDM discrepancies as deemed by the service provider. This aligned with the task's objective to quickly characterize hundreds

of cracks within the best of NDE ability before down-selecting cracks for ILI and destructive characterization. A limitation of this approach, however, is that it is vastly not possible to assess the individual inspection performance of MPI with shear wave sizing, PAUT, or TOFD. Overall, this did not dampen the ability to understand the current state of leading ILI and ITDM designed for crack-like anomalies.

Nineteen cracks were identified as ILI validation candidates and underwent metallography and fractography for confirmation of actual crack size and type. Although this anomaly subset is not large enough for statistically derived conclusions, valuable trends and observations can be drawn. They are as follows for each inspection technique:

Electromagnetic Acoustic Transducer (EMAT) Inline Inspection (ILI) for Longitudinal Seam Cracks

- EMAT technologies performed to their reported crack detection specification[***] even with challenging seam flaws in uneven trim and/or connected to underlying laminations. This specification was met despite each tool missing one crack, which not only existed in uneven trim but also hovered just above the service provider's minimum size threshold.
- In general, seam crack-like anomalies tend to be called slightly longer and shallower than reality by EMAT. 17 of 21 EMAT calls were overstated +0.4" to +4.7". The remaining four seam calls were undersized in length:
    - Anomaly #9: an EMAT reported no crack while actual length 2.6 inches
    - Anomaly #10: an EMAT reported 1.7 inches while actually 1.8 inches long
    - Anomaly #15: an EMAT reported 1.7 inches while actually 3.7 inches long
    - Anomaly #15: a different EMAT tool reported 3.4 inches length while the feature was actually 3.7 inches long
- EMAT depth calls were found to be typically within +/- 25% if the seam crack was detected *and* shallower than 70% NWT. Near through wall features (90%+ NWT)

[***] Depending on the EMAT tool, the minimum crack length for 90% POD confidence varied from 1-inch to 1.97-inches. Minimum depth varied from 0.04-inch to 20% of wall thickness.

were typically sized 15 to 40% shallower than reality. However, in these scenarios crack depths 50% or deeper were still reported by EMAT for these severe cracks.

- EMAT depth call accuracy appeared independent of crack length as features became longer. Note that all cracks in this study were shorter than 6 inches.
- EMAT length call accuracy generally increased as features became deeper and approached through-wall.
- As for identifying a seam crack's precise location (i.e. denoting if a crack is in a ERW weld bondline, HAZ, or body), gathering that particular insight from ILI is not developed at this time. Current EMAT ILI resolution restricts this specific identification ability, with limited sensor size and frequency being the major driving factor.
- If complex trim (e.g. irregular, uneven, cut-ins) or ID/OD seam alignment is present or suspect, it is recommended to closely work with the ILI provider(s) as they may have prior, similar case studies as the pipeline in question to provide adjusted POD and sizing tolerances.

Magnetic Flux Leakage (MFL) Inline Inspection (ILI) for Longitudinal Seam Cracks

- While it is generally accepted that MFL technology is not well suited for detection and sizing of all cracks types, MFL still has a suitable role in crack inspection; when paired with EMAT, it commonly is used as a screening tool for identifying the long seam and pipe fabrication processes and also aides in discriminating crack-like anomalies from seam variations such as excess trim. MFL can also be used independently for "crack-like" anomalies that are sufficiently open and have a metal loss volume, which is not uncommon for certain hook cracks, for example. Transverse MFL is meant for long, narrow, axially oriented metal loss or these crack-like anomalies with volume.
- In general, MFL undersized the long-seam anomalies in this study. In the case of near-through wall cracks, MFL severely undersized them, reporting 30% NWT depths when in reality they exist at 90%+. Therefore, additional conservatism may be required for dig criteria and fatigue analysis when using this method.

- As for identifying a seam crack's precise location (in bondline, HAZ, or body), gathering that particular insight from ILI is not developed at this time. Current EMAT ILI resolution restricts this specific identification ability, with limited sensor size and frequency being the major driving factor.

Magnetic Particle Inspection (MPI) and Ultrasonic (UT) In-the-Ditch Methods for Longitudinal Seam Cracks

- Investigation revealed that MPI and UT shear wave can be unreliable, as it twice falsely reported near-through-wall features where no crack existed. Trim tool markings and human error are suspected source of error in these incidents.
- It is strongly recommended that MPI and shear wave UT approach not be used alone to locate and then size significant longitudinal seam cracks. That is, if shear wave reports near through-wall features, it may be advisable to verify with another technology in the event that the call is a false positive similar to those witnessed here.
- It is recommended to take caution when sizing seam anomalies with complex alignment (e.g. uneven trim or flash, ID/OD misalignment) only with single beam shear wave. This was the reported cause of error on a critical false positive (i.e. a crack was reported as nearly through wall deep reported but later deemed non-existent in reality) observed in this limited subset of cracks.

Full Matrix Capture (FMC) as Represented by IWEX for Longitudinal Seam Cracks

- Investigation of full matrix capture inspection performance versus actual fracture sizes of anomalies showed encouraging improvements from the two generations employed under this study. The 2016 version tested correctly identified the majority of crack and lamination geometries (e.g. denoting cold weld versus hook crack versus lamination). This was the best defect characterization of tools employed in this study. Although minor, those misinterpreted geometries were falsely calling hook cracks and stringers as cold welds.

- As for anomaly sizing, full matrix capture was the most accurate of technologies employed. It sized 14 of the 16 simple flaws (i.e., not overlapped with a lamination) lengths within +/- 0.5". However, the remaining two were fairly large outliers as they were under sized by an average of 1.7inches in length. Of these outliers one was a stringer (#13) and the other a hook crack (#15). With respect to depth sizing, 13 of 16 simple flaws were sized within +/-16%. The remaining three flaws were oversized in depth by approximately 30% to 55% and were either stringers or hook cracks. Even with these outliers, the overall sizing accuracy was viewed as generally reliable.
- Full Matrix Capture (i.e. IWEX) *depth* call accuracy increased as anomalies' became longer and approached 4 inches long.
- Full Matrix Capture (i.e. IWEX) *length* calls tended to be undersized for features approximately 50% through-wall or shallower. The opposite trend was observed for deeper anomalies where FMC tended to overstate length.
- Full Matrix Capture (i.e. IWEX) can characterize crack type, which could then be used to infer most likely crack location. That is, a true cold weld will be located along the bondline. Hook cracks are generally contained in the HAZ, although they can extend to the bondline and pipe body. How far they extend into the pipe body depends on the extent of the inclusion or lamination that curved up to form the hook crack.

Hydrostatic Tests for Model Validation of Longitudinal Seam Cracks

- The two deepest cracks collected (#1 and #2) were hydrostatically tested to failure. Their re-sealing behavior upon de-pressurization and subsequent metallography indicated that post-weld repairs were completed at these cold welds and executed without post-weld heat treatment. This poor longitudinal weld seam repair likely introduced weld residual stresses. Therefore, these experimental burst tests are not appropriate validation cases for PipeAssess PI™ and other failure pressure prediction models which do not consider weld residual stresses.

While results of each inspection method are compared herein, it is reasonable to expect ITDM to be capable of higher accuracy and precision than ILI. ILI is optimal for inspecting extended distances first and locating discrete sites for further, pinpointed evaluation via ITDM afterwards. ITDM and ILI are complementary inspection techniques in this manner.

Overall, ITDM and ILI technologies are evolving and maturing. For ITDM, IWEX exemplified considerable improvements with the two generations tested one year apart within this program. For ILI, considerable improvements were observed with the addition of EMAT tools for crack detection in pipe with diameters 16 inches and less as compared to MFL and liquid coupled UT ILI being the only tools available at the beginning of this program. Technology improvements are evident by comparing multiple generations of ILI on the same crack (see Figure 22 and Figure 26) and also through ILI assessment reports over time. For instance, the 2013 Kiefner ILI track record report [11] showed that while these tools can find anomalies, some will be missed and sizing is not particularly accurate. Therefore, the probability of finding the few crack-like anomalies that would fail a hydrotest in an operating pipeline was low with 2013 ILI systems. This is becoming different with today's technologies. Now, with commercial EMAT ILI tools available and field-experience growing, operators are beginning to have the ability to identify cracks that could potentially fail a hydrotest. EMAT technology can also detect smaller anomalies that would go undetected in a hydrotest and the sizing capability appears to be sufficient to dismiss these smaller anomalies from further investigation.

Appendix

A. NPS 16 Metallographic Examination Results of Seam Weld Anomalies

B. Material Testing Results of Phase II Pipe

Works Cited

[1] B. N. Leis, B. A. Young and e. al., "Final Summary Report and Recommendations for the Comprehensive Study to Understand Longitudinal ERW Seam Failures -- Phase One," < http://primis.phmsa.dot.gov/matrix/FilGet.rdm?fil=8501&s=EC16005513FE40EE867254CFB69090FD&c=1 >, DTPH56-11-T-000003, 2013.

[2] B. Leis, "Subtask 4.2: Time-Trending and Like-Similar Analysis for ERW-Seam Failures," < http://primis.phmsa.dot.gov/matrix/FilGet.rdm?fil=8421&s=EC16005513FE40EE867254CFB69090FD&c=1 >, DPH56-11-T-000003, 2013.

[3] ApplusRTD, "Long Seam Assessment On RFQ-15092 with IWEX: NDT ILI Verifications for Battelle," 2015.

[4] C. Holmes, B. W. Drinkwater and P. D. Wilcox, "The post-processing of ultrasonic aray data using the Total Focusing Method," *Insight 46(11)*, pp. 677-680, 2005.

[5] N. Pörtzgen, D. Gisolf and G. Blaquière , "Inverse Wave Field Extrapolation: a different NDI approach to imaging defects," *IEEE Transactions on Ultrasonics, Ferroelectrics, and Frequency Control 54(1)*, pp. 118-127.

[6] H. H. Haines, L. Hörchens and P. Tomar, "IPC2016-64069: Identifying and Sizing Axial Seam Weld Flaws in ERW Pipe Seams and SCC in the Pipe Body Using Ultrasonic Imaging," Proceedings of the 2016 11th International Pipeline Conference, (to be published October 2016).

[7] RTD Quality Services USA, L.P., "In-Ditch Validation Methodology for Determination of Defect Sizing," < https://primis.phmsa.dot.gov/matrix/PrjHome.rdm?prj=503 >, DTPH56-13-T-000008, 2013.

[8] B. A. Young, S. Nanney, B. Leis and J. M. Smith, "IPC2014-33226: Overview of a Comprehensive Study to Understand Longitudinal ERW Seam Failures," International Pipeline Conference, 2014.

[9] Iowa State University, "Advanced Nondestructive Characterization of Pipeline Materials," < http://primis.phmsa.dot.gov/matrix/prjHome.rdm?prj=511 >, DTPH56-13-H-CAAP07, 2015.

[10] R. B. Stonesifer, F. W. Brust and B. N. Leis, "Stress-Intensity Factors for Long Axial Outer Surface Cracks in Large R/t Pipes," Fracture Mechanics: Twenty-Second Symposium (Volume II), American Society for Testing and Materials (ASTM) STP 1131, Philadelphia, 1992.

[11] J. F. Kiefner, K. M. Kolovich and et. al., "Subtask 1.3: Track Record of In-Line Inspection as a Means of ERW Seam Integrity Assessment"," < http://primis.phmsa.dot.gov/matrix/PrjHome.rdm?prj=390 >, DTPH56-11-T-000003L, 2013.

Appendix A

0533-1302 Final Battelle NPS 16Metallographic Examination Results

Battelle

Final Report No. 16-161

NPS 16 Metallographic Examination Results of Seam Weld Anomalies

Pushpendra Tomar & Bruce Nestleroth

October 18, 2016

Kiefner

0533-1302

Intentionally blank

Final Report No. 16-161

Final Report

on

NPS 16 METALLOGRAPHIC EXAMINATION RESULTS OF SEAM WELD ANOMALIES

to

BATTELLE

October 18, 2016

Prepared by

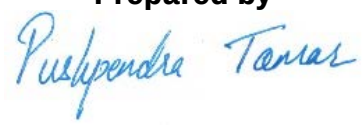

_____

Pushpendra Tomar
Engineer II

Approved by

_____

Dyke Hicks
Senior Principal Engineer

Kiefner and Associates, Inc.
4480 Bridgeway Avenue, Suite D
Columbus, OH 43219

0533-1302

DISCLAIMER

This document presents findings and/or recommendations based on engineering services performed by employees of Kiefner and Associates, Inc. The work addressed herein has been performed according to the authors' knowledge, information, and belief in accordance with commonly accepted procedures consistent with applicable standards of practice, and is not a guaranty or warranty, either expressed or implied.

The analysis and conclusions provided in this report are for the sole use and benefit of the Client. No information or representations contained herein are for the use or benefit of any party other than the party contracting with Kiefner. The scope of use of the information presented herein is limited to the facts as presented and examined, as outlined within the body of this document. No additional representations are made as to matters not specifically addressed within this report. Any additional facts or circumstances in existence but not described or considered within this report may change the analysis, outcomes and representations made in this report.

TABLE OF CONTENTS

LIST OF FIGURES

LIST OF TABLES

NPS 16 Metallographic Examination Results of Seam Weld Anomalies

Pushpendra Tomar and Bruce Nestleroth

SUMMARY

Kiefner performed metallographic and fractographic examinations on five NPS 16 pipe samples as part of the DOT PHMSA's Comprehensive Study to Understand Longitudinal ERW Seam Failures. In 2015, Battelle performed a series of in-line inspection (ILI) pull tests at their facility in West Jefferson, Ohio. The pipe samples were for Keifners test were extracted from testing in Battelle's ILI pull rig (see Figure 1) and pull tests were conduct with tools from two ILI vendors. Both ILI vendors reported detected anomalies on the five pipe samples to Battelle. Anomalies reported in the seam weld area and adjacent to seam weld area were of interest for this study.

The goal was to provide detailed examples of anomalies that the ILI and in the ditch methods had detected. Nearly one hundred images are presented for 17 anomaly locations.

BACKGROUND

Commercial ILI tools and external inspection methods were used to precisely locate anomalies for fracture analysis. The ILI tools included electromagnetic acoustic transducer (EMAT) and magnetic flux leakage (MFL) tools. Ultrasonic (UT) imaging using inverse wave field extrapolation (IWEX) was used in external inspection. IWEX is an emerging NDE technique that is being applied to improve discrimination and sizing of anomalies in pipelines. IWEX finds its origin in the application field of seismic exploration, where acoustic wave fields are used to reconstruct structures and layers in the subsurface. With the introduction of ultrasonic array technology, the principles to reconstruct images from measured wave fields became useful for other applications such as girth weld inspection. A goal of IWEX imaging is to produce images capable of detecting, discriminating, and sizing crack-like features such as cold welds, surface breaking hook cracks, and fatigue cracks and discriminate these from non-surface breaking upturned fiber indications, poor trim, offset plate edges, laminations and inclusions. In mapping these anomalies the sizing needs to be sufficiently accurate to qualify in-line inspection tools used for crack inspection.

After pull testing, these pipe samples were removed from the pull rig and sent to Kiefner's facility in Columbus, Ohio for nondestructive testing and fracture analysis. Anomalies reported

in multiple ILI runs along with the results of nondestructive examinations were used to select locations for metallographic examinations. Seventeen locations on the five pipe samples were selected for metallographic examination. Results and findings from the metallographic examination of these 17 locations are presented in this report.

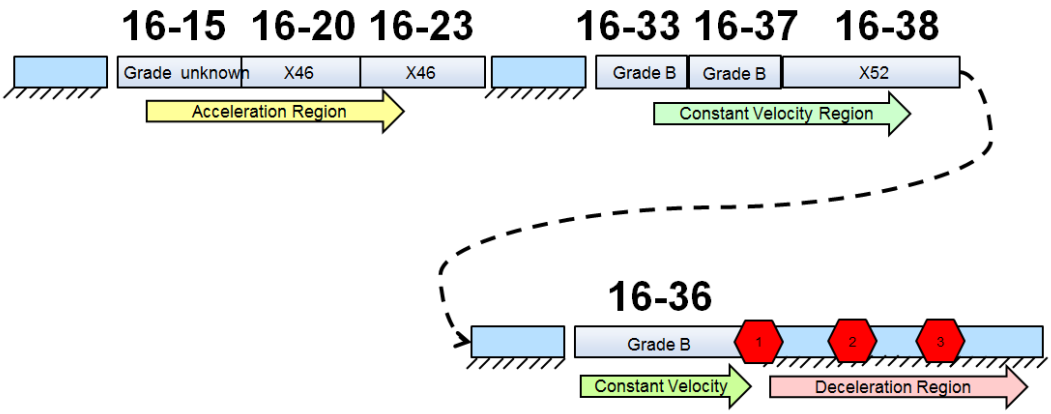

Figure 1. NPS 16 pipe rig layout, (Sketch provided by Battelle)

The pipe joint identification, pipe grade and wall thickness, both nominal and actual, of the five pipe samples selected for the study are provided in Table 1.

Table 1. Pipe Sample Details

Joint #	Pipe Grade	Nominal Wall Thickness	Actual Wall Thickness
16-20	X46	0.340	0.323
16-33	Grade B	0.250	0.268
16-37	Grade B	0.250	0.274
16-38	X52	0.250	0.252
16-36	Grade B	0.250	0.268

SELECTION OF SWA LOCATIONS FOR METALLOGRAPHIC EXAMINATION

Seam weld anomalies (SWA) reported by two ILI vendors and IWEX were correlated to select locations for metallographic examination. SWAs/locations were selected based on one or more of the following criteria:

- Depth of SWA: ILI/IWEX reported depth of 20% NWT or above
- Length of SWA: ILI/IWEX reported length of 1.0 inch or above

- Location of SWA: External/Internal, both were selected

Effort was also made to select SWA from every pipe sample to evaluate performance with varying seam geometry. Seventeen pipe locations were selected for metallographic evaluation. Table 2 presents details of the selected locations. Axial location in Table 2 represents location from the start of the ILI Pull Rig.

Table 2. Selected SWA Locations for Metallographic Examination

SWA #	Axial Location*	Joint #	Cut out Start (ft.)	Cut out End (ft.)
1	155.48	16-37	155.1	156.1
2	125.29	16-33	125	123
3	224.57	16-36	224.25	225.2
4	223.1	16-36	223.05	223.9
5	49.1	16-20	48.9	50
	49.19			
	49.36			
6	37.47	16-20	37	38
	37.6			
7	222.7	16-36	222.25	223.05
	222.83			
8	164.01	16-38	163.9	166
9	173.13	16-38	172.9	174
10	185.68	16-38	185	186.5
	185.98			
	186.22			
11	221.49	16-36	221	223
12	170.02	16-38	169.75	171
	170.2			
13	187.95	16-38	186.9	189
14	167.1	16-38	166	168
15	182.81	16-38	181.9	183.5
	182.96			
16	225.55	16-36	225.25	227
17	168.25	16-38	168.2	169

* Axial location in Table 2 represents axial location with reference to the start of the ILI Pull Rig

Metallographic Examination: Selected locations from ILI-IWEX correlation were evaluated using metallographic examination. The following steps were involved in the Metallurgical Examination of Anomalies:

Visual Inspection and Documentation

This examination involved documentation of the physical appearance of the samples and any significant features. The external and internal surfaces of the pipe were examined for evidence of the presence of a longitudinal seam. Measurements were made of the sample dimensions, including wall thickness and significant features. Digital pictures were taken for documentation of all samples.

Non-destructive Examination (MT)

Magnetic Test (MT) is a non-destructive test method for the detection of surface and near-surface discontinuities in ferrous materials. This examination helped in the detection of any surface or near surface discontinuities in the seam area of the pipe samples.

Fractography

Anomalies that appeared to be relatively deep planar flaws, such as hook cracks, upturned fiber imperfections, or cold welds in ERW seams were examined as follows. A coupon of material containing the flaw was cut out, chilled in liquid nitrogen to promote brittle behavior, and broken open to expose the flaw surfaces. The flaw surfaces were visually examined and cleaned as necessary to allow for optical examination at magnifications up to 10X. Examination results were documented with digital photographs.

Anomalies that did not appear to break in the flaw detected by NDE analysis were examined by metallographic sectioning as described next under metallography.

Metallography

Metallographic cross sections through anomalies were prepared and examined. The section was cut out, mounted in a resin, polished, and etched with a 3% nital solution. The samples were examined on a metallographic microscope at magnifications of 12.5X and 25X.

The Discussion Section contains detailed pictures of Metallographic Examination results.

Comparison - Metallographic Examination, ILI and IWEX: Results of the metallographic examination were compared with correlated features from ILI and IWEX reported anomalies. Table 3, “Metallographic Examination Results,” presents the results of the comparison between metallographic examination, IWEX, and ILI calls.

Seam Weld Anomalies on Pipe ID 16-36

Multiple anomalies were reported on Pipe ID 16-36 by both ILI vendors and IWEX. Five SWA (3, 4, 7, 11, 16 and 18) from Pipe 16-36 were selected after the correlation for metallographic examination. Details for these anomalies are given in Table 2.

An individual metallographic examination was performed on SWA (3, 4, 7, 11, 16 and 18) and it was discovered that these anomalies are interconnected by a lamination and therefore should be considered as one anomaly. The anomaly details along with details of ILI and IWEX reported anomalies on 16-36 are presented in Figure 2. This figure illustrates the metallographic results (top graph), the in the ditch sizing results (middle graph) and the results of the two ILI vendors in the bottom graph. It should be noted that the ILI methods detect the presence of a crack and provide a depth but cannot define whether the crack is connected to the ID, OD or midwall. The anomaly starts at 221.54 feet and ends at 227.05 feet. Multiple metallographic sections were taken along with fractography to characterize this anomaly. Metallographic sections of this anomaly show one continuous lamination anomaly that turns into surface breaking hook crack at three instances between 222.73 ft. to 223.20ft, 224.54 ft. to 224.85 ft. and 225.55 ft to 226.17 ft.

It is unclear what may have caused this anomaly but there are two possible scenarios:

1. This pipe could have been manufactured by slit skelp. The ingot solidifies from the outside surface inward, and therefore impurities are pushed towards the center of the ingot where they become trapped during solidification. During hot rolling, the impurities are compressed and elongated, sometimes becoming laminations in the center of the hot rolled plate or coil. Slitting the plate or coil will move the edge of the coil to a mid-width position closer to the interior of the plate or coil. During pipe manufacturing these edges are brought together at the ERW seam weld.

2. The edge of the plate used for making ERW welds may have a lamination on the fusion face and some areas were closer to the edge than others. That explains why the anomaly is surface breaking in certain regions and non-surface breaking for the rest of the length.

Table 3. Metallographic Examination Results

Anomaly #	Axial Location	Joint #	Length (Inch)				Depth (% Wall Thickness***)					Anomaly Type
			IWEX	ILI Y Avg.	ILI Z Avg.	Fracture Surface	IWEX (inches)	IWEX	ILI Y Avg.	ILI Z Avg.	Fracture Surface	
1	155.48	16-37	2.8	3.4	3.4	3.0	0.252	92	84	62	**99**	CW
2	125.29	16-33	2.5	2.8	3.2	2.0	0.268	100	70	46	**92**	CW
3*	224.57	16-36	3.1	2.6	12.8	3.8	0.252	94	46	17	**60**	HC (due to Lamination)[2]
4*	223.1	16-36	0.6	SWA# 4 and #7 were reported as one by ILI		1.2	0.181	68			**63**	HC (due to Lamination)[2]
5	49.1	16-20	1.4	1.9	< Spec;	1.0	0.181	56	50	< Spec;	**68**	CW
											44	CW
	49.36		0.1			0.2	0.051	16			**12**	CW
6	37.47	16-20	0.2	1.7	< Spec;	0.3	0.157	49	38	< Spec;	**50**	CW
	37.6		0.1			0.1	0.102	32			**31**	CW
7*	222.7	16-36	5.4	4.5	22.4	5.7	0.197	74	38	27	**63**	HC (due to Lamination)[2]
8	164.01	16-38	2.6	2.1	2.5	1.7	0.114	45	32	39	**56**	HC
9	173.13	16-38	2.7	3.1	N/A	2.6	0.201	80	32	N/C	**34**	HC
10	185.68	16-38	1.3	1.7	4.0	1.1	0.114	45	38	26	**32**	HC
	185.98		0.4			0.5	0.122	48			**16**	HC
	186.38		1.7			1.8	0.114	45			**44**	HC
11	206.3	16-36	No Calls reported by ILI or IWEX									
12	115.6	16-33	No Calls reported by ILI or IWEX									
13	187.95	16-38	0.1	6.3	5.5	1.6	0.102	40	10	38	**24**	Stringer
14	167.1	16-38	0.3	< Spec;		0.6	0.185	73			**18**	Stringer
15	182.81	16-38	1.9	1.7	3.4	3.7	0.114	45	21	25	**32**	HC
16*	225.55	16-36	6.6	5.1	5.7	7.4	0.252	94	61	27	**75**	HC (due to Lamination)
17	168.25	16-38	1.8	2.5	3.6	1.5	0.110	44	32	35	**52**	HC
18*	221.49	16-36	23.9	Lamination, No ILI calls		56.0	0.000	0			**7**	Lamination
19	170.02	16-38	2.2	3.0	3.9	2.3	0.091	36	32	26	**48**	HC
	170.2		0.4				0.000	0				

* 3, 4, 7, 16 & 18 orginate from one lamination with 3 surface breaking hook cracks

** Further analysis required to determine defect type.

*** Nominal Wall thickness used for ILI data and Actual Wall thickness used for IWEX data and fracture surface

< Spec defined as Length < 1.5inches & Depth <25%

Glossary:

IWEX: Inverse Wave Field Extrapolation

CW: CW

HC: Hook Crack

HC/UFI: Hook Crack OR Upturned Fiber Imperfection

SWA-A: Seam Weld Anomaly-A

SWA-B: Seam Weld Anomaly-B

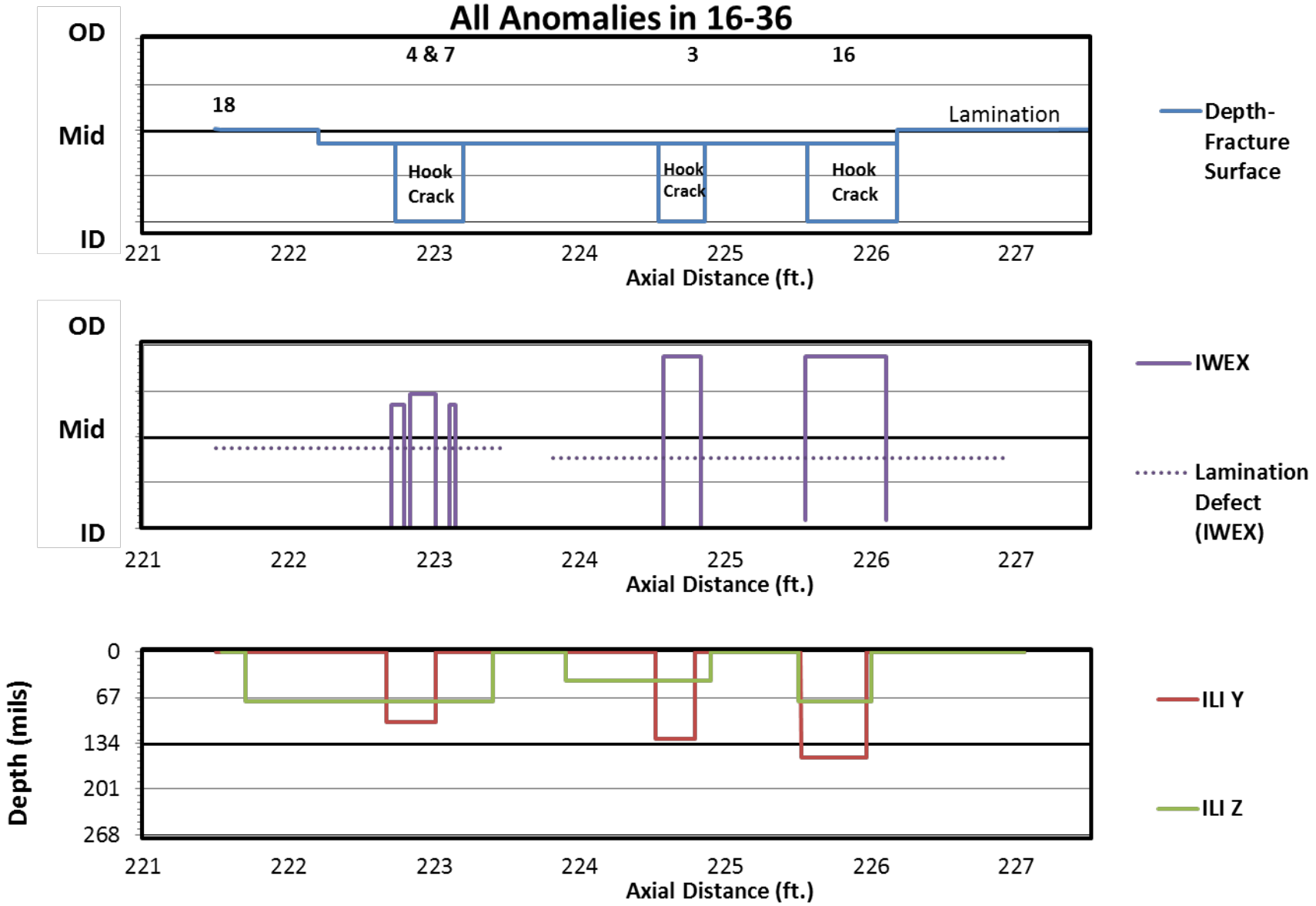

Figure 2. Depth profile and inspection results of all SWA on Pipe #16-36

DISCUSSION

The detailed results of the fractographic and metallographic examination of each seam weld anomaly (SWA) are presented in this section.

SWA #1: SWA #1 was located on Pipe #16-37. Metallographic examination revealed this SWA to be a cold weld. Metallographic cross sections also revealed the presence of a repair weld (possibly a mill repair) in the seam weld area. Figure 3 shows the pipe marked in preparation for the fractographic specimens. Figure 4 though Figure 6 show the metallographic, metallurgical, and fractographic results. The anomaly location details along with details of ILI and IWEX reported anomalies are presented in Figure 7.

Figure 3. Break location marked on SWA #1

Figure 4. SWA #1, Break location and fracture surface

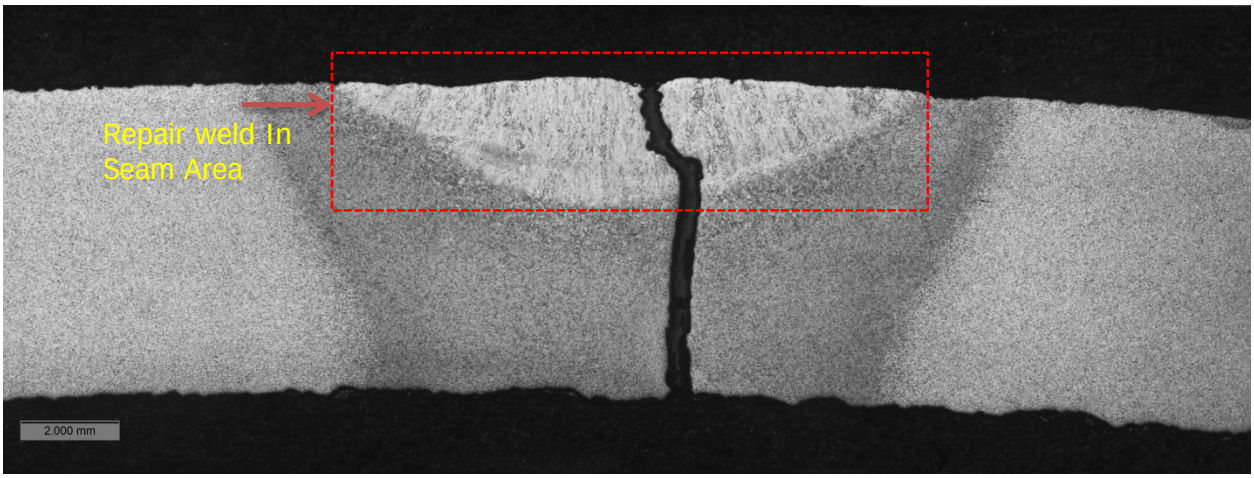

Figure 5. SWA #1, metallographic image 12.5X

Figure 6. SWA #1, metallographic image 25X

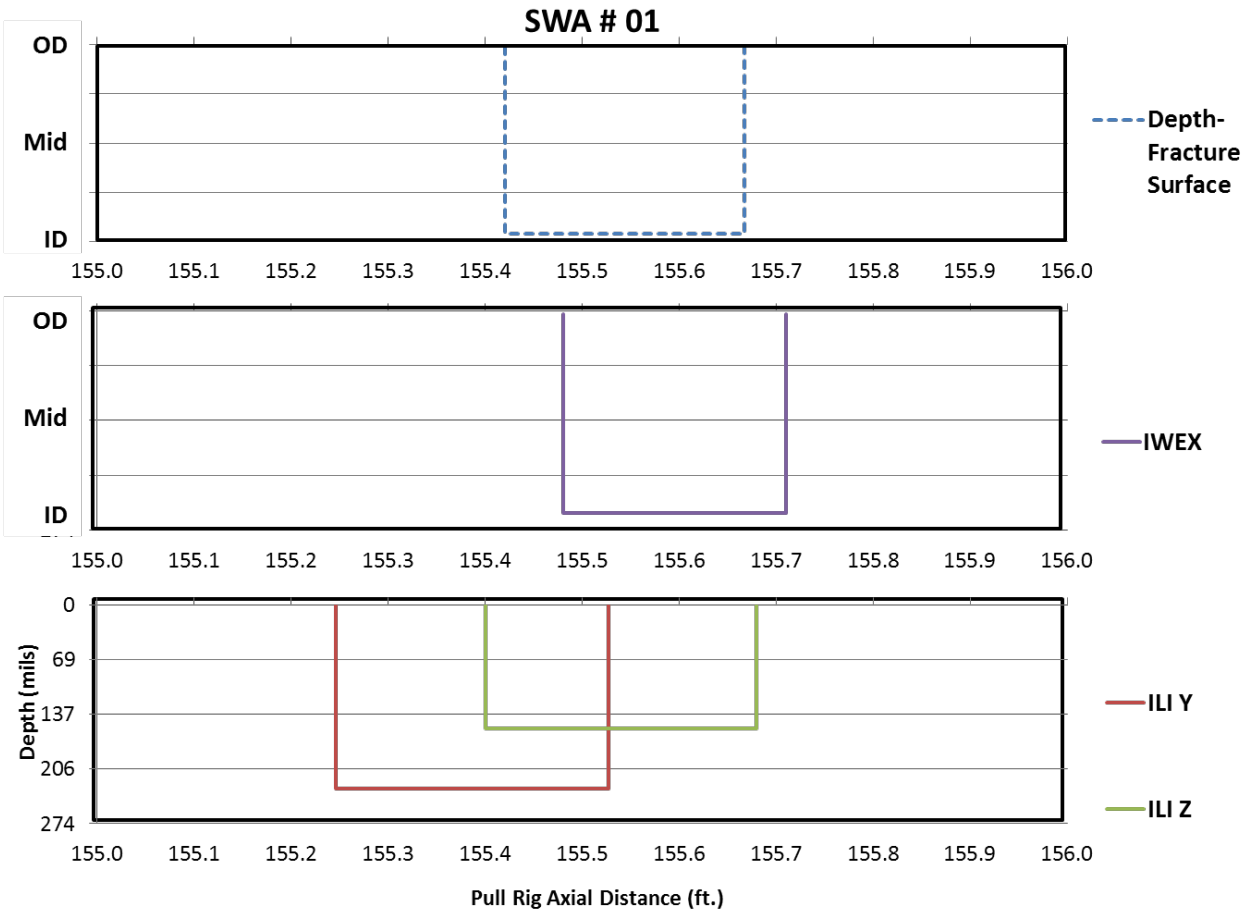

Figure 7. Depth profile and inspection results of SWA #1

SWA #2: SWA #2 was located on Pipe #16-33. Metallographic examination revealed this SWA to be a cold weld. Metallographic cross sections also revealed the presence of a repair weld (possibly a mill repair) in the seam weld area. Figure 8 shows the pipe marked in preparation for the fractography specimens. Figure 9 through Figure 11 show the metallographic, metallurgical, and fractographic results. An ID SWA can be seen in the picture on the right in Figure 9. The anomaly location details along with details of ILI and IWEX reported anomalies are presented in Figure 12.

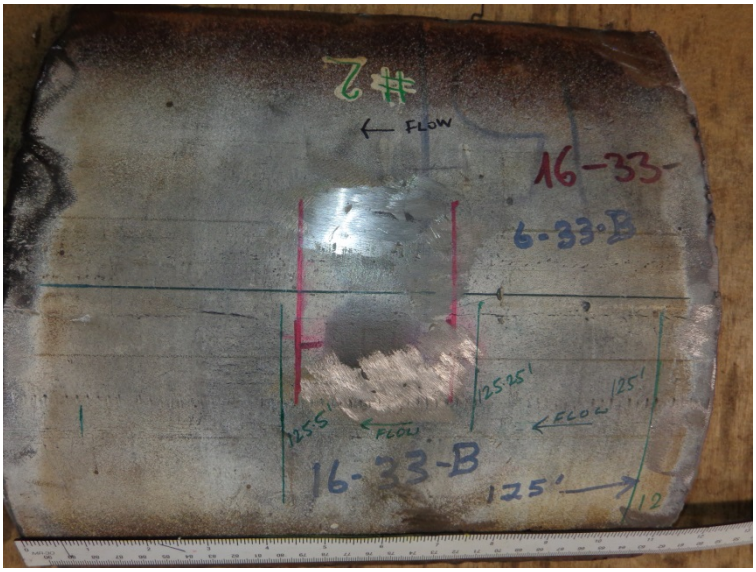

Figure 8. Break location marked on SWA #2.

Figure 9. SWA #1, break location and fracture surface

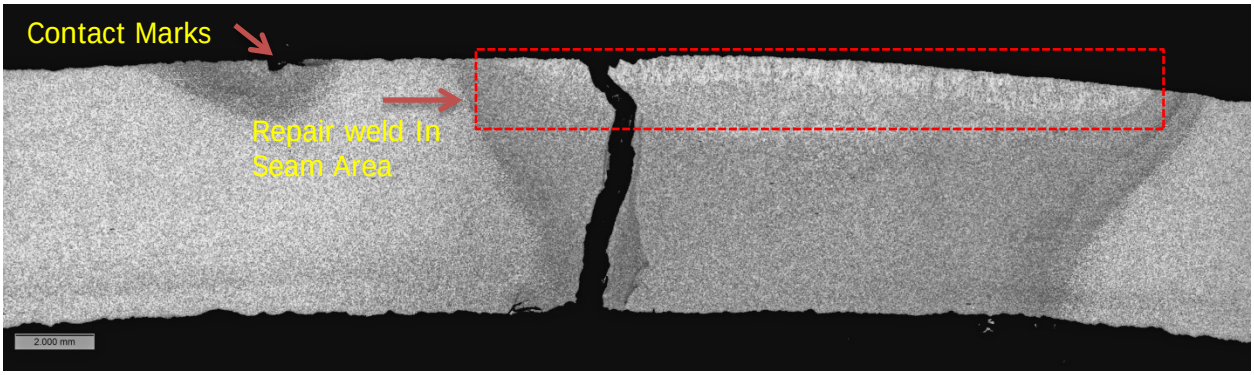

Figure 10. SWA #2, metallographic image 12.5X

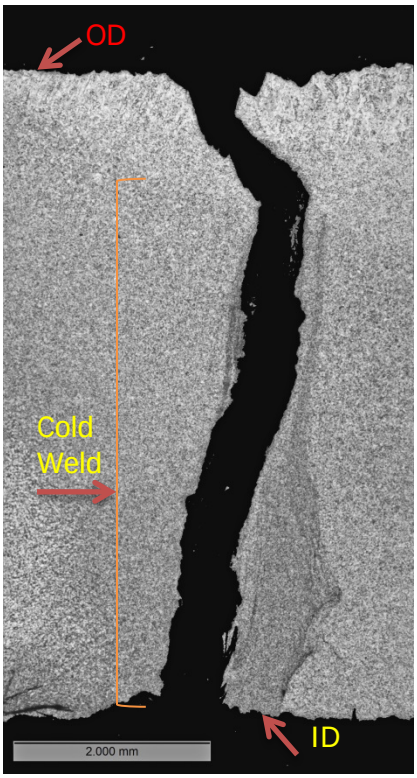

Figure 11. SWA #2, metallographic image 25X

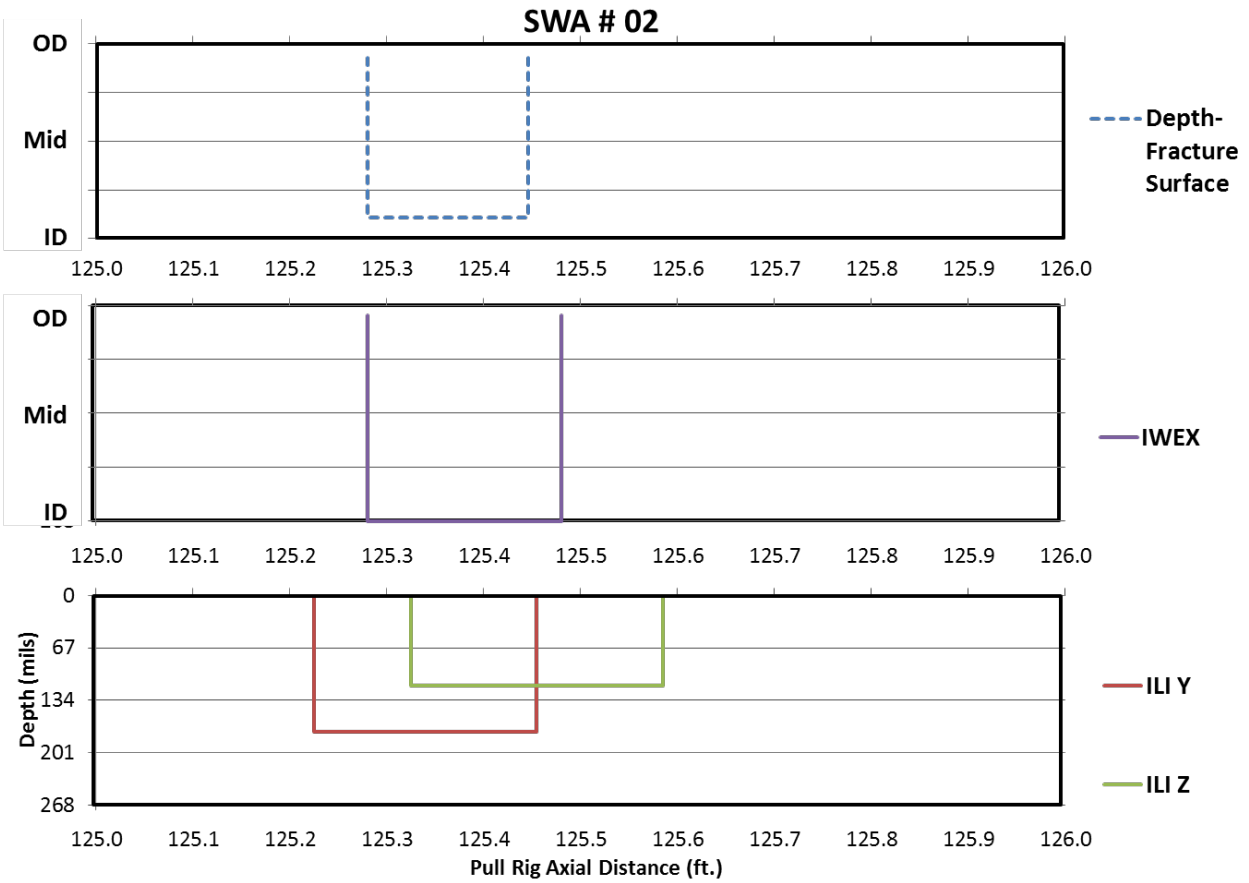

Figure 12. Depth profile and inspection results of SWA #2

SWA #3: SWA #3 was located on Pipe #16-36. Metallographic examination revealed this SWA to be a hook crack. A metallographic cross section also revealed the presence of a near mid-wall lamination feature in SWA #3. The presence of a lamination feature connected to the hook crack suggests that this hook crack was formed due to the lamination feature disturbing the seam in the electric resistance weld (ERW) process. Figure 13 shows the pipe marked in preparation for the fractography specimens. Figure 14 though Figure 16 show the metallographic, metallurgical, and fractographic results. The anomaly location details along with details of ILI and IWEX reported anomalies are presented as the feature in Pipe 16-36.

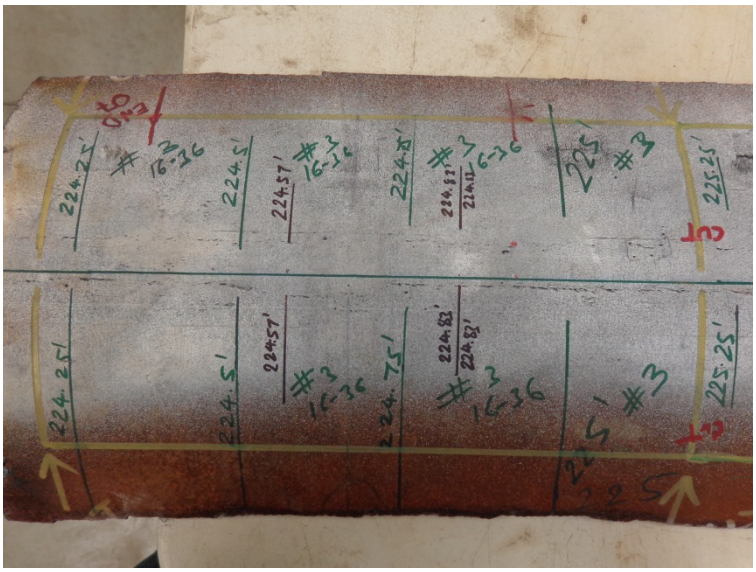

Figure 13. Break location marked on SWA #3

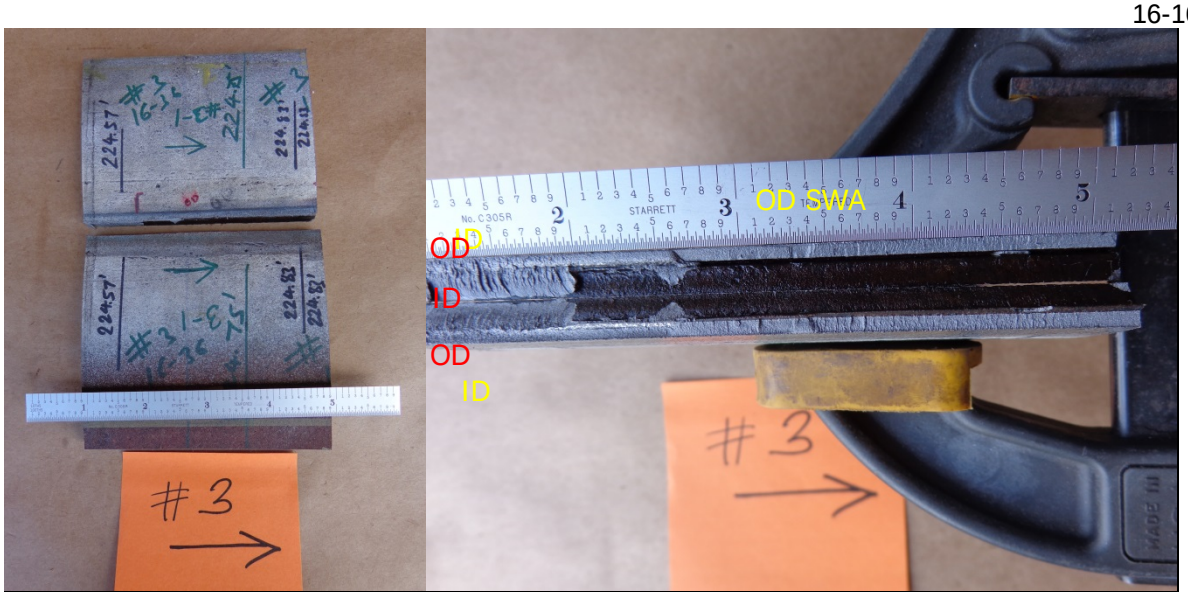

Figure 14. SWA #3, break location and fracture surface

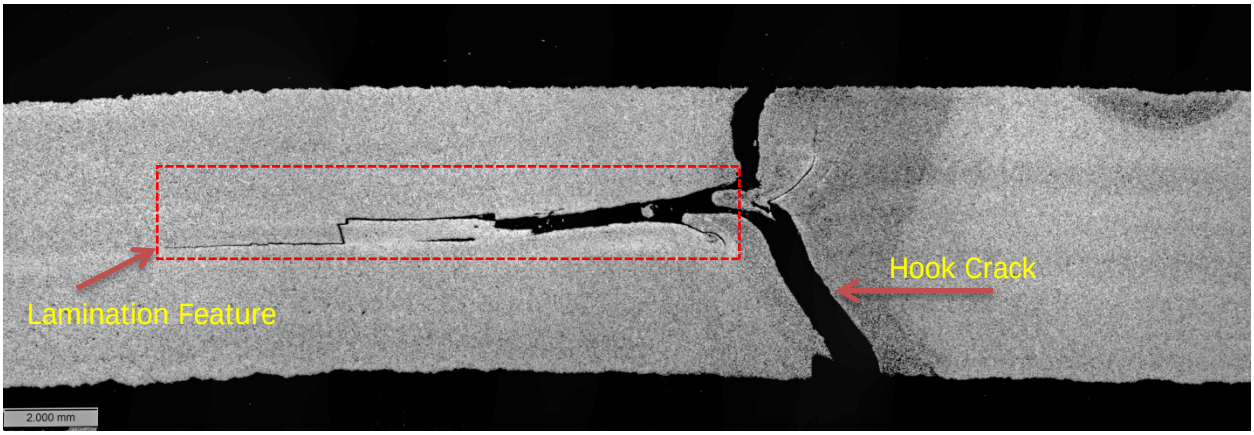

Figure 15. SWA #3, metallographic image 12.5X

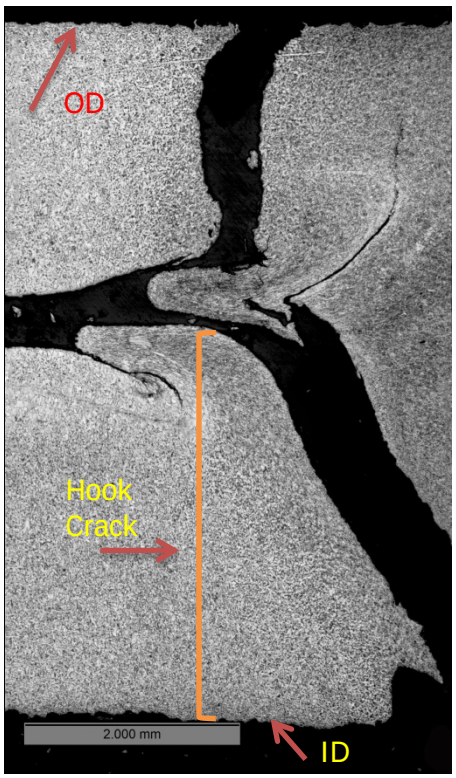

Figure 16. SWA #3, metallographic image 25X

SWA #4: SWA #4 was located on Pipe #16-36. Metallographic examination revealed this SWA to be a hook crack. Similar to SWA#3, the presence of a lamination feature connected to the hook crack suggests that this hook crack was formed due to the lamination feature disturbing the seam in the ERW process. Figure 17 shows the pipe marked in preparation for the fractography specimens and Figure 18 shows the fractographic results. An ID SWA can be seen in the picture on the right side. The anomaly location details along with details of ILI and IWEX reported anomalies are presented as the feature in Pipe 16-36.

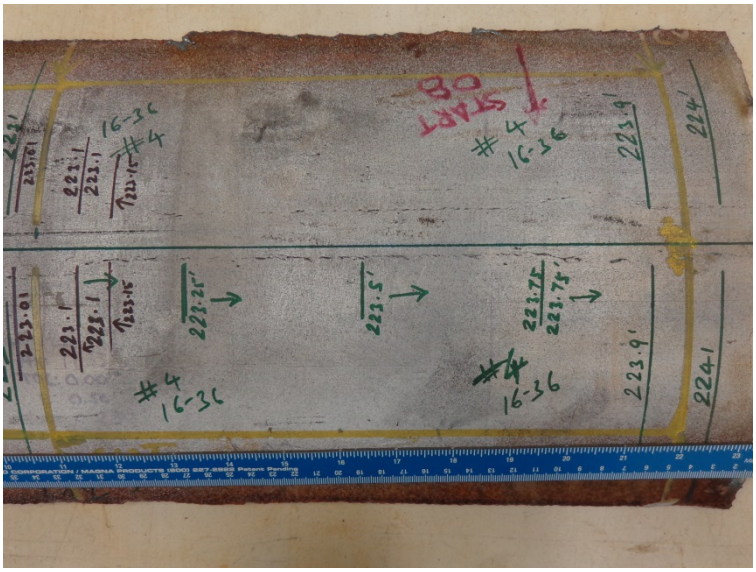

Figure 17. Break location marked on SWA #4

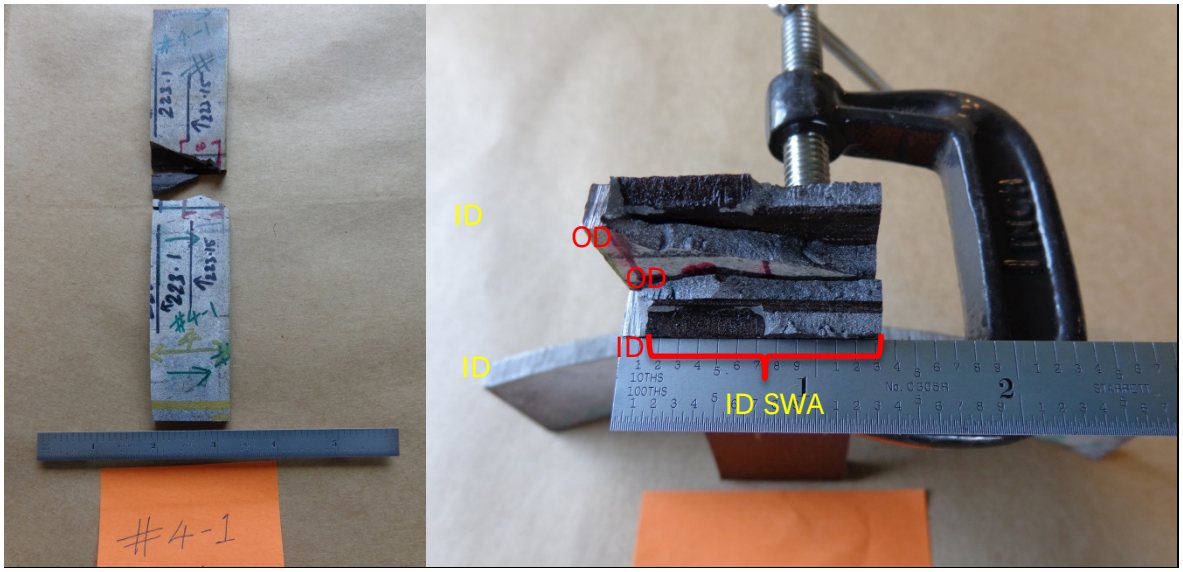

Figure 18. SWA #4, Break location and fracture surface

SWA #5: SWA #5 was located on Pipe #16-20. Metallographic examination revealed this SWA to be a cold weld. Figure 19 shows the pipe marked in preparation for the fractography specimens and Figure 20 through Figure 22 show the fractographic results. An ID SWA can be seen in the picture on the right side. The scanning electron microscope (SEM) images (Figure 23 through Figure 25) of the intact material between the surface breaking feature and non-surface breaking feature on SWA #5-3 showed characteristics of cleavage fracture suggesting the presence of intact material between the features. The anomaly location details along with details of ILI and IWEX reported anomalies are presented in Figure 28. Two OD anomalies were grouped for comparison to the ILI since they were less than an inch apart. However, the combined length of the two anomalies is less than most ILI tool specifications.

Figure 19. Break location marked on SWA #5

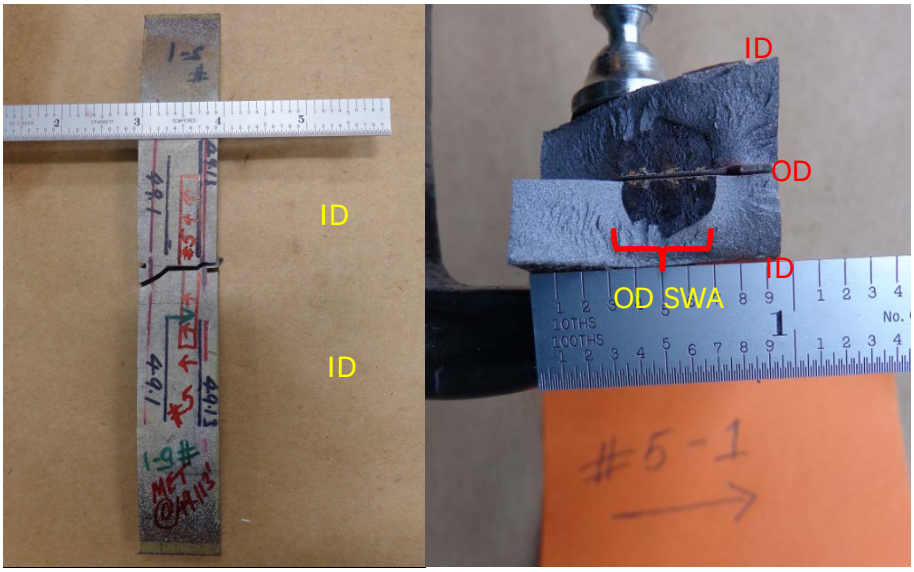

Figure 20. SWA #5-1, break location and fracture surface

Figure 21. SWA #5-2, break location and fracture surface

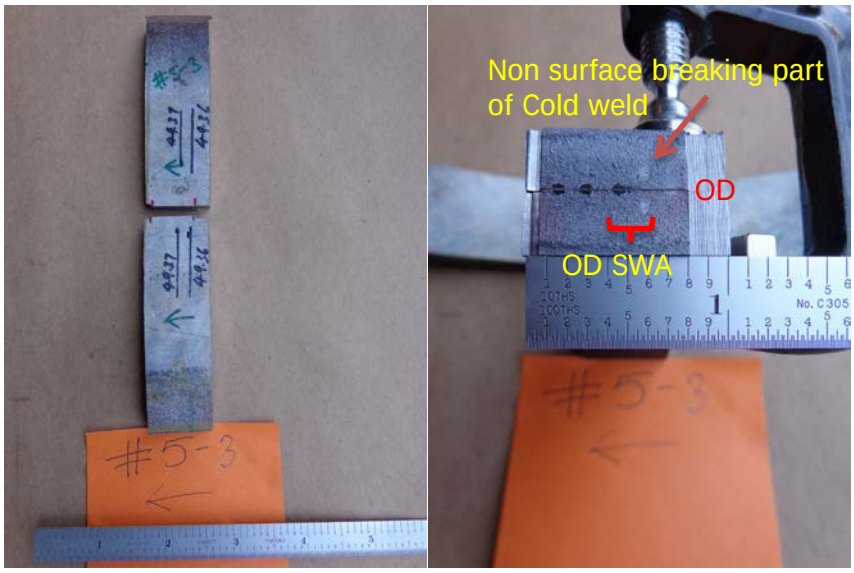

Figure 22. SWA #5-3, break location and fracture surface

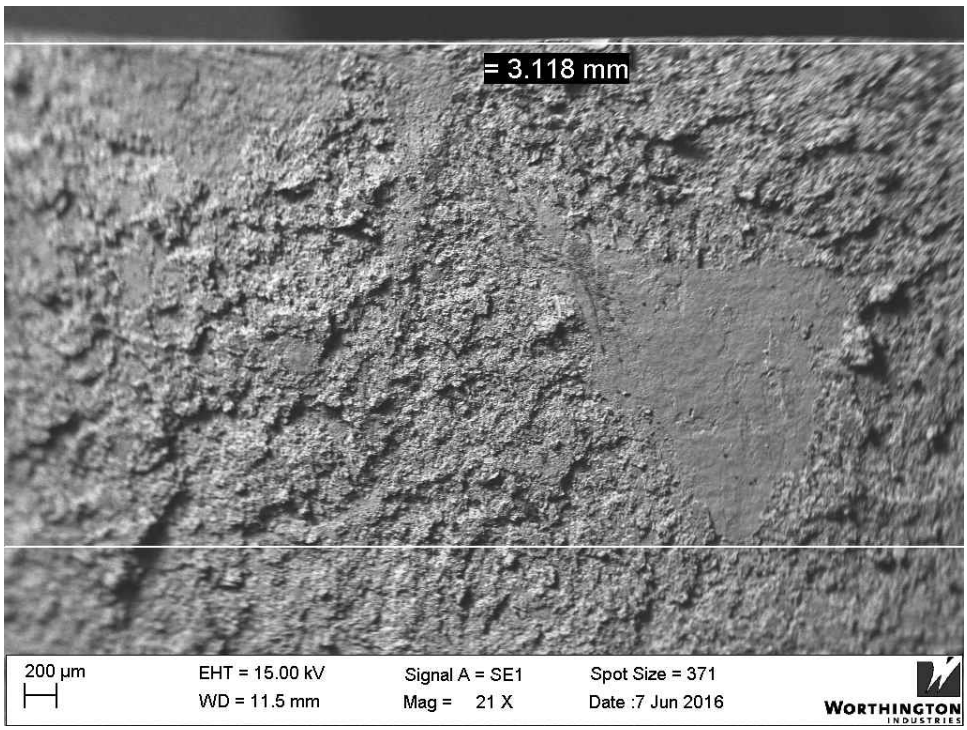

Figure 23. SEM image of non-surface breaking part of cold weld feature; SWA #5-3

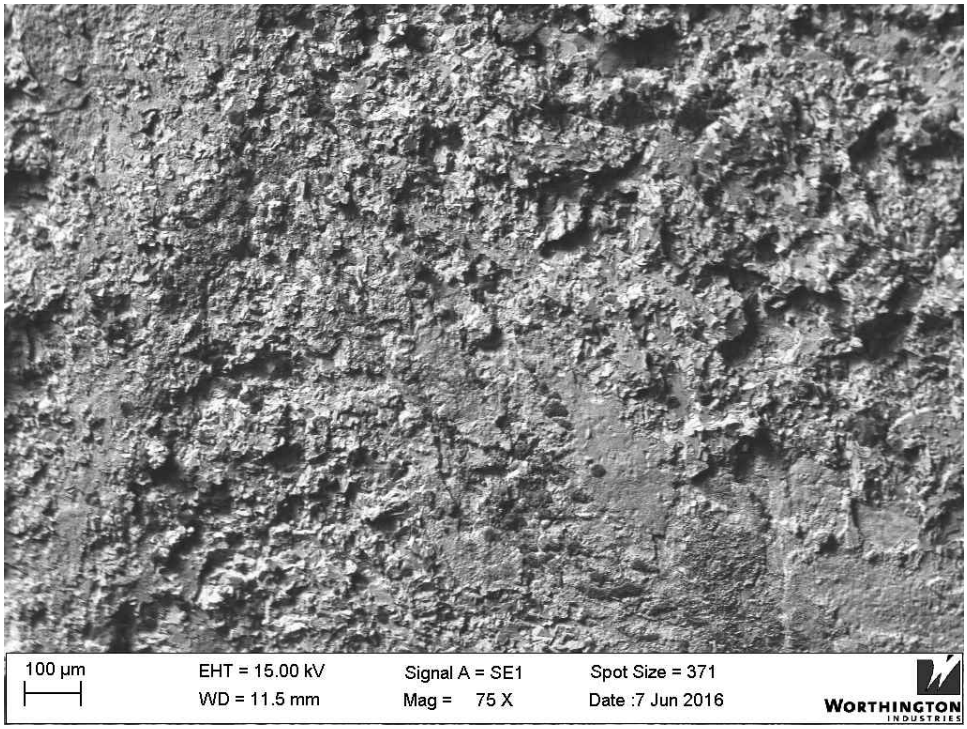

Figure 24. SEM image of intact material between cold weld features; SWA #5-3 to confirm if the surface breaking feature is connected to the non-surface breaking feature.

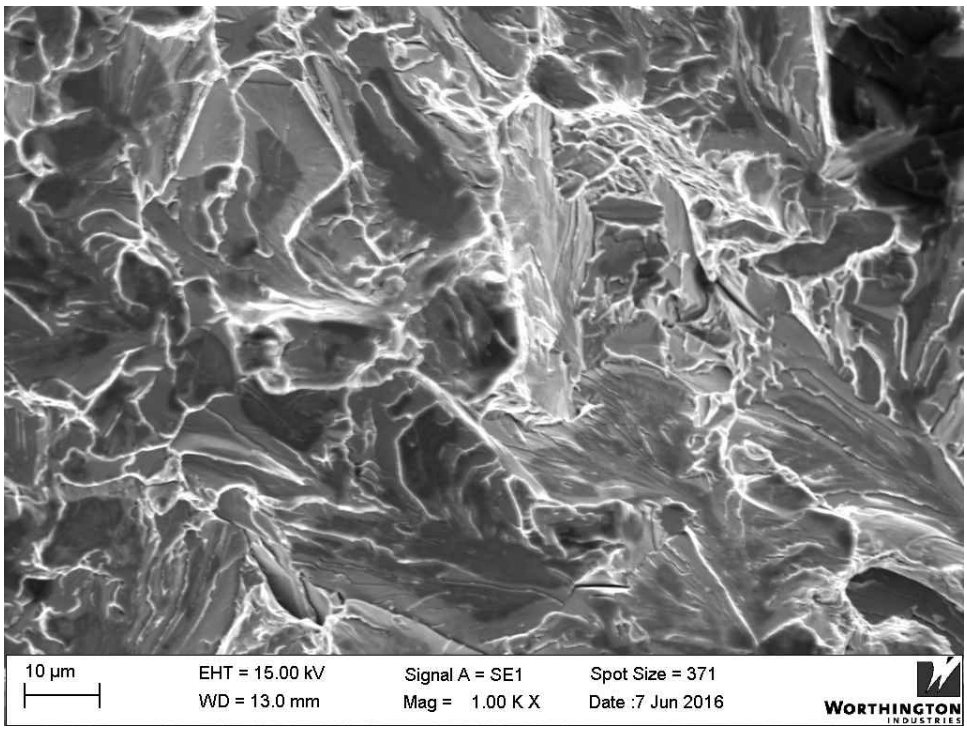

Figure 25. SEM image of non-surface breaking part of cold weld feature; SWA #5-3

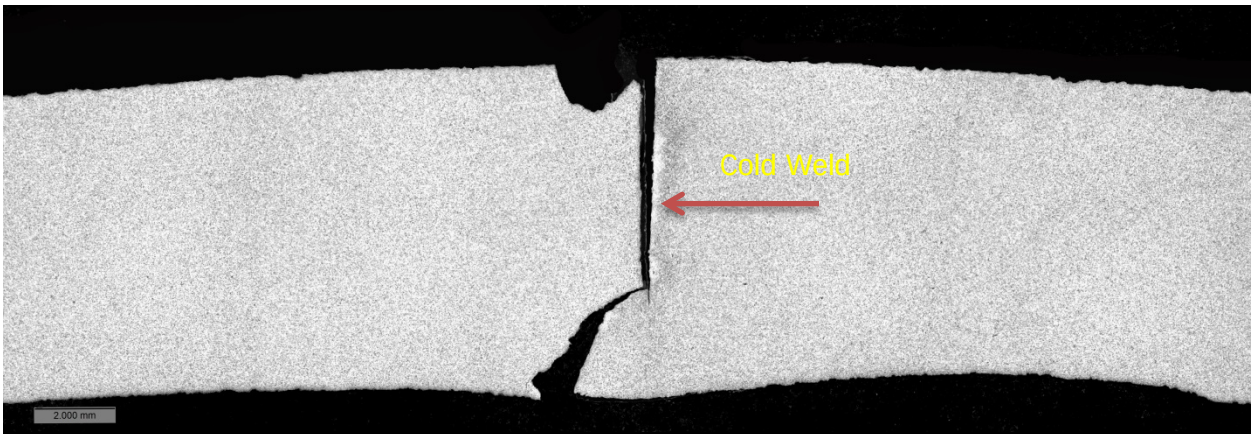

Figure 26. SWA #5-1, metallographic image 12.5X

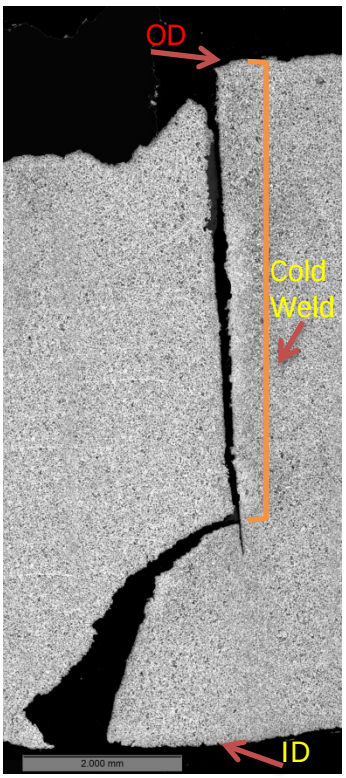

Figure 27. SWA #5-1, metallographic image 25X

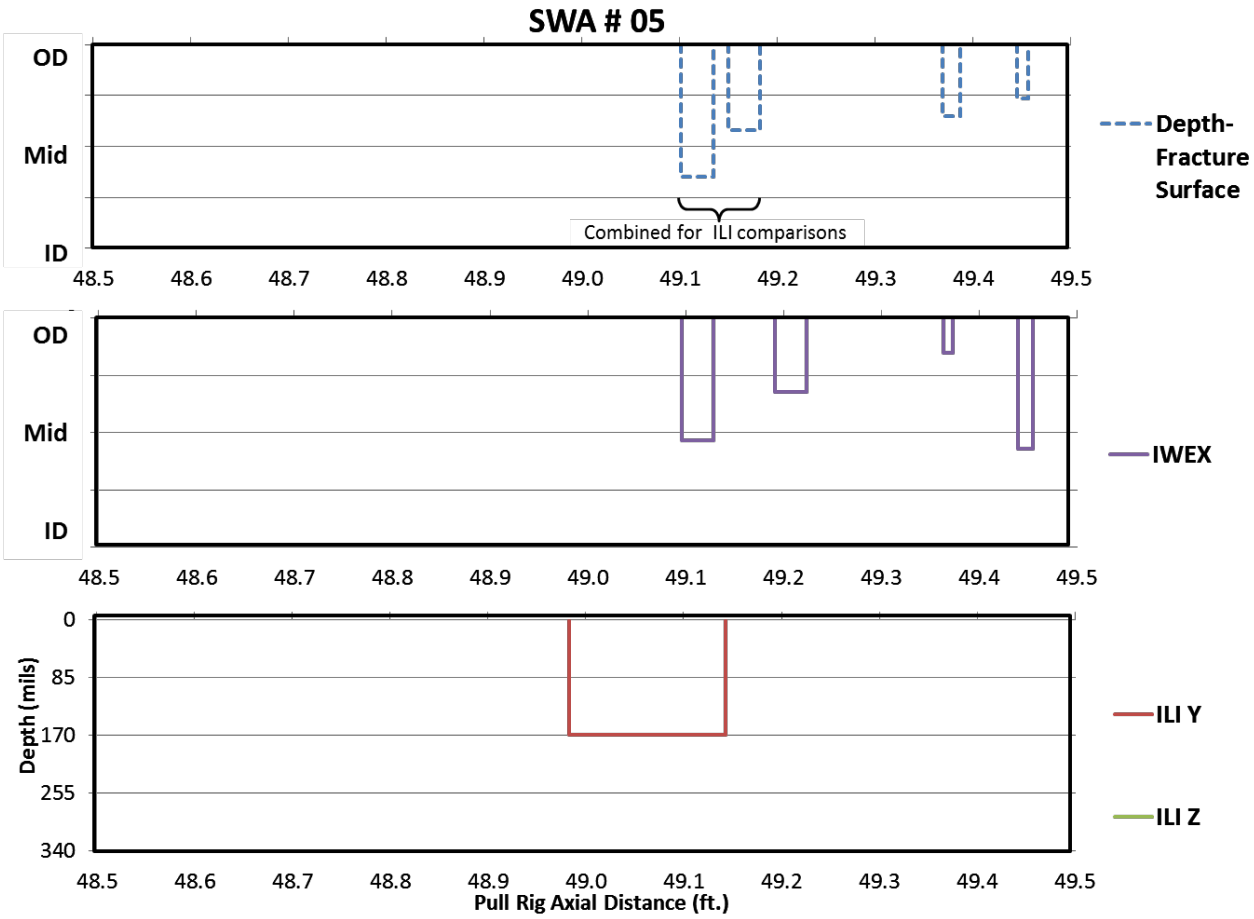

Figure 28. Depth profile and inspection results of SWA #5

SWA #6: SWA #6 was located on Pipe #16-20. Metallographic examination revealed this SWA to be a cold weld. Figure 29 shows the pipe marked in preparation for the fractography specimens and Figure 30 and Figure 31 show the fractographic results. An ID SWA can be seen in the pictures on the right side. The metallographic images in Figure 32 and Figure 33 show the extent of the cold weld. The anomaly location details along with details of ILI and IWEX reported anomalies are presented in Figure 34. The two ID anomalies were grouped for comparison to ILI since they were less than an inch apart. However, the combined length of the two anomalies is less than most ILI tool specifications.

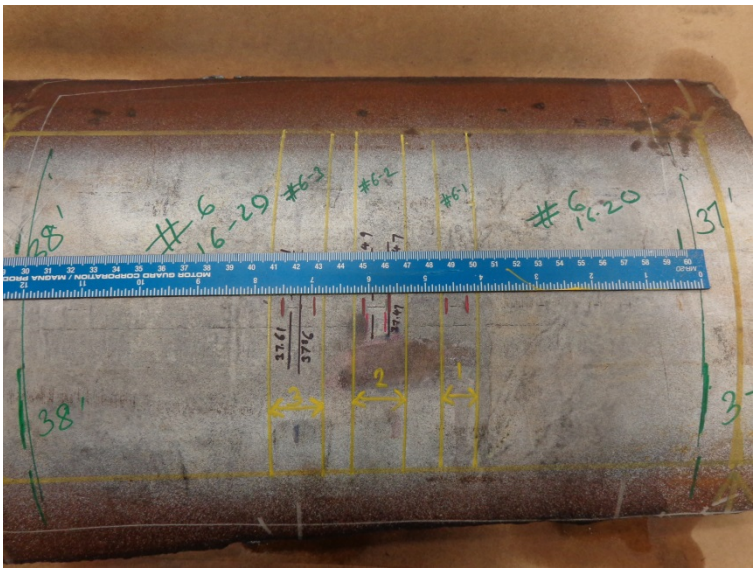

Figure 29. Break location marked on SWA #6

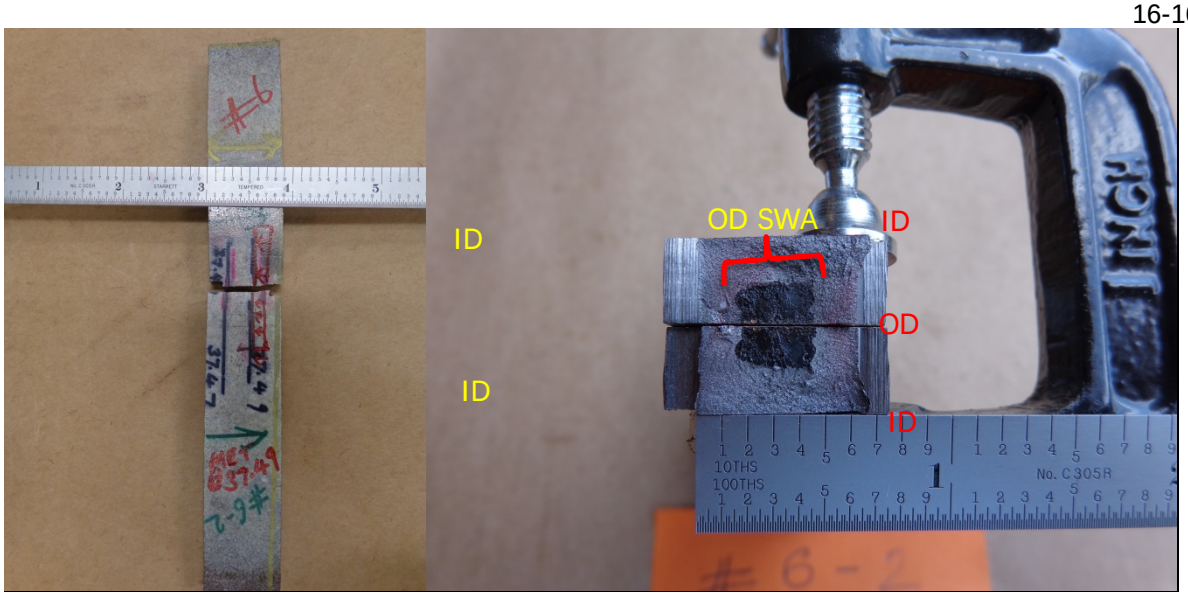

Figure 30. SWA #6-1, break location and fracture surface. This location shows an ID SWA which can be seen in the picture on the right.

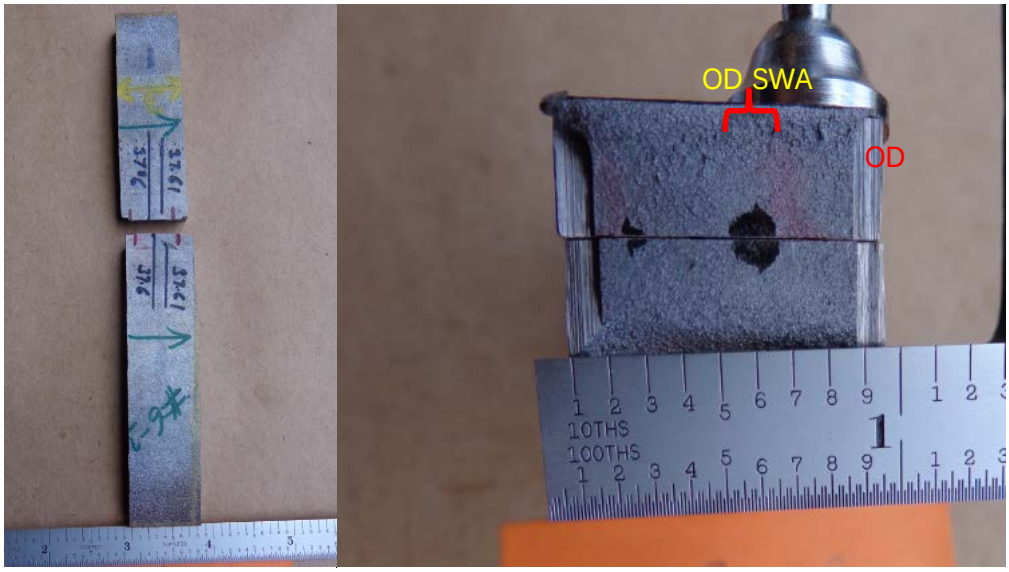

Figure 31. SWA #6-2, Break location and fracture surface

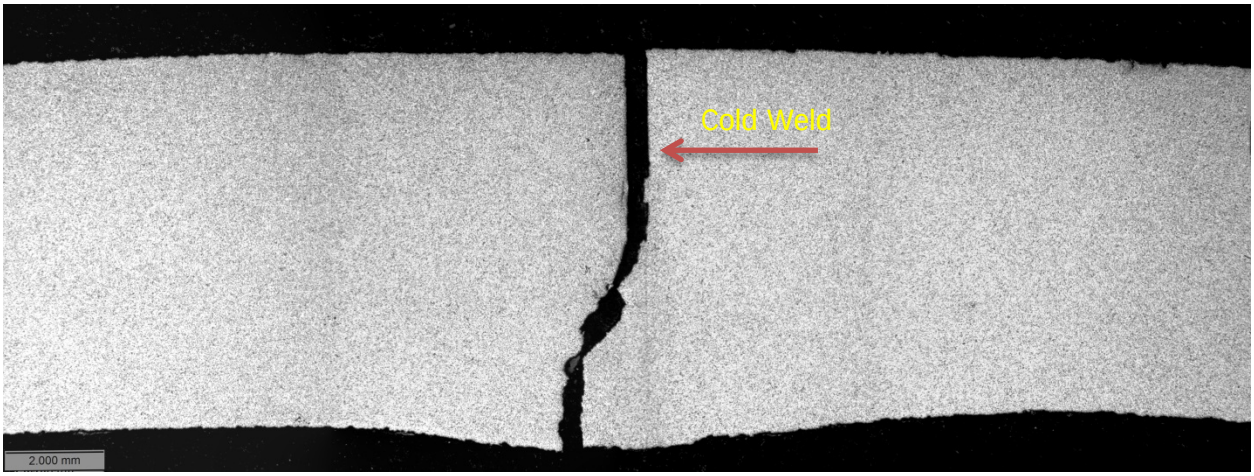

Figure 32. SWA #6-1, metallographic image of the larger cold weld 12.5X

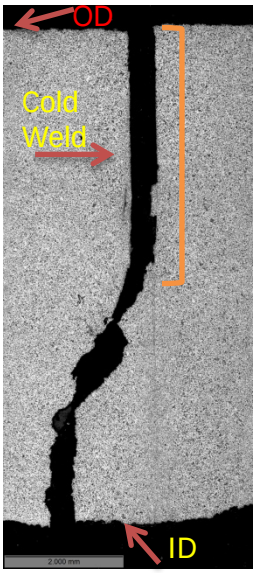

Figure 33. SWA #6-1, metallographic image 25X

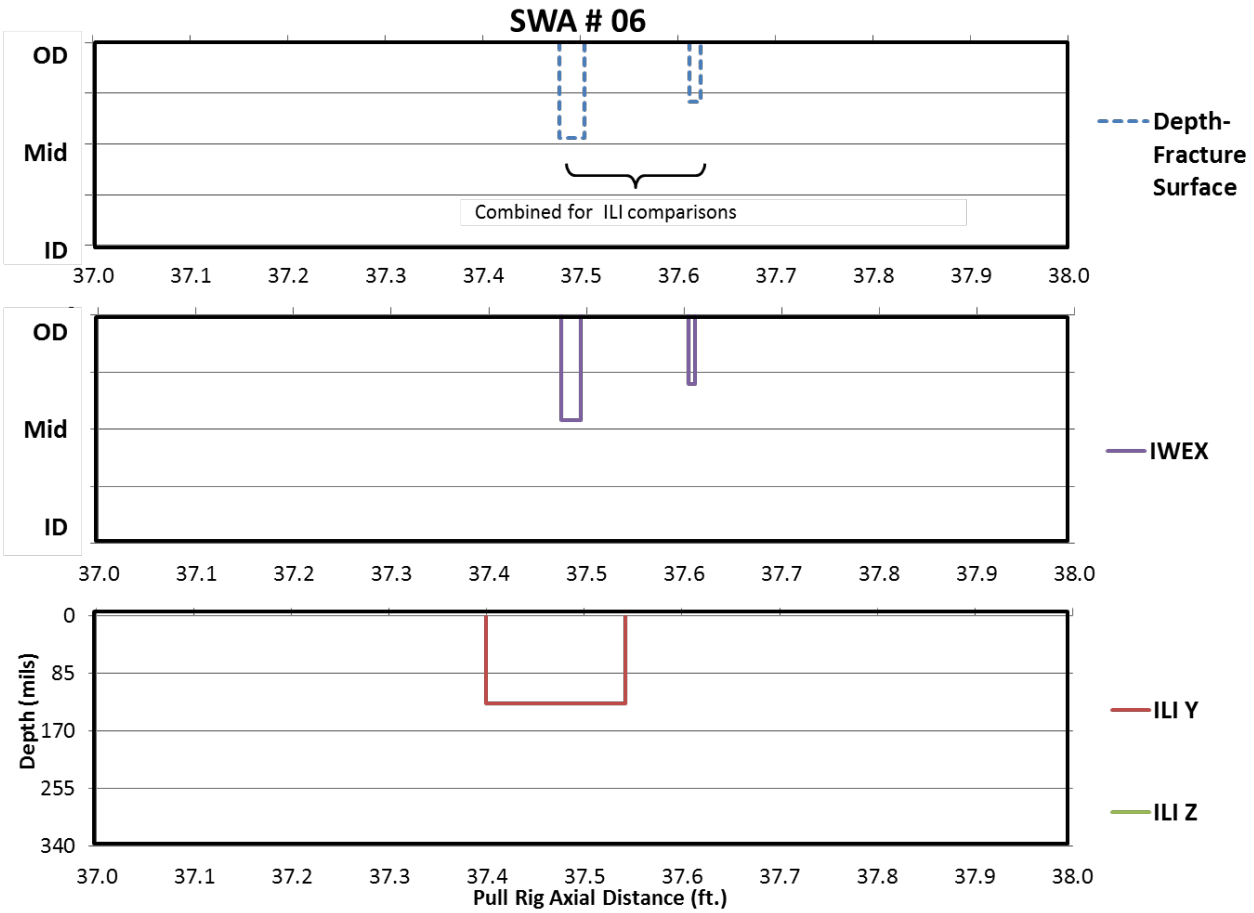

Figure 34. Depth profile and inspection results of SWA #6

SWA #7: SWA #7 was located on Pipe #16-36. Metallographic examination revealed this SWA to be a hook crack. A metallographic cross section also revealed the presence of a near mid-wall lamination feature in SWA #7. The presence of a lamination feature connected to the hook crack suggests that this hook crack was formed due to the lamination feature disturbing the seam in the ERW process. A metallographic section for SWA #7 was cut before performing fractography to obtain an intact seam metallographic cross section. SWA #7 was divided into three break sections to achieve a full anomaly profile. Figure 35 shows the pipe marked in preparation for the fractography specimens and Figure 36 through Figure 38 show the fractographic results. An ID SWA can be seen in the pictures on the right side.

The SEM image in Figure 39 shows the lamination feature in SWA #7-3. Energy dispersive spectroscopy (EDS) was performed to confirm the presence of nonmetallic impurities that may have contributed to the development of crack like features. EDS results presented in Figure 40 show the presence of carbonates and oxygen and no evidence was found that may suggest the presence of any nonmetallic impurities such as silicates. EDS results (Figure 41) of fracture surface in the hook crack area also suggested the presence of carbonates and oxygen; no evidence of any nonmetallic impurities was found.

The metallographic images in Figure 42 and Figure 43 show the hook crack and lamination features. The anomaly location details along with details of ILI and IWEX reported anomalies are presented with Pipe 16-36 shown in Figure 2.

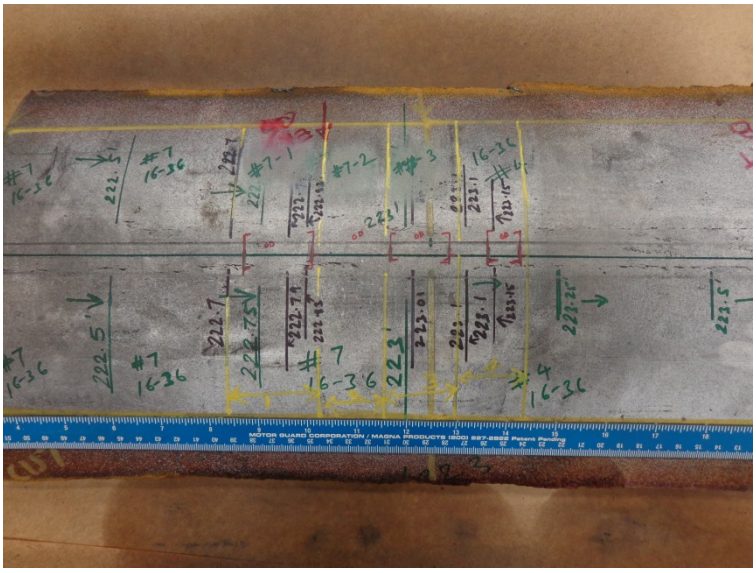

Figure 35. Break location marked on SWA #7

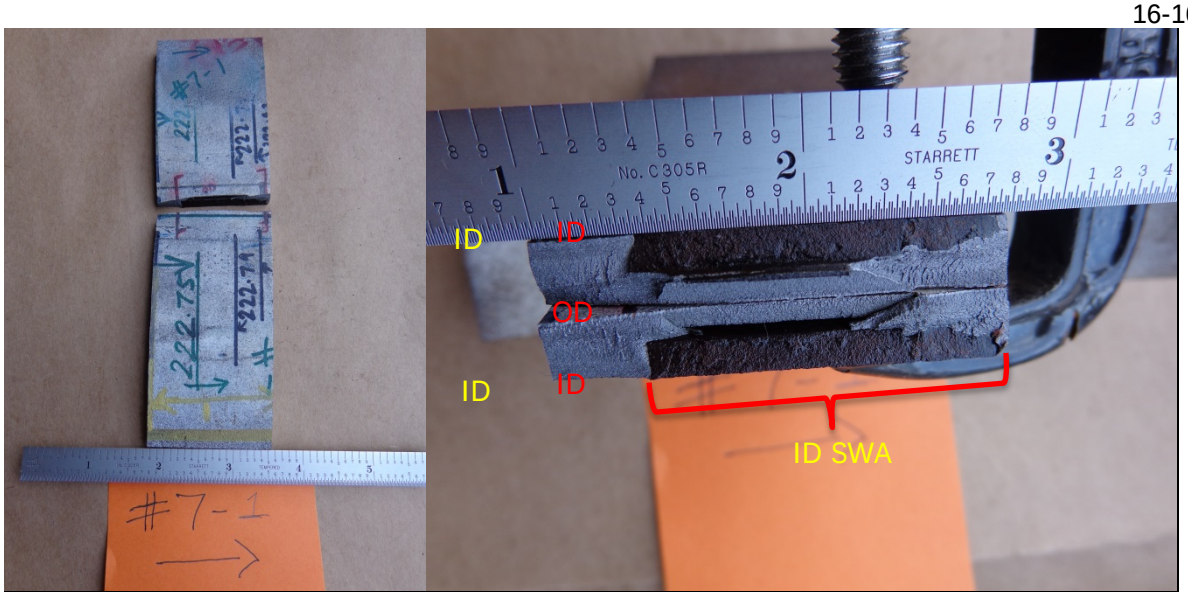

Figure 36. SWA #7-1, Break location and fracture surface

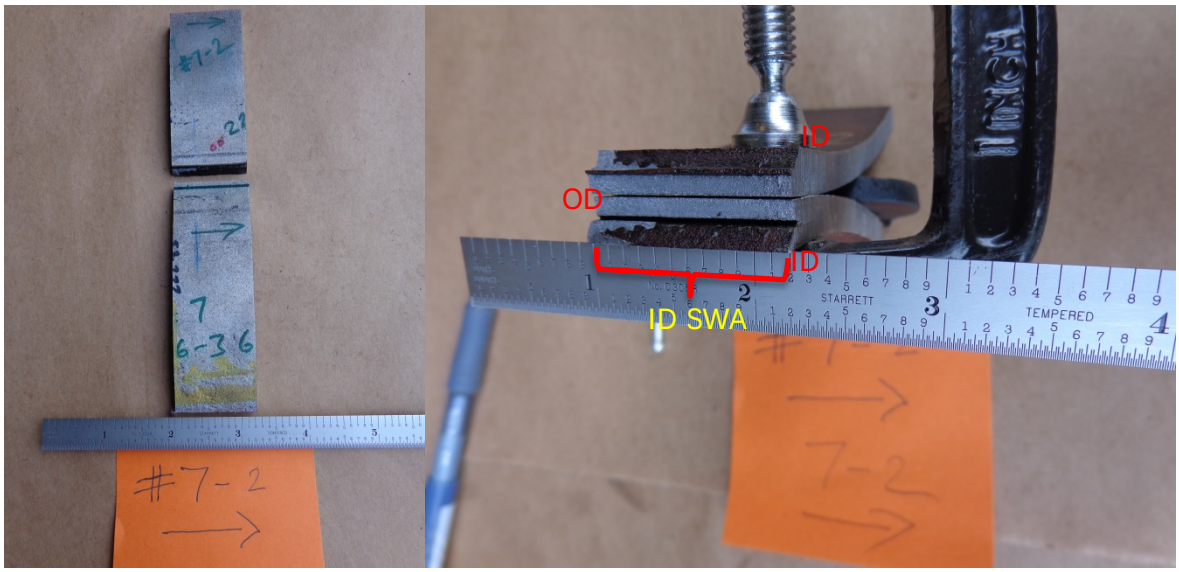

Figure 37. SWA #7-2, break location and fracture surface

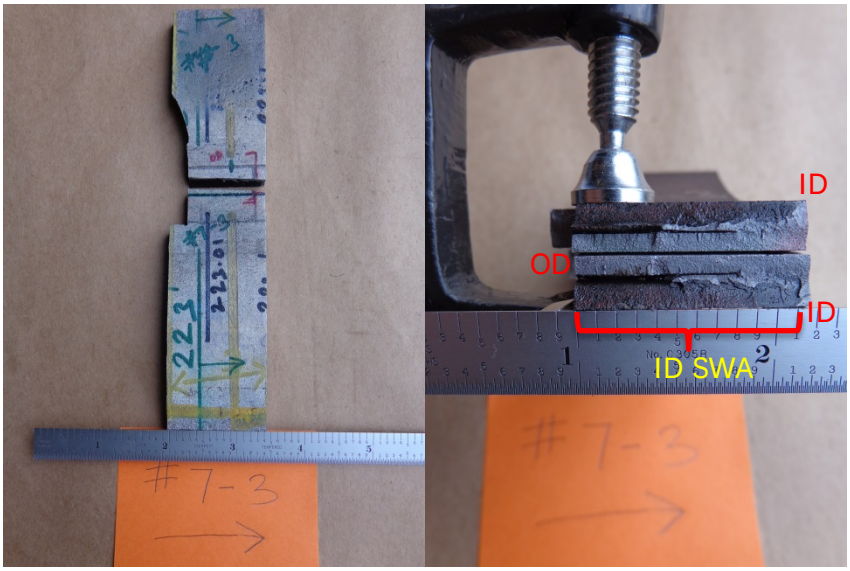

Figure 38. SWA #7-3, break location and fracture surface

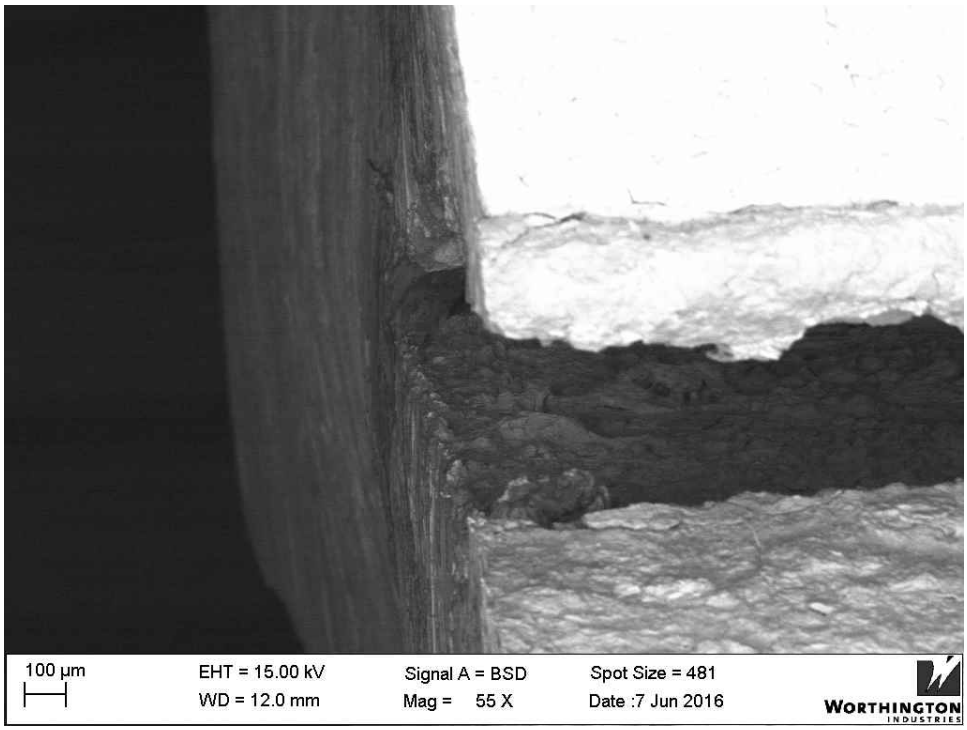

Figure 39. SEM image of fracture surface of lamination feature SWA #7-3

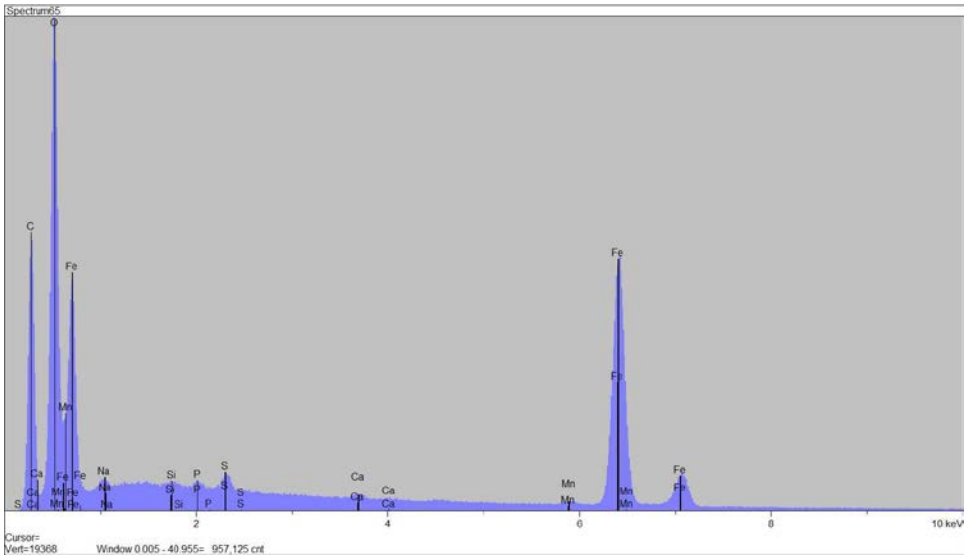

Figure 40. EDS of material in fracture surface of lamination feature, SWA #7-3

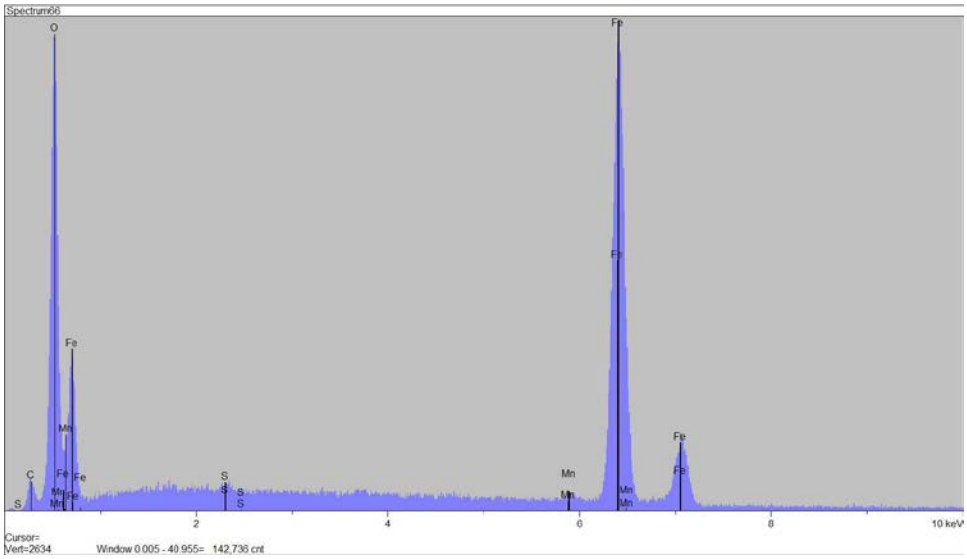

Figure 41. EDS of material in fracture surface of hook crack, SWA #7-3

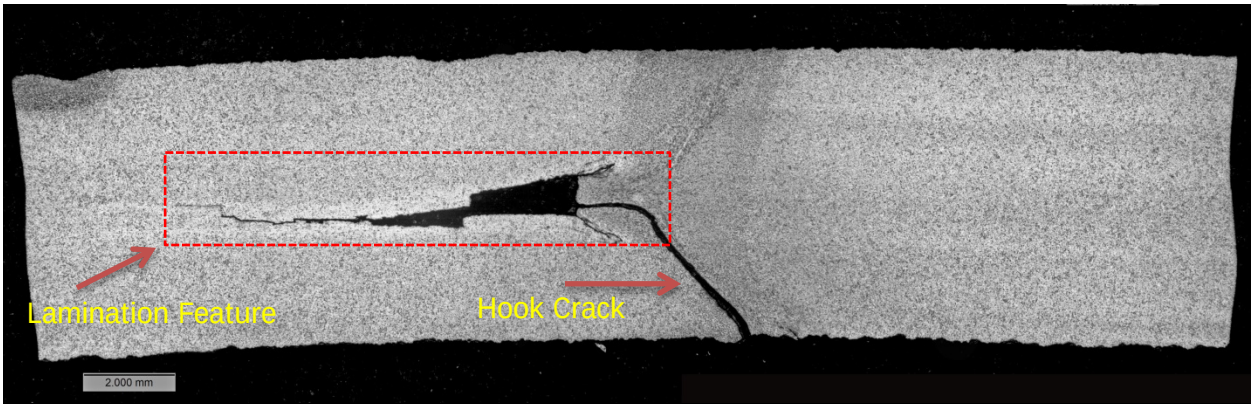

Figure 42. SWA #7, metallographic image 12.5X

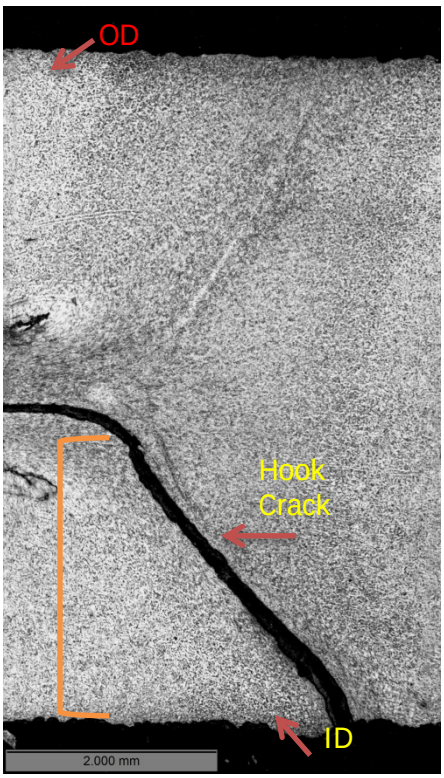

Figure 43. SWA #7, metallographic image 25X

SWA #8: SWA #8 was located on Pipe #16-38. Metallographic examination revealed this SWA to be a mid-wall stringer as shown in the metallographic cross section. Figure 44 shows the pipe marked in preparation for the fractography specimens and Figure 45 shows the fractographic results; a midwall SWA as can be seen in the picture on the right side.

The SEM image in Figure 47 and Figure 48 shows the midwall feature at 25X and 100X. EDS was performed to confirm presence of nonmetallic impurities that that may have contributed to the development of crack like features. EDS of the mid-wall feature on SWA #8 detected high levels of aluminum and silica as can be seen in Figure 49.

The metallographic images in Figure 50 and Figure 51 show the hook crack and lamination features. The anomaly location details along with details of ILI and IWEX reported anomalies are presented in Figure 52. Note that additional anomalies were detected by IWEX, however these did not break in the anomaly when tested. Since they had very short length, metallographic cross section was not attempted.

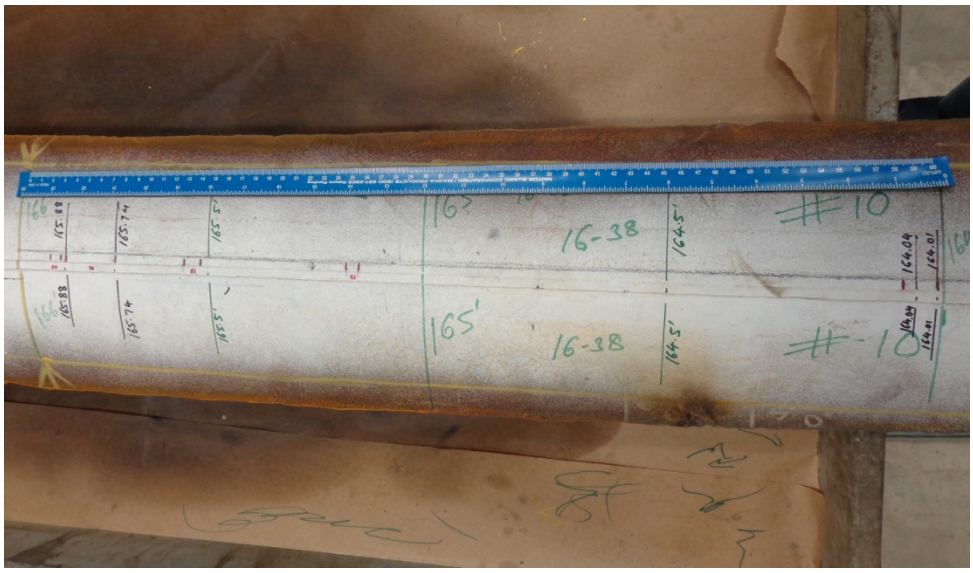

Figure 44. Break location marked on SWA #8

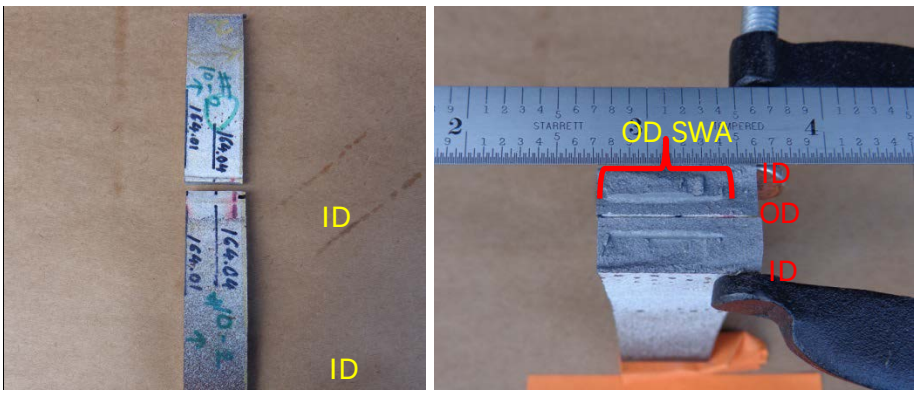

Figure 45. SWA #8-1, break location and fracture surface

Figure 46. SWA #8-2, break location and fracture surface

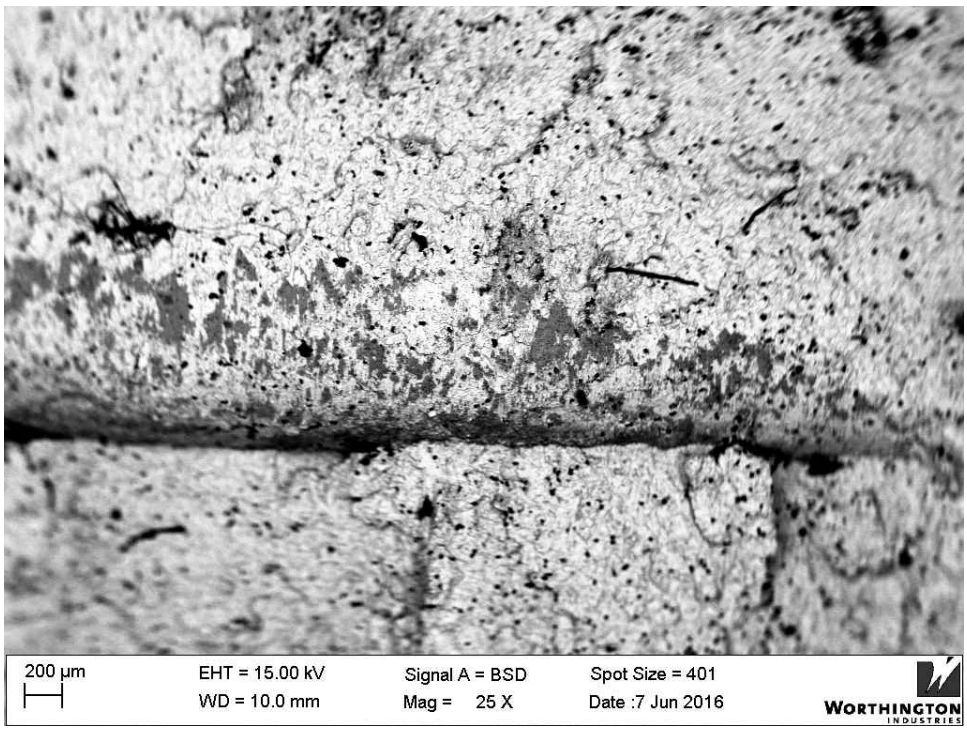

Figure 47. SEM image (25X) of mid-wall feature on SWA #8-1

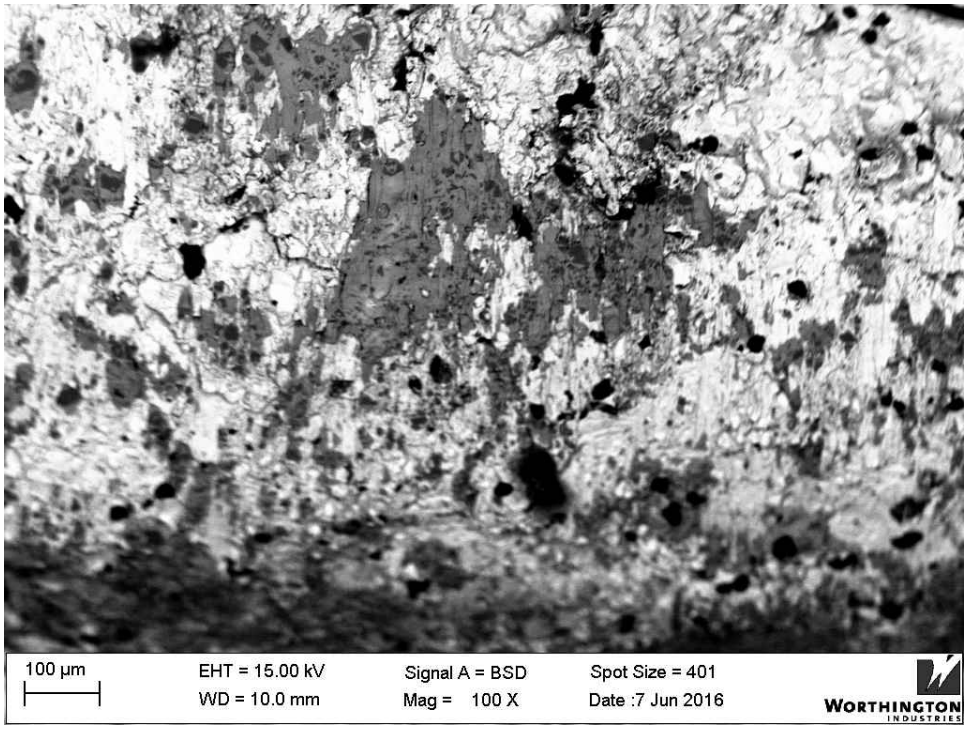

Figure 48. SEM image (100X) of mid-wall feature on SWA #8-1

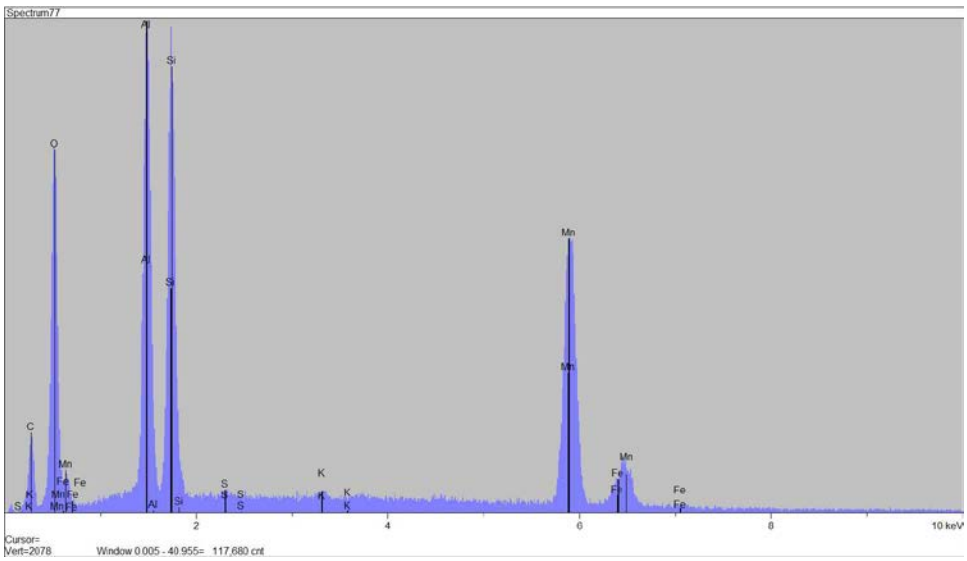

Figure 49. EDS of material of mid-wall feature on SWA #8-1

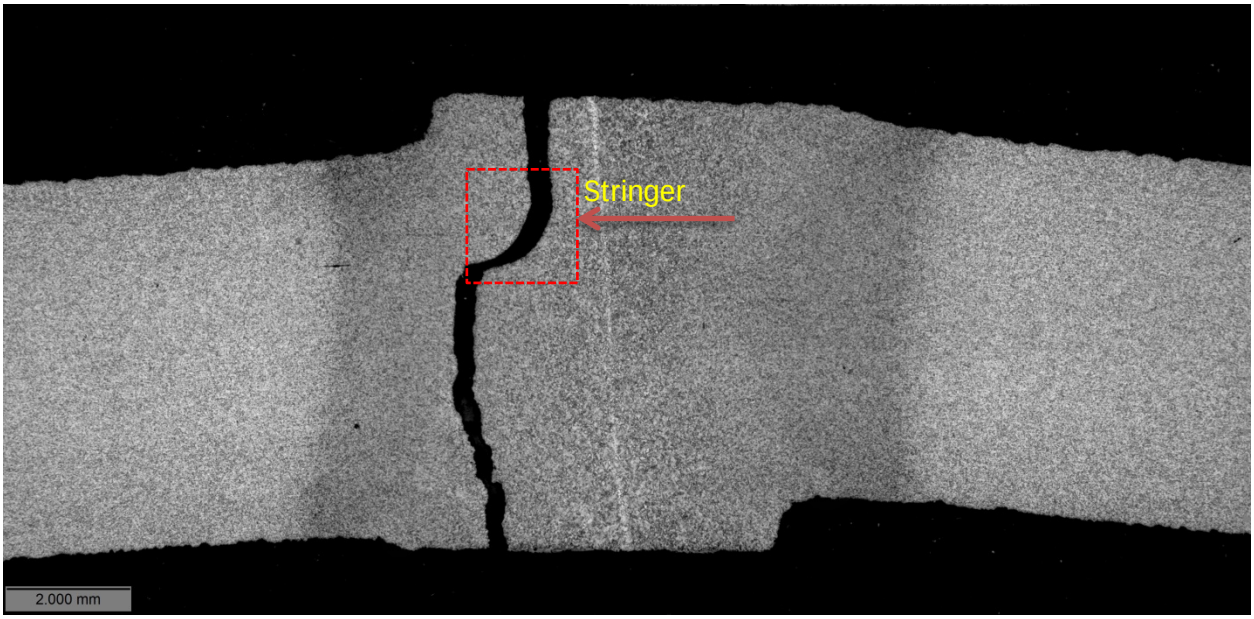

Figure 50. SWA #8-1, metallographic image 12.5X

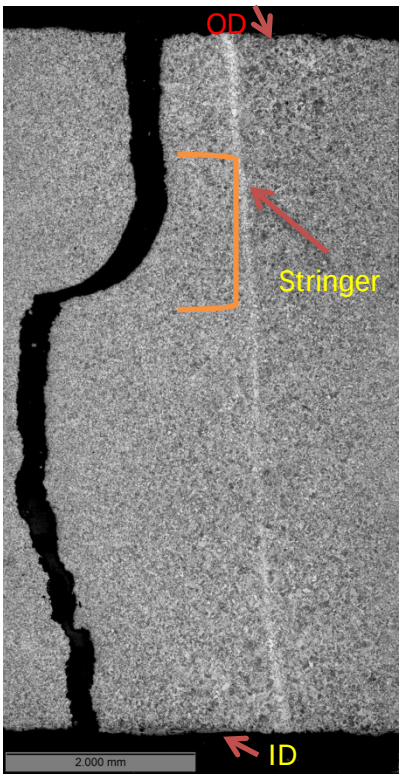

Figure 51. SWA #8-1, metallographic image 25X

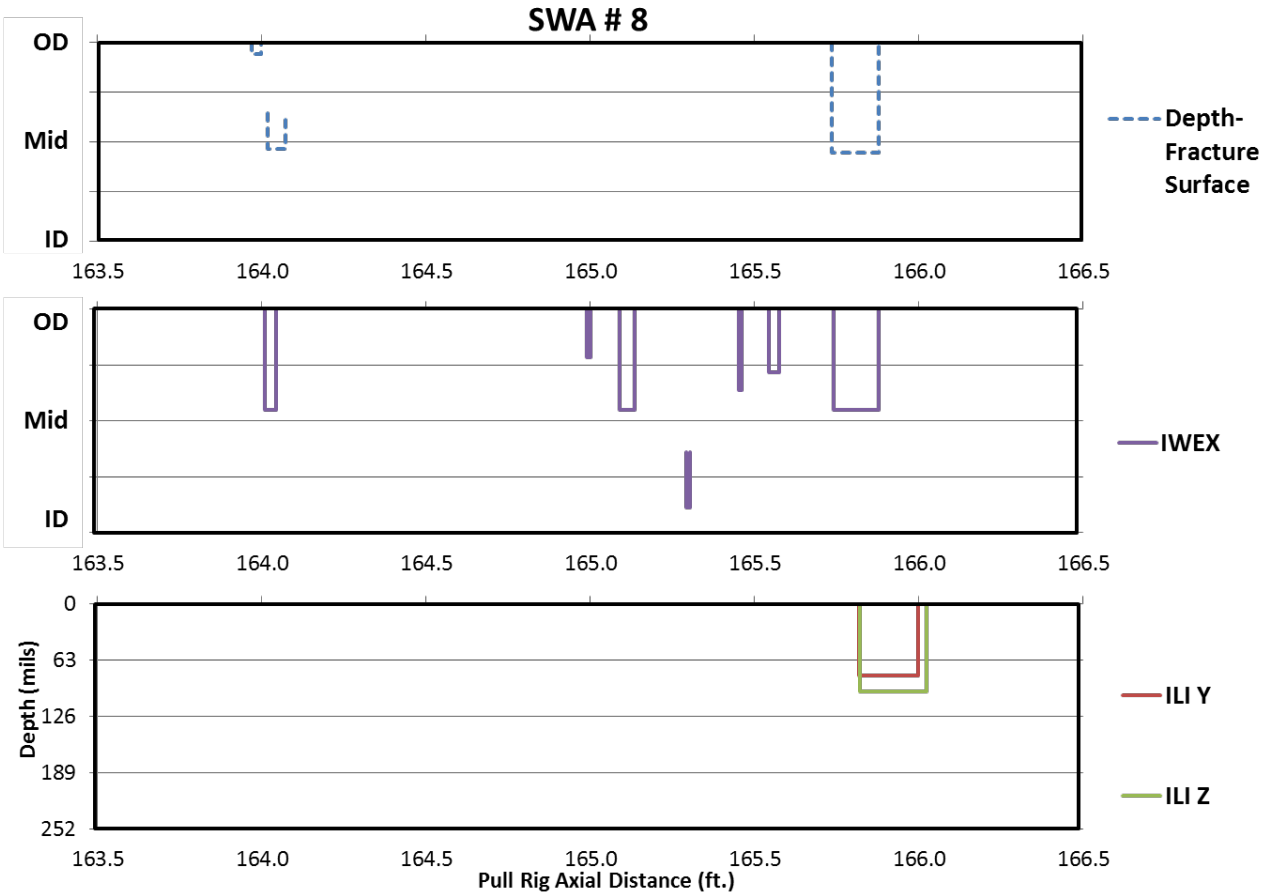

Figure 52. Depth profile and inspection results of SWA #8

SWA #9: SWA #9 was located on Pipe #16-38. Metallographic examination revealed this SWA to be a hook crack. Figure 53 shows the pipe marked in preparation for the fractography specimens and Figure 54 shows the fractographic results. A hook crack can be seen in the picture on the right side. The metallographic images in Figure 55 and Figure 56 show the hook crack. The anomaly location details along with details of ILI and IWEX reported anomalies are presented in Figure 57.

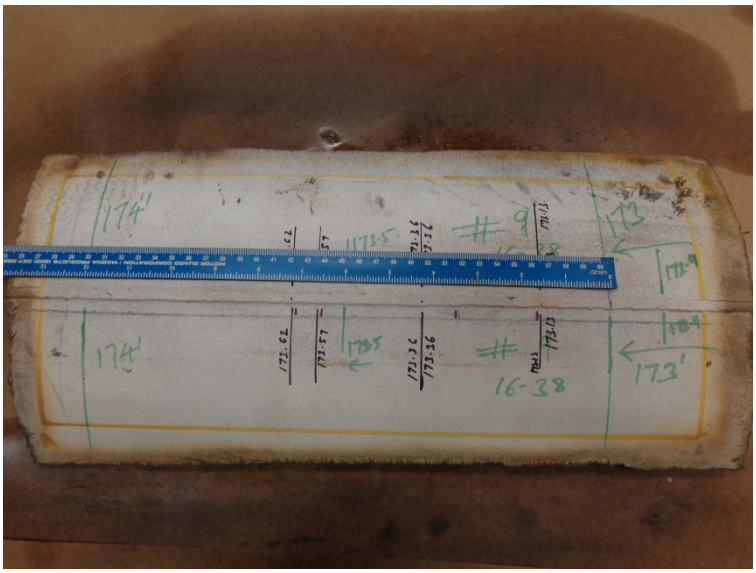

Figure 53. Break location marked on SWA #9

Figure 54. SWA #9, break location and fracture surface

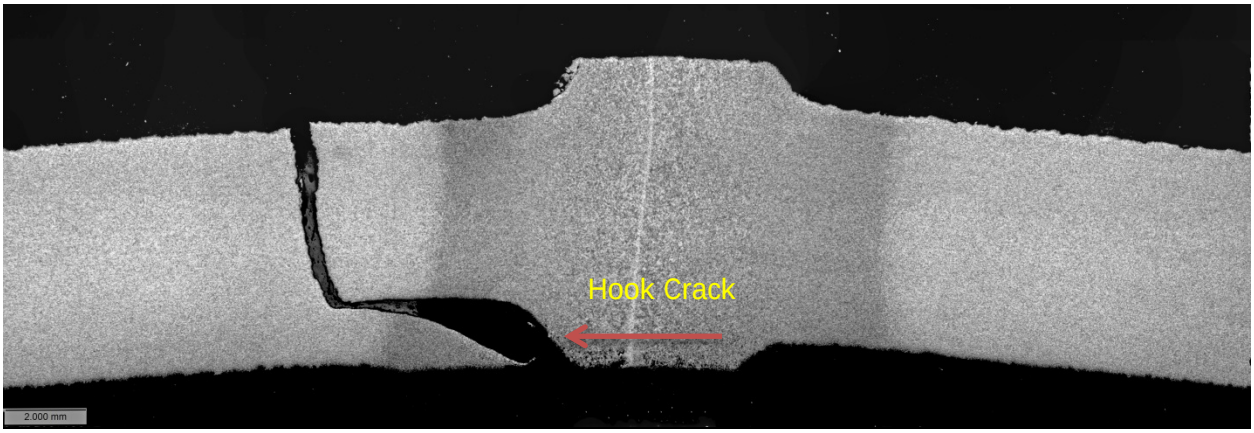

Figure 55. SWA #9, metallographic image 12.5X

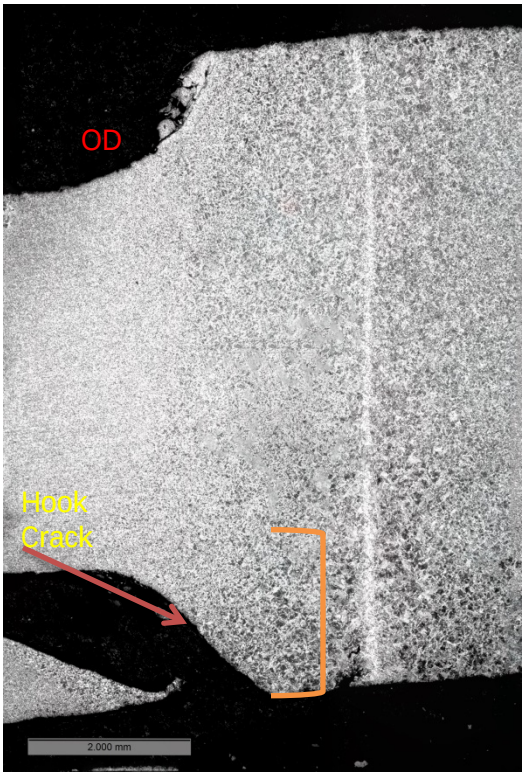

Figure 56. SWA #9, metallographic image 25X

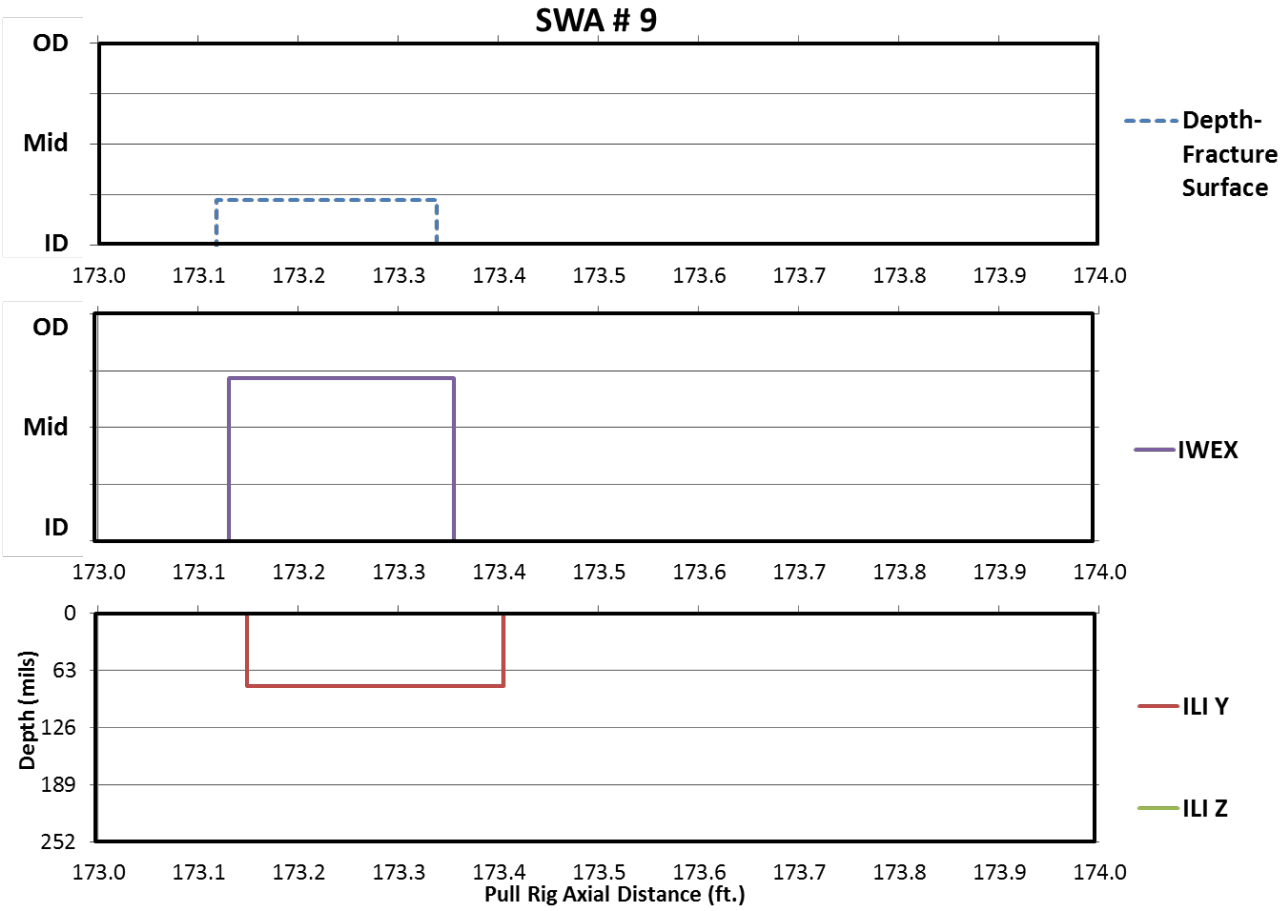

Figure 57. Depth profile and inspection results of SWA #9

SWA #10: SWA #10 was located on Pipe #16-38. Metallographic examination revealed this SWA to be multiple hook cracks. Figure 58 shows the pipe marked in preparation for the fractography specimens and Figure 59 through Figure 61 show the fractographic results. A hook crack can be seen in the picture on the right side. The metallographic images in Figure 62 and Figure 63 show the hook cracks. The anomaly location details along with details of ILI and IWEX reported anomalies are presented in Figure 64.

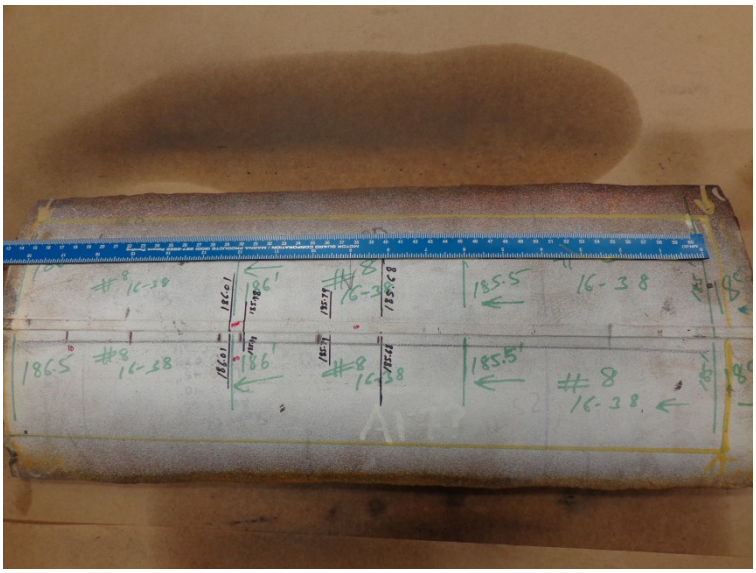

Figure 58. Break location marked on SWA #10

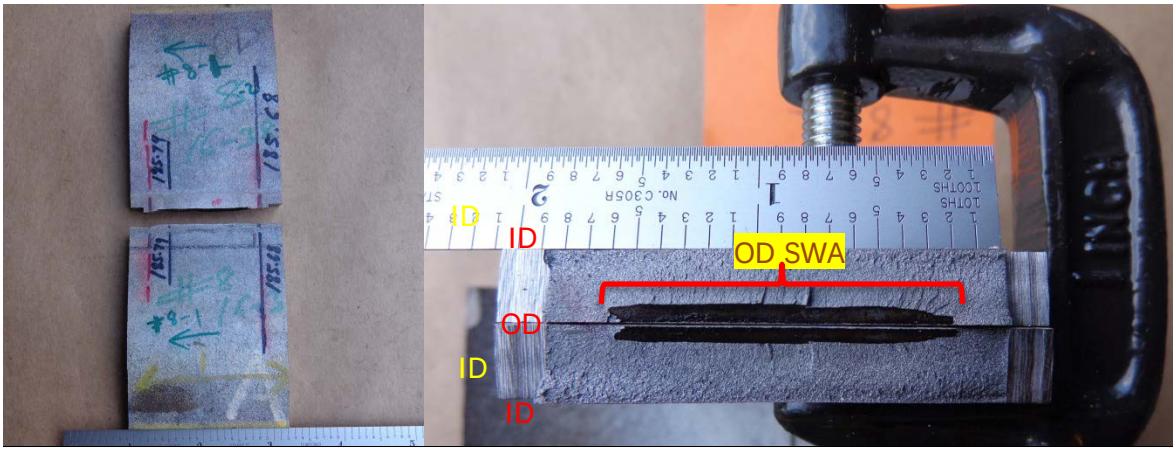

Figure 59. SWA #10-1, break location and fracture surface

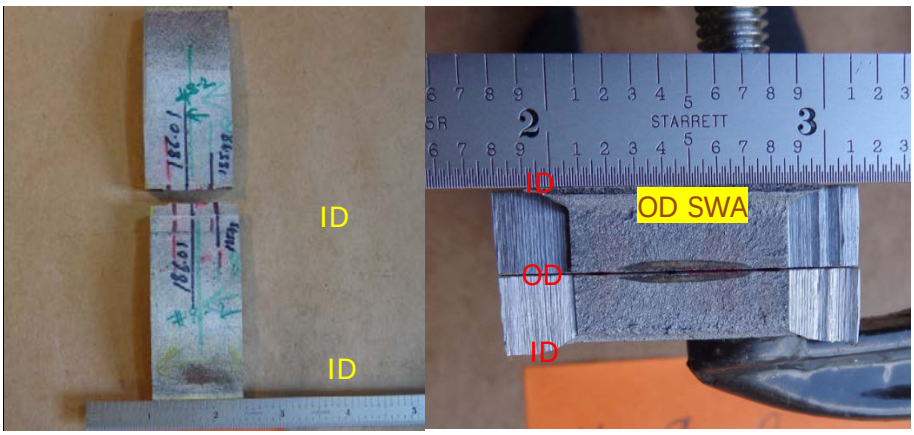

Figure 60. SWA #10-2, break location and fracture surface

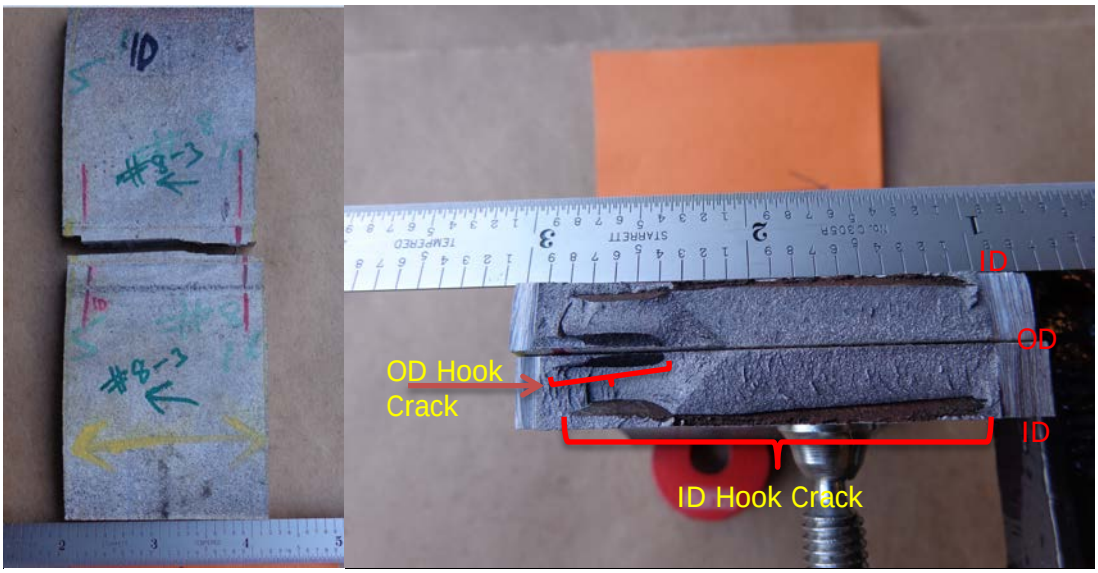

Figure 61. SWA #10-3, break location and fracture surface

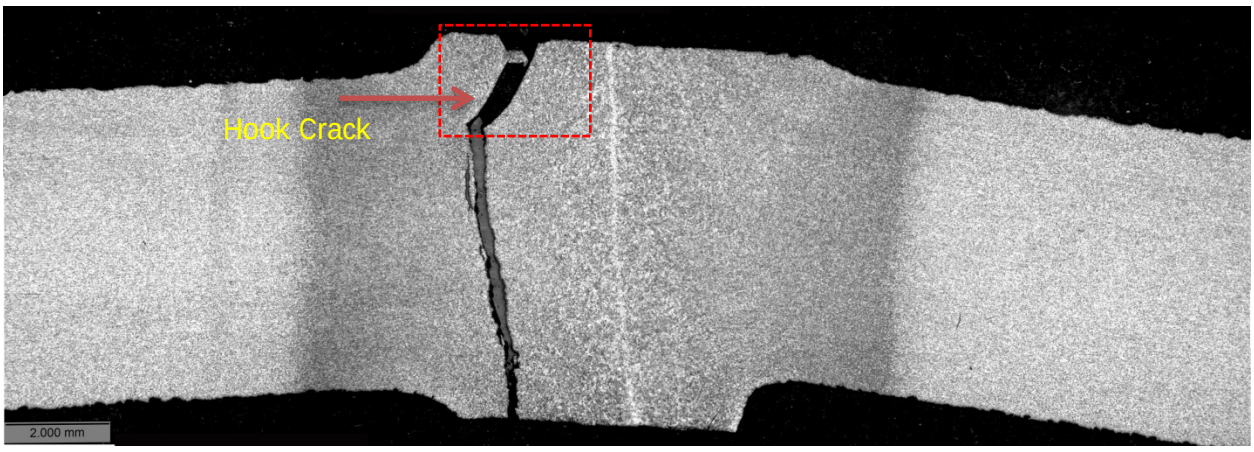

Figure 62. SWA #10-1, metallographic image 12.5X

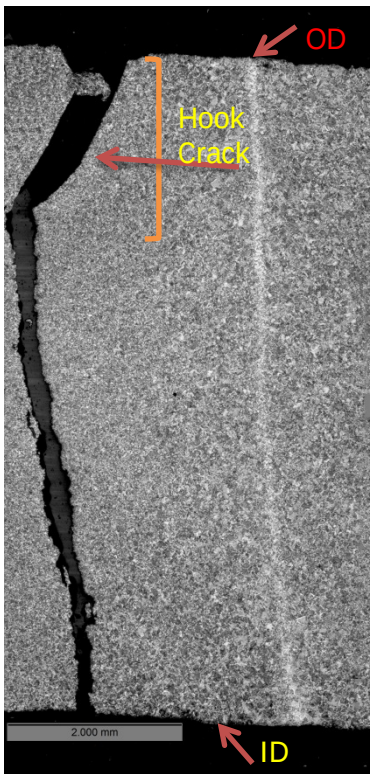

Figure 63. SWA #10-1, metallographic image 25X

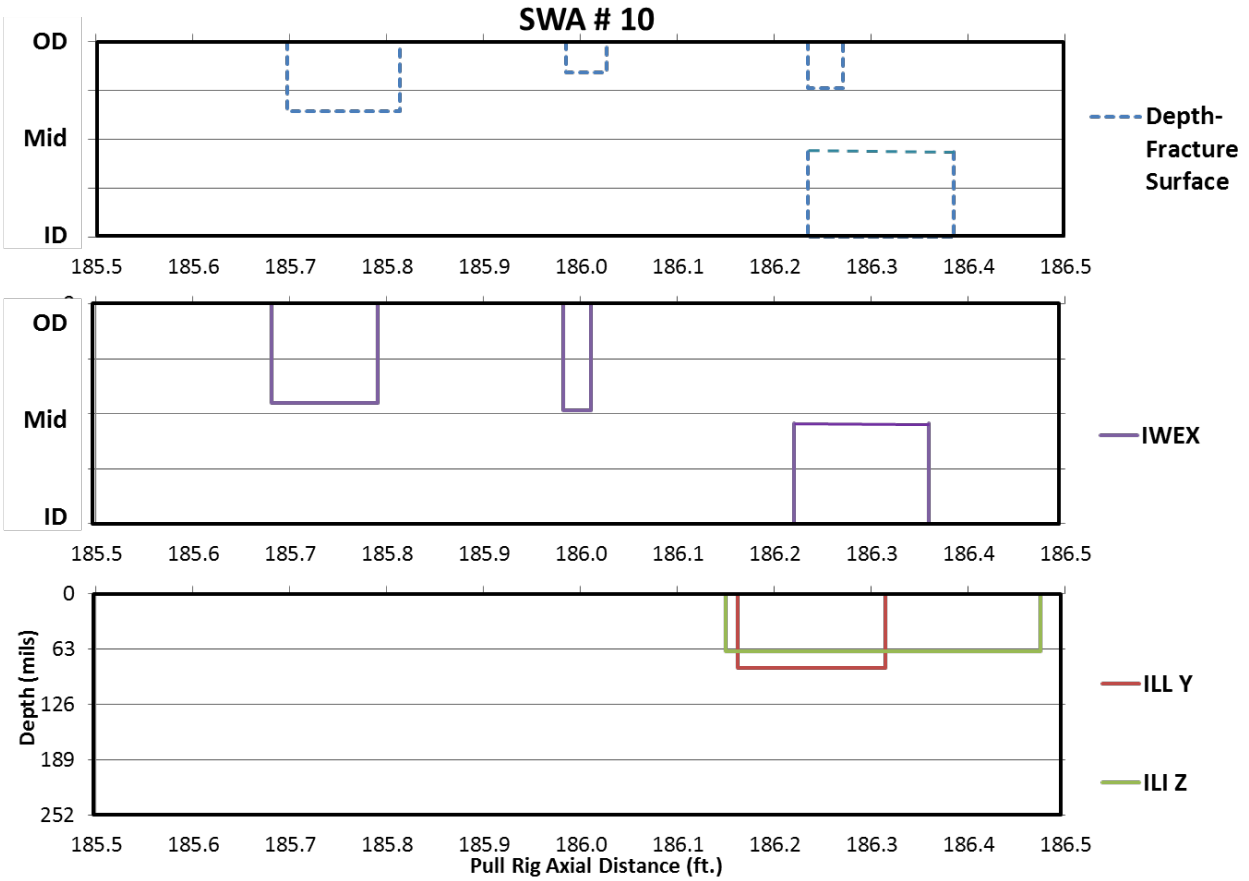

Figure 64. Depth profile and inspection results of SWA #10

SWA #13: SWA #13 was located on Pipe #16-38. Metallographic examination revealed this SWA to be a non-surface breaking stringer and cold weld. Figure 65 shows the pipe marked in preparation for the fractography specimens and Figure 66 shows the fractographic results. A stringer can be seen in the picture on the right side. The metallographic image in Figure 67 shows the stringer. The anomaly location details along with details of ILI and IWEX reported anomalies are presented in Figure 68. The ILI tools appeared to conservatively group the largest anomaly by area with one 2.3 inches away.

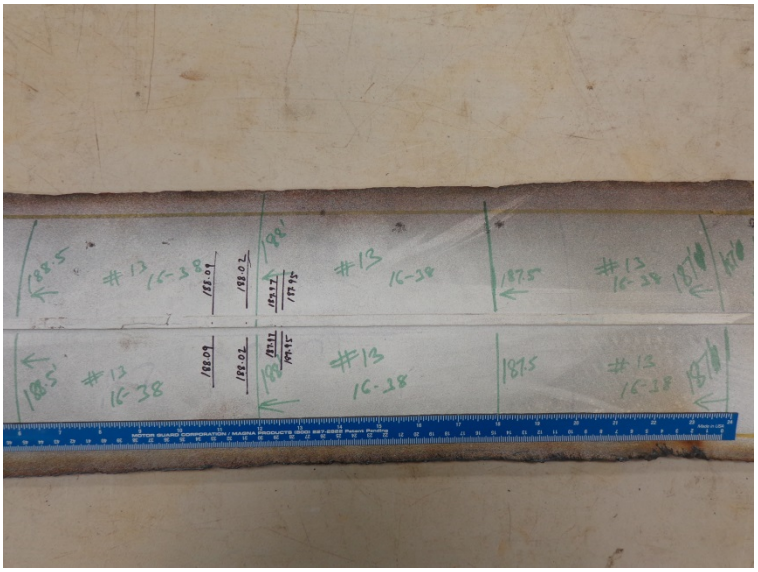

Figure 65. Break location marked on SWA #13

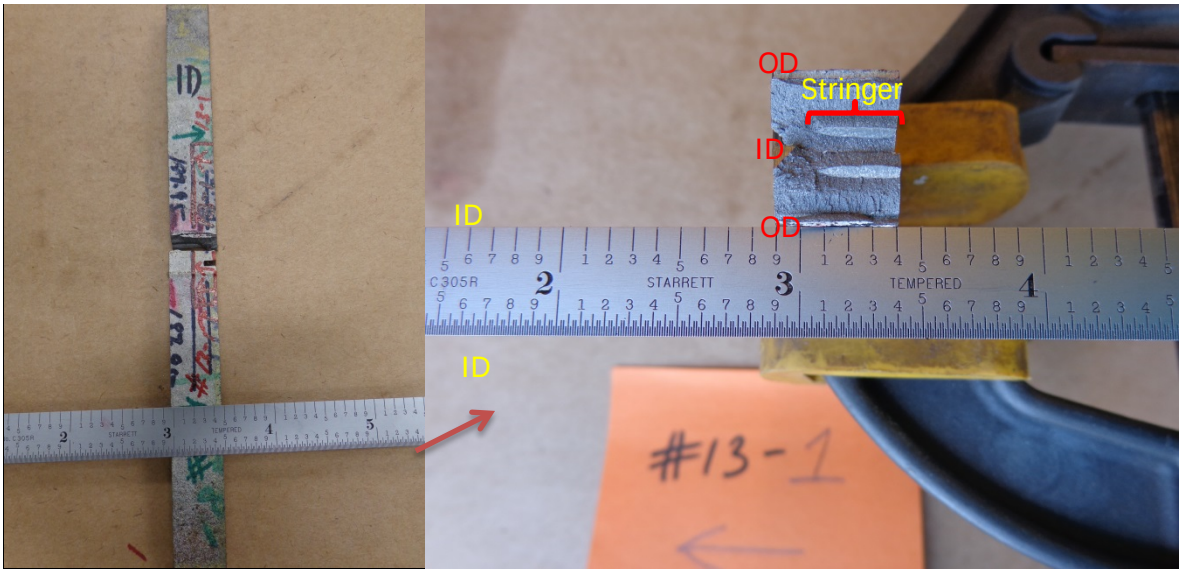

Figure 66. SWA #13, break location and fracture surface

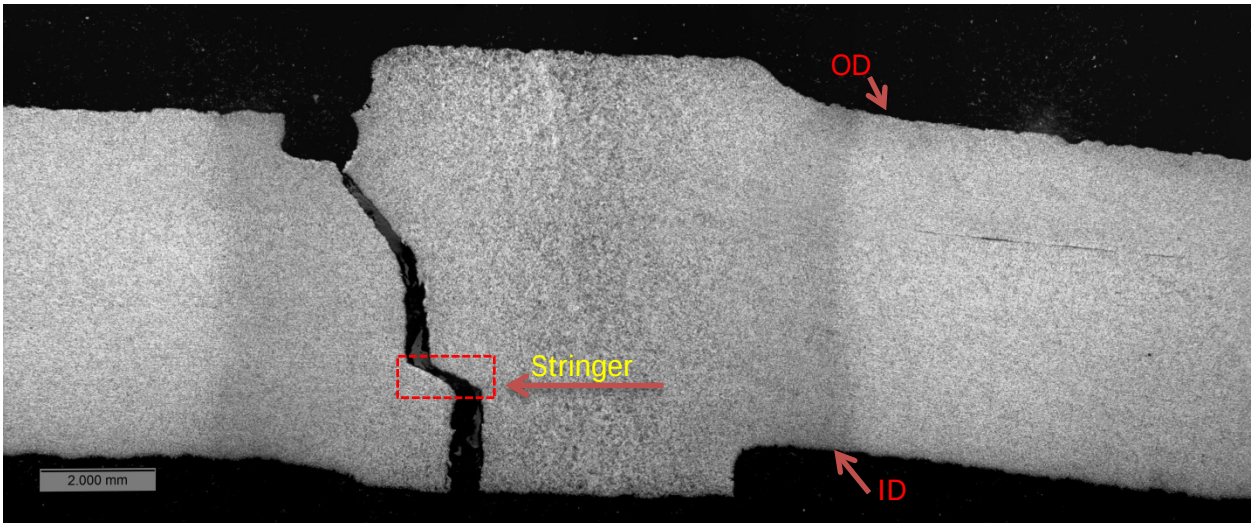

Figure 67. SWA #13, metallographic image 12.5X

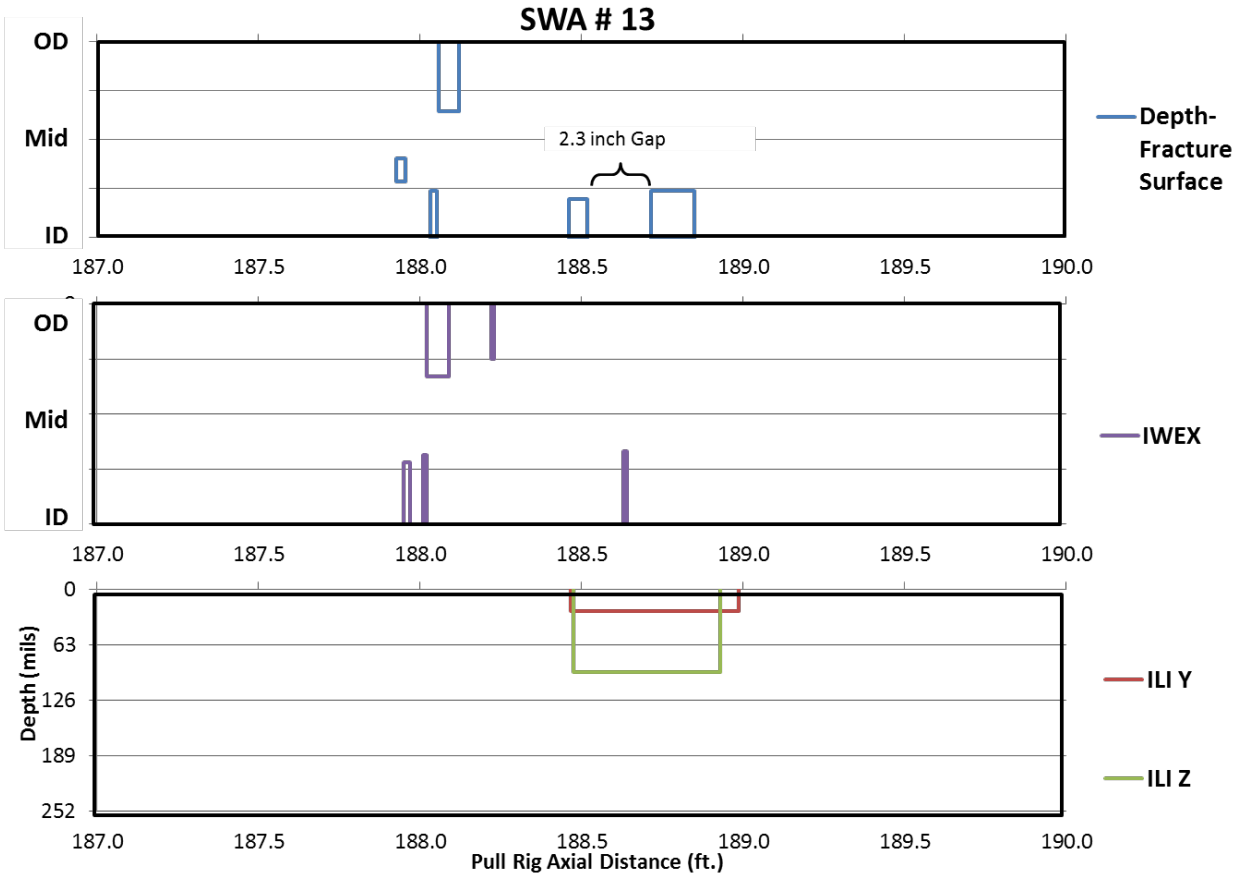

Figure 68. Depth profile and inspection results of SWA #13

SWA #14: SWA #14 was located on Pipe #16-38. Metallographic examination revealed this SWA to be a stringer. A metallographic cross section shows the presence of a mid-wall stringer. Figure 69 shows the pipe marked in preparation for the fractography specimens and Figure 70 shows the fractographic results; a stringer can be seen in the picture on the right. The metallographic image in Figure 71 and Figure 72 shows the stringer. This anomaly was below the detection threshold of both ILI tools and no anomalies were reported.

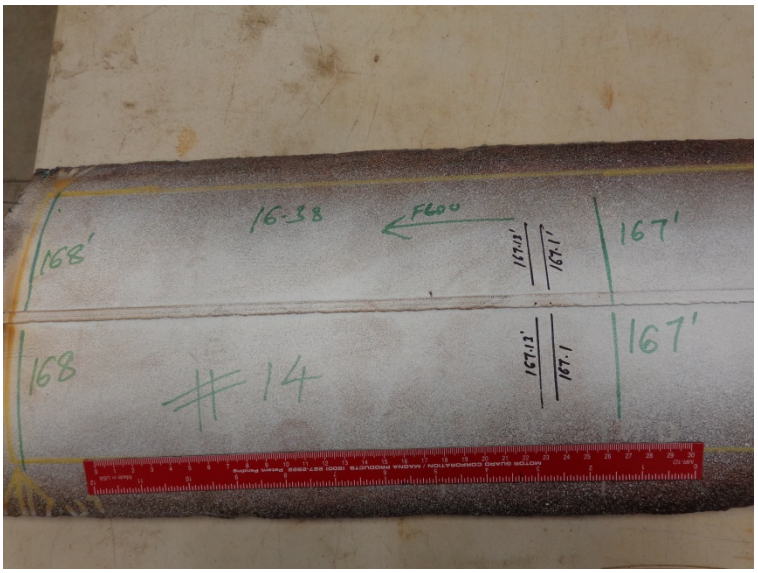

Figure 69. Break location marked on SWA #14

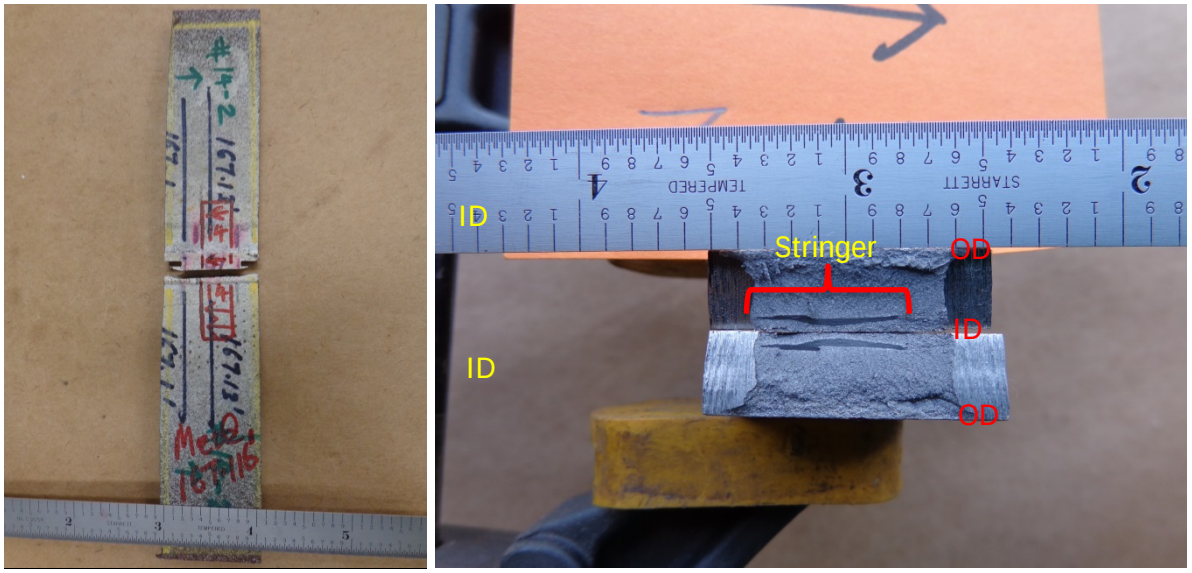

Figure 70. SWA #14, break location and fracture surface

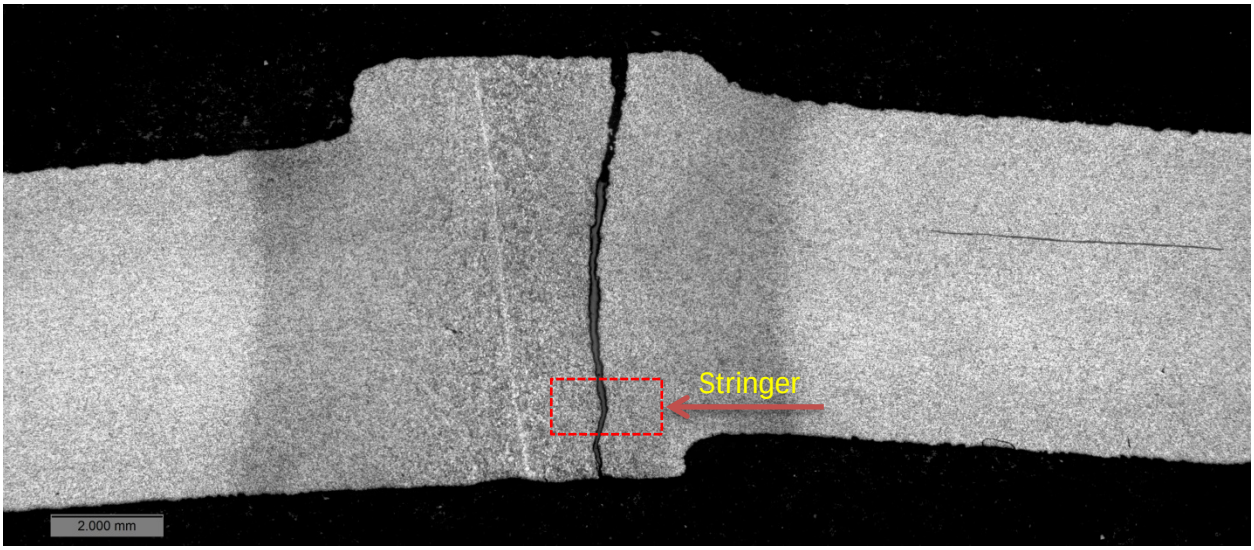

Figure 71. SWA #14, metallographic image 12.5X

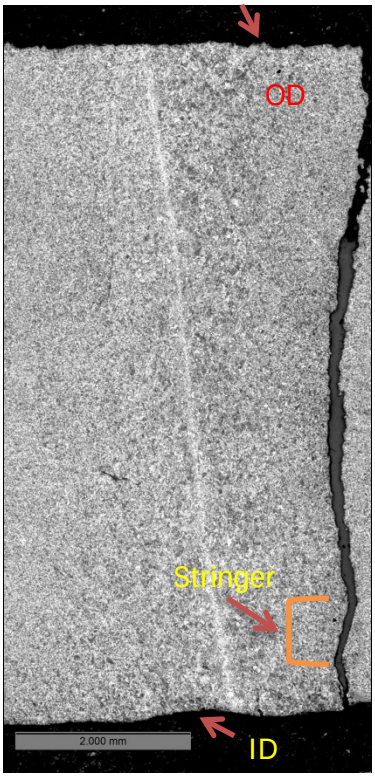

Figure 72. SWA #14, metallographic image 25X

SWA #15: SWA #15 was located on Pipe #16-38. Metallographic examination revealed this SWA to be a hook crack. Figure 73 shows the pipe marked in preparation for the fractography specimens and Figure 75 shows the fractographic results; a hook crack can be seen in the picture on the right side. The metallographic image in Figure 77 shows the hook crack. The anomaly location details along with details of ILI and IWEX reported anomalies are presented in Figure 78. The ID anomaly and nearby mid-wall anomaly were grouped for comparison to ILI since they were less than an inch apart.

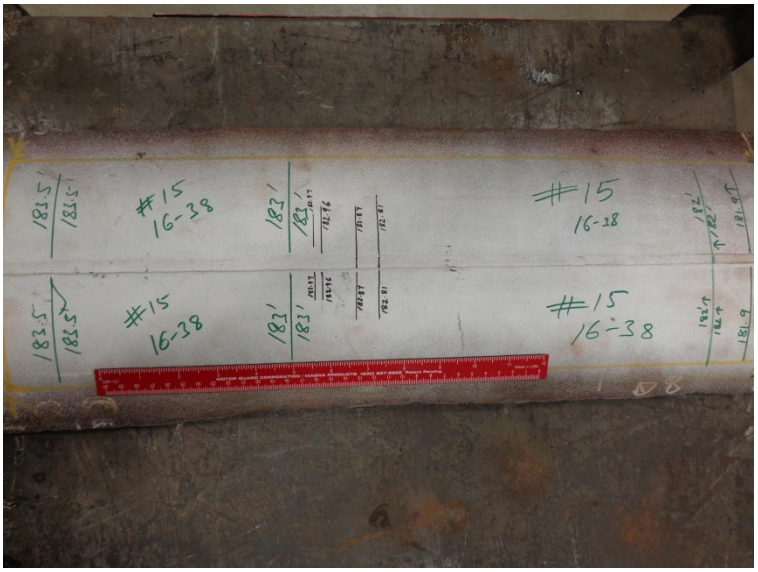

Figure 73. Break location marked on SWA #15

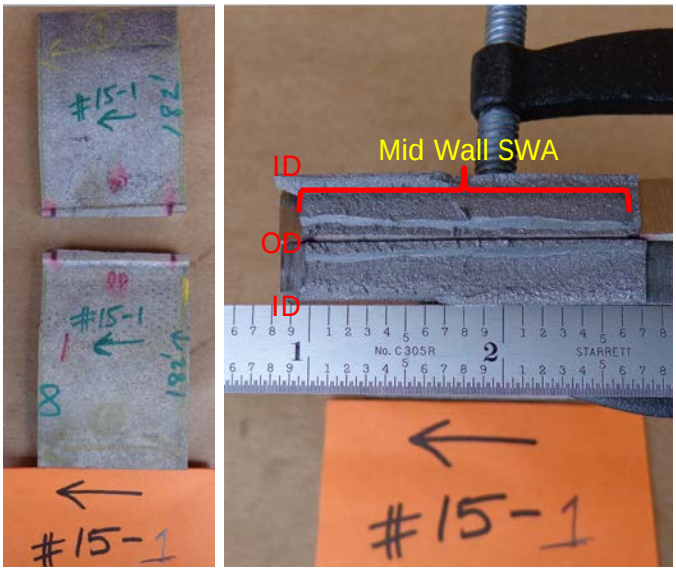

Figure 74. SWA #15-1, break location and fracture surface

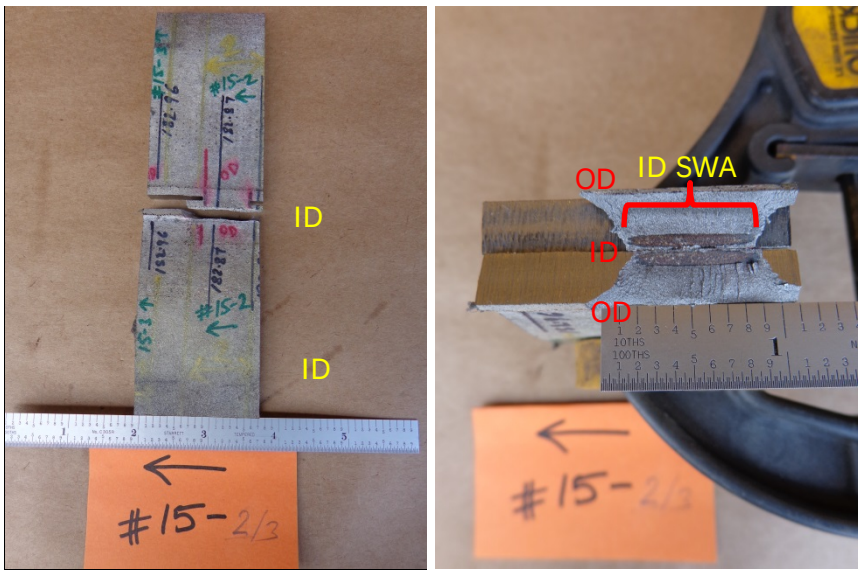

Figure 75. SWA #15-2, break location and fracture surface

Figure 76. SWA #15-3, break location and fracture surface

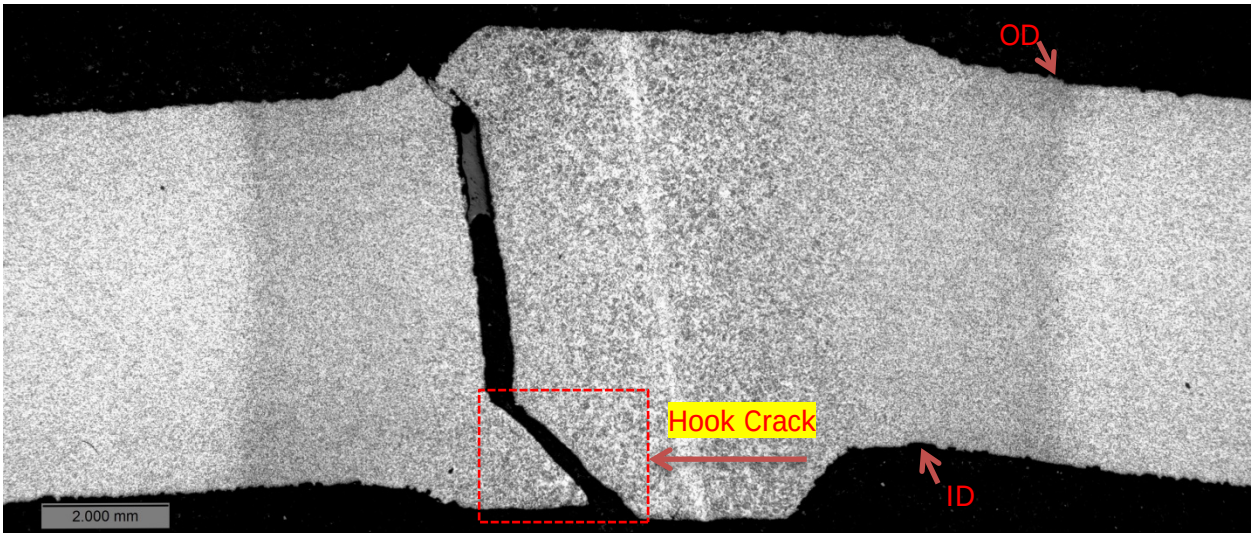

Figure 77. SWA #15-1, metallographic image 12.5X

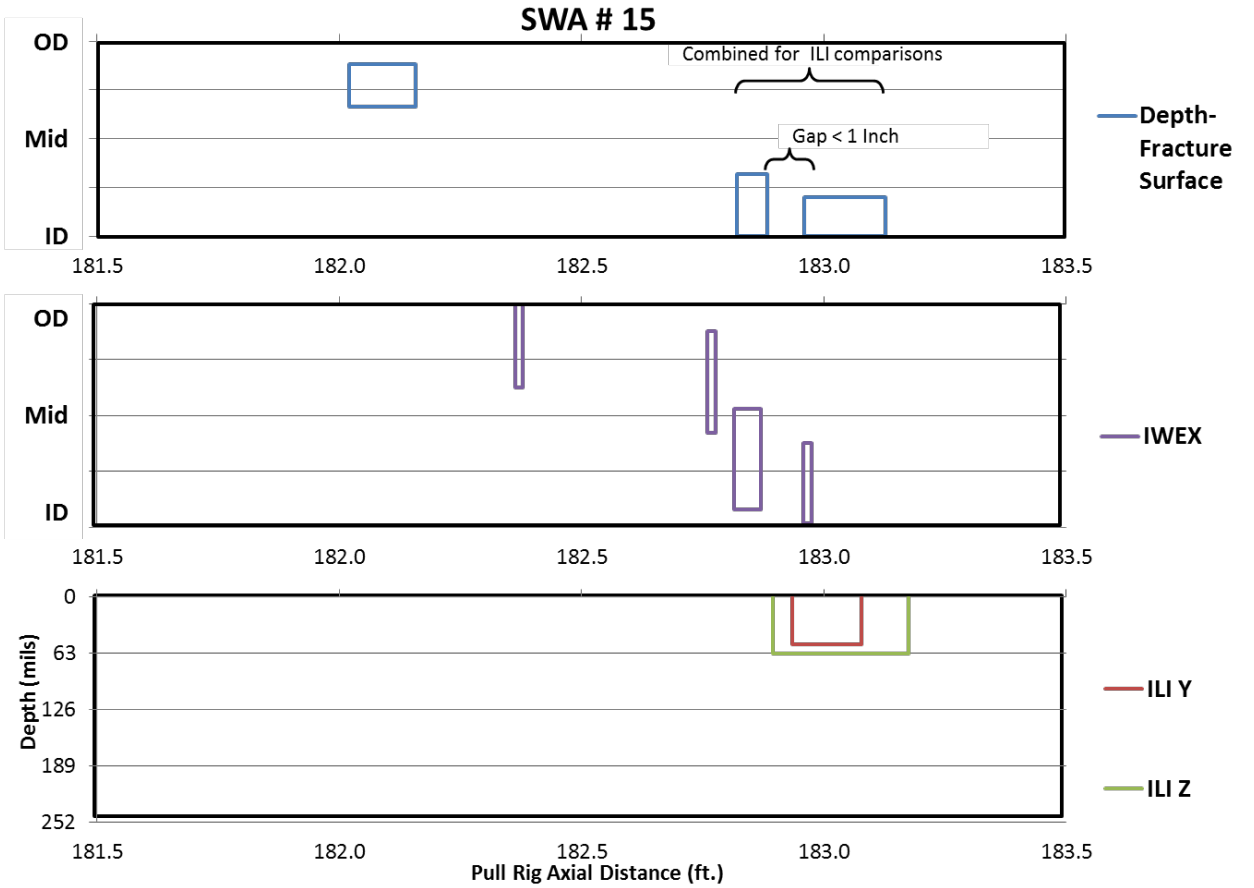

Figure 78. Depth profile and inspection results of SWA 15

SWA #16: SWA #16 was located on Pipe #16-36. Metallographic examination revealed this SWA to be a hook crack. A metallographic cross section also revealed the presence of a near mid-wall lamination feature in SWA #16. The presence of a lamination feature connected to the hook crack suggests that this hook crack was formed due to the lamination feature disturbing the seam in the ERW process. This feature appears to be connected to SWA# 3, 4, 7 and 18. This feature was divided into two parts (16-1 and 16-2) to acquire a complete feature profile. Two metallographic sections were taken from this SWA. One metallographic section of the intact seam was taken at axial distance of 225.828 feet and after fractography one metallographic section at 225.70 feet axial location was obtained.

Figure 79 shows the pipe marked in preparation for the fractography specimens and Figure 80 though Figure 85 show the metallographic, metallurgical, and fractographic results. The hook cracks that originate at this lamination extend towards the ID and also the OD for a small extent; only the inner hook crack broke to the surface. This location shows an ID connected hook crack as can be seen in the picture on the right side. The anomaly location details along with details of ILI and IWEX reported anomalies are presented as the feature in Pipe 16-36.

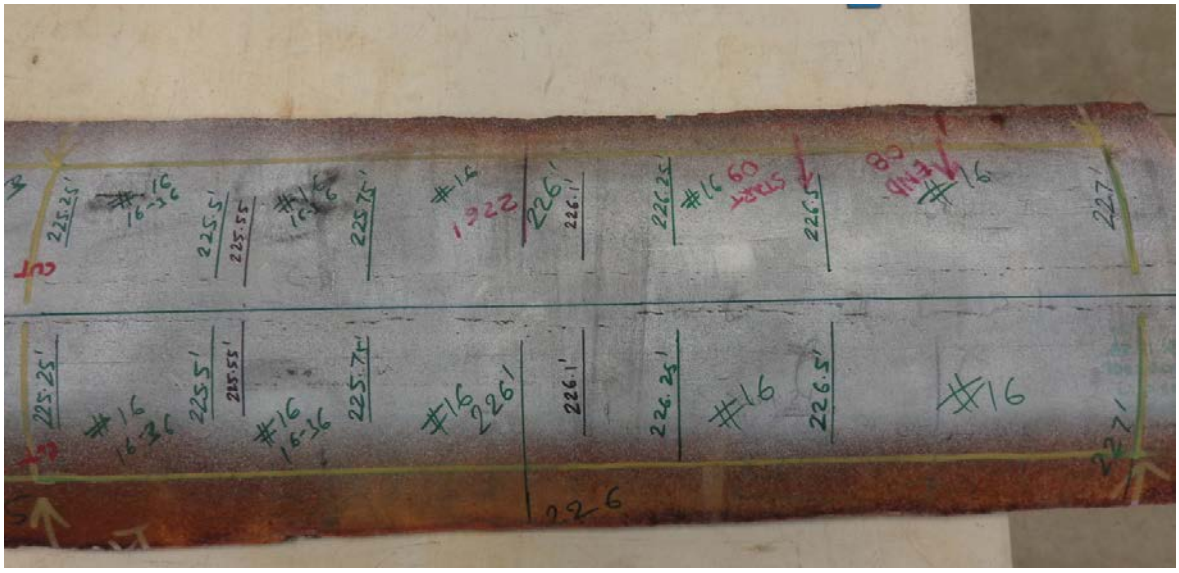

Figure 79. Break location marked on SWA #16

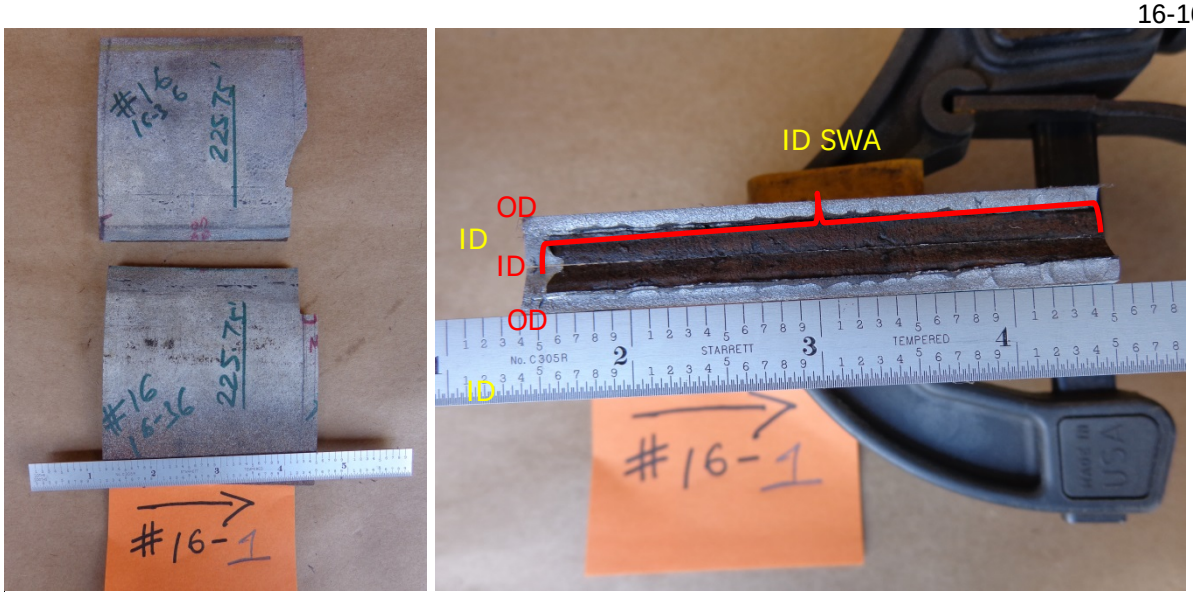

Figure 80. SWA #16-1, break location and fracture surface

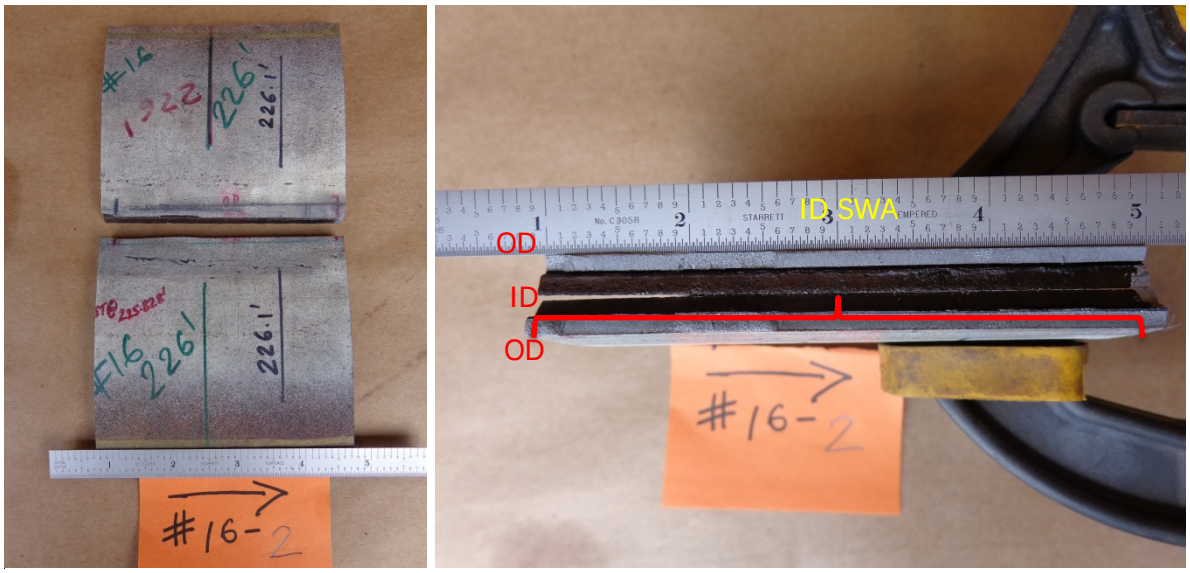

Figure 81. SWA #16-2, break location and fracture surface

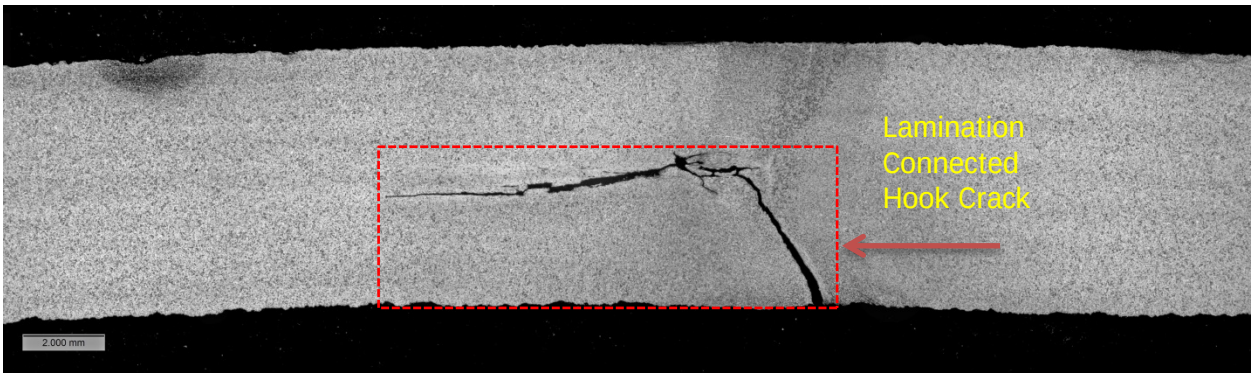

Figure 82. SWA #16, metallographic image 12.5X of intact seam at 225.83 feet

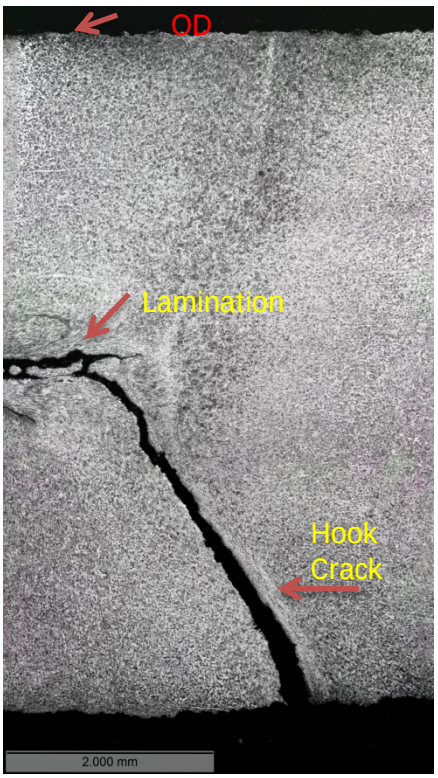

Figure 83. SWA #16, metallographic image 25X of intact seam at 225.83 feet

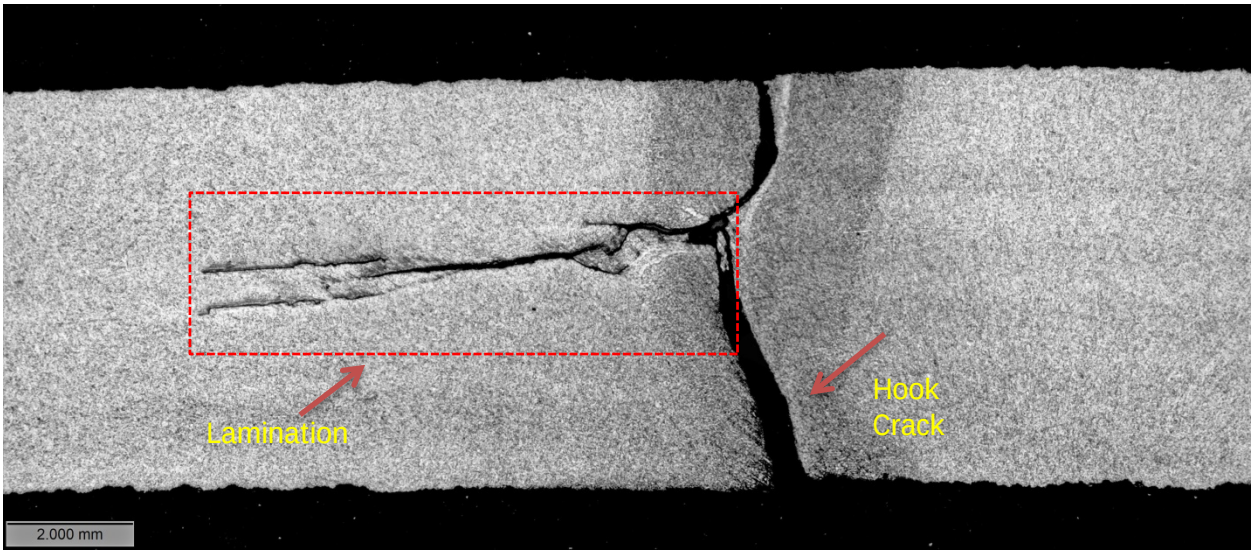

Figure 84. SWA #16, metallographic image 12.5X at Axial Location 225.70 feet after fractography

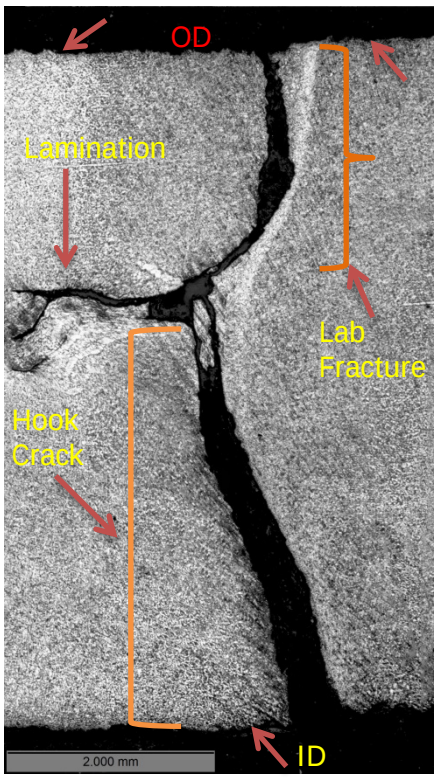

Figure 85. SWA #16, metallographic image 25X at Axial Location 225.70 feet after fractography

SWA #17: SWA #17 was located on Pipe #16-38. Metallographic examination revealed this SWA to be a hook crack. Figure 86 shows the pipe marked in preparation for the fractography specimens and Figure 87 shows the fractographic results; a hook crack can be seen in the picture on the right side. The anomaly location details along with details of ILI and IWEX reported anomalies are presented in Figure 88.

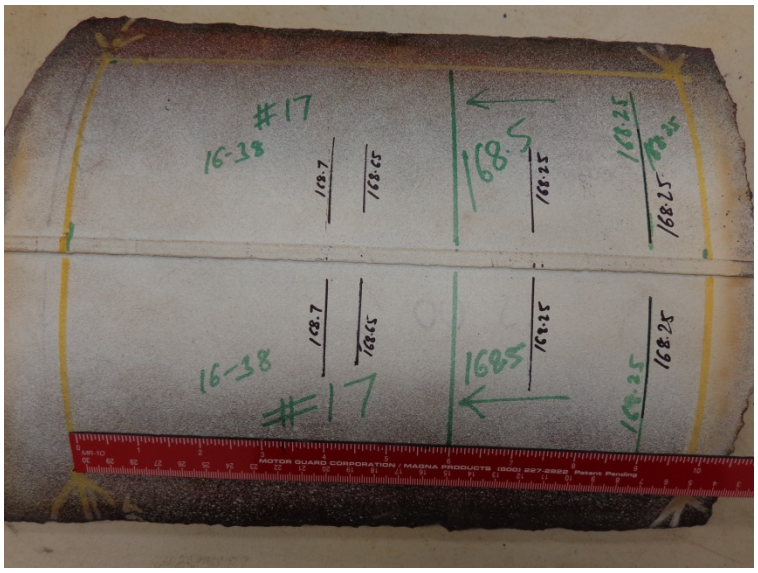

Figure 86. Break location marked on SWA #17

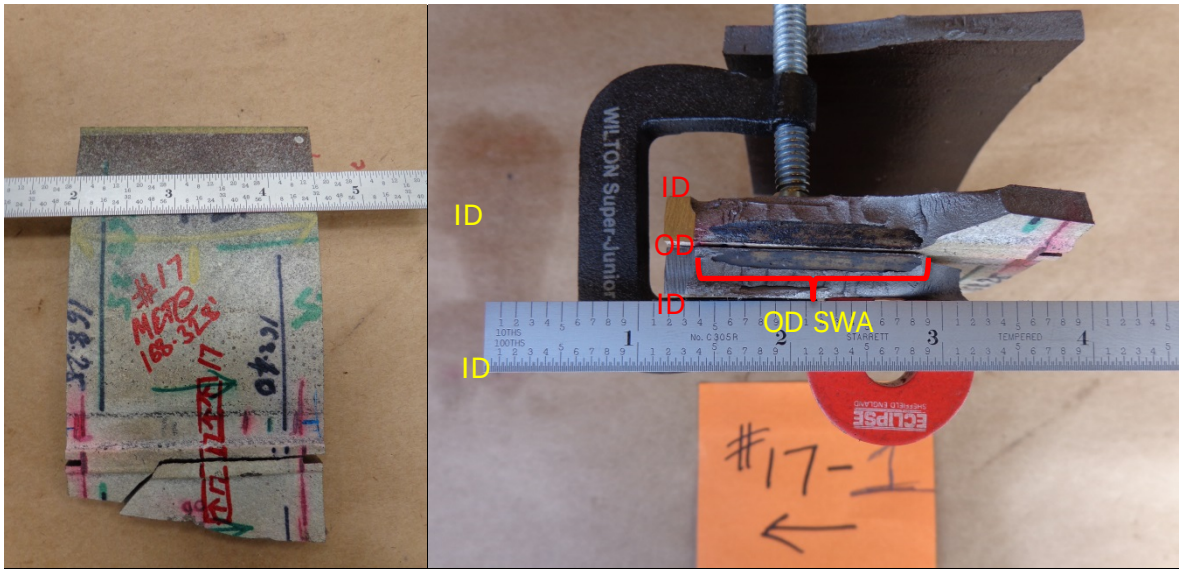

Figure 87. SWA #17, break location and fracture surface

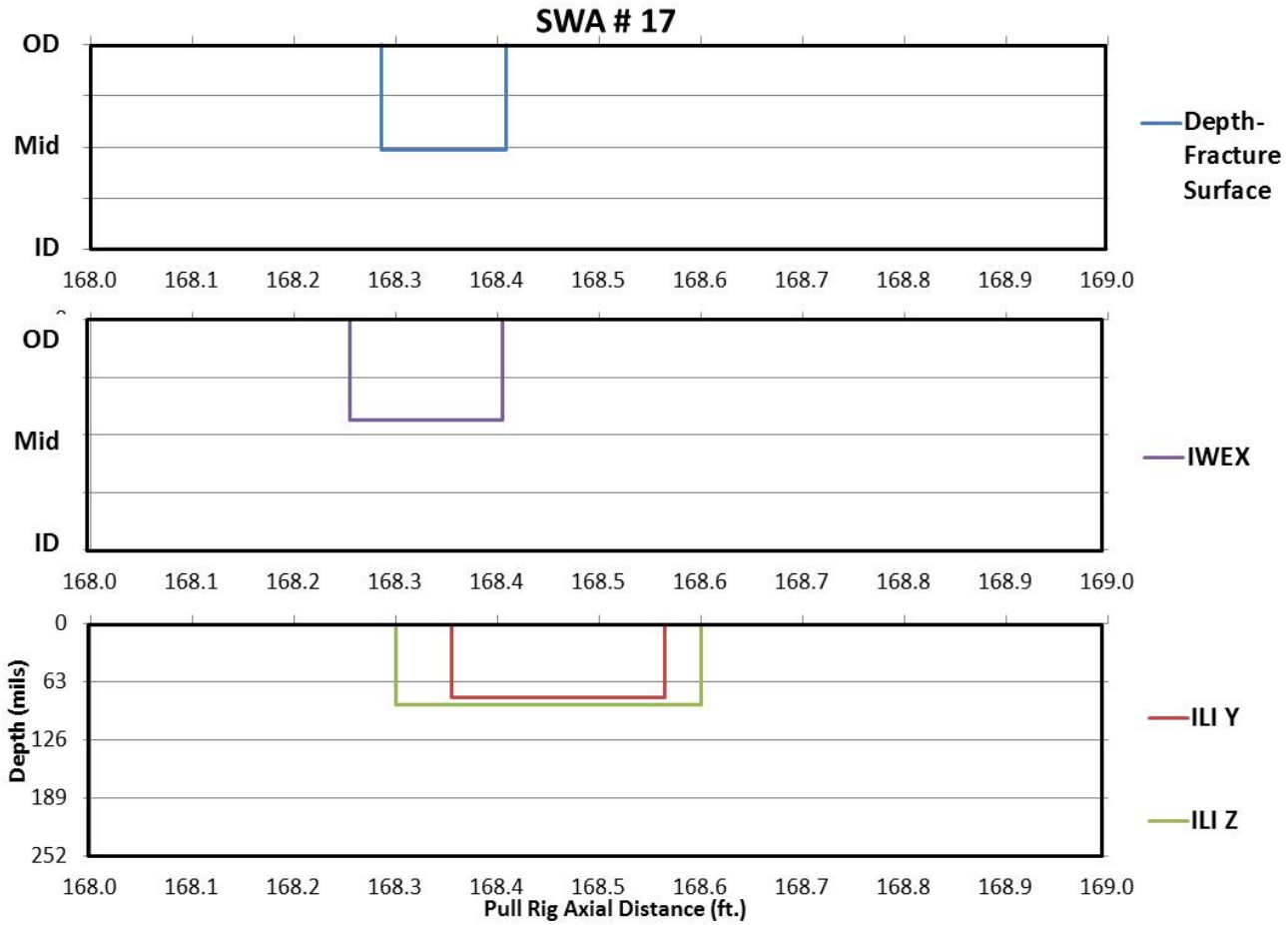

Figure 88. Depth profile and inspection results of SWA #17

SWA #18: SWA #18 was located on Pipe #16-36. Metallographic examination revealed this SWA to be a mid-wall lamination. A metallographic cross section was taken at 222.2ft axial distance which shows the presence of a near mid-wall lamination. The direction of flow line and the location of the fusion line show that the metal was pushed in towards the void created by lamination during the welding process. Figure 89 shows the pipe marked in preparation for the fractography specimens. Figure 90 and Figure 91 show the metallographic results. This lamination feature is part of one continuous feature which includes SWA #3, 4, 7, 16 and 18.

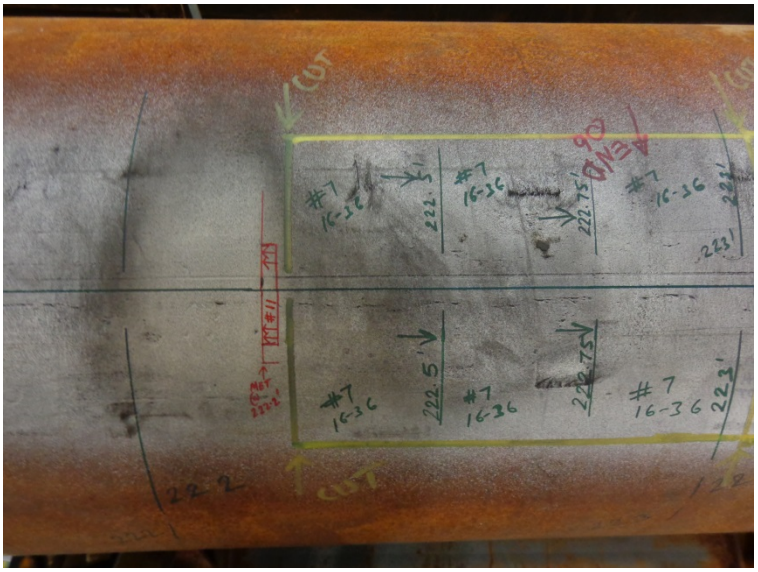

Figure 89. Break location marked on SWA #18

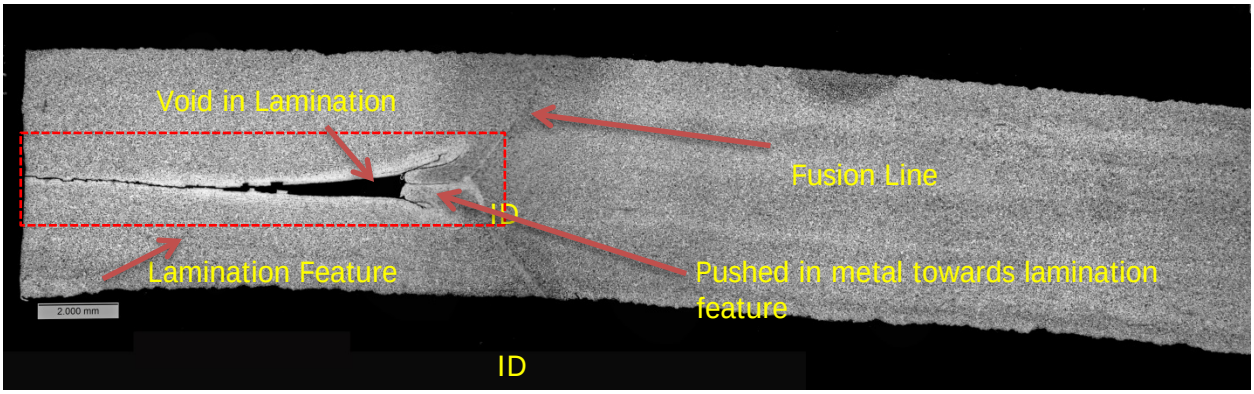

Figure 90. SWA #18, metallographic image 12.5X

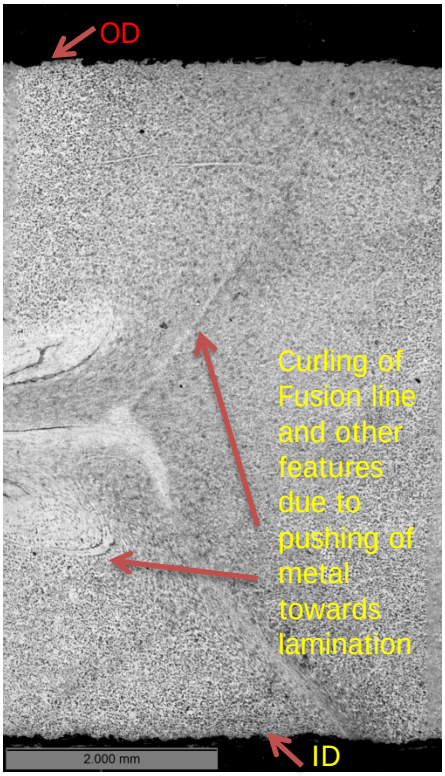

Figure 91. SWA #18, metallographic image 25X

SWA #19: SWA #19 was located on Pipe #16-38. A metallographic cross section shows the presence of an OD hook crack and another stringer feature on the opposite side of fusion line. Figure 92 shows the pipe marked in preparation for the fractography specimens. Figure 93 shows the fractographic results; a hook crack can be seen in the picture on the right side. Figure 94 shows the metallographic results with the OD hook crack and another stringer feature. The anomaly location details along with details of ILI and IWEX reported anomalies are presented in Figure 95.

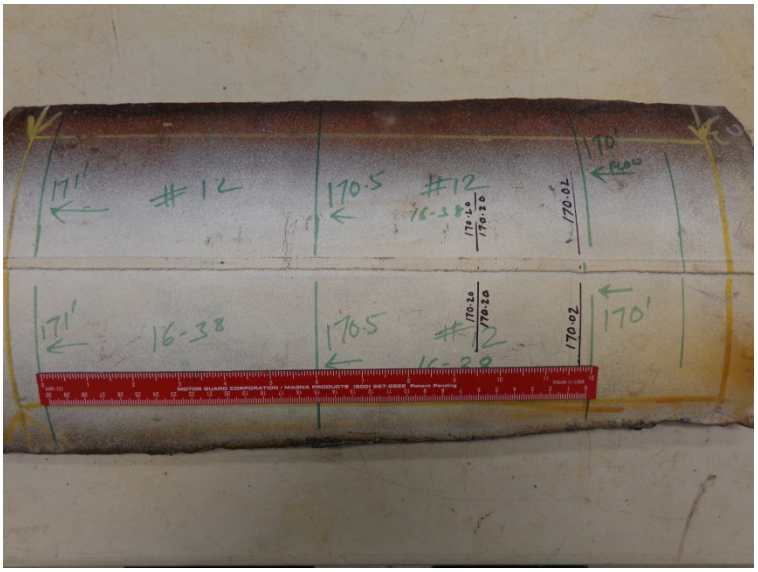

Figure 92. Break location marked on SWA #19

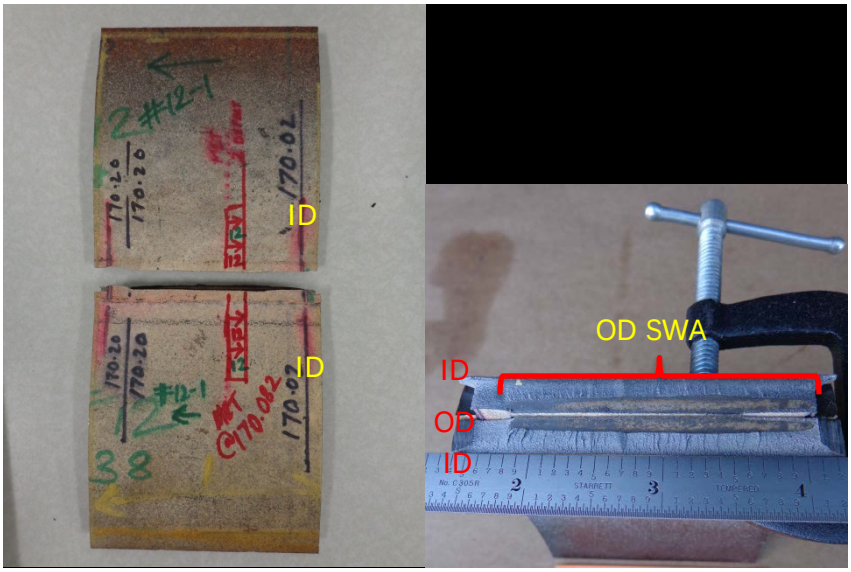

Figure 93. SWA #19, break location and fracture surface

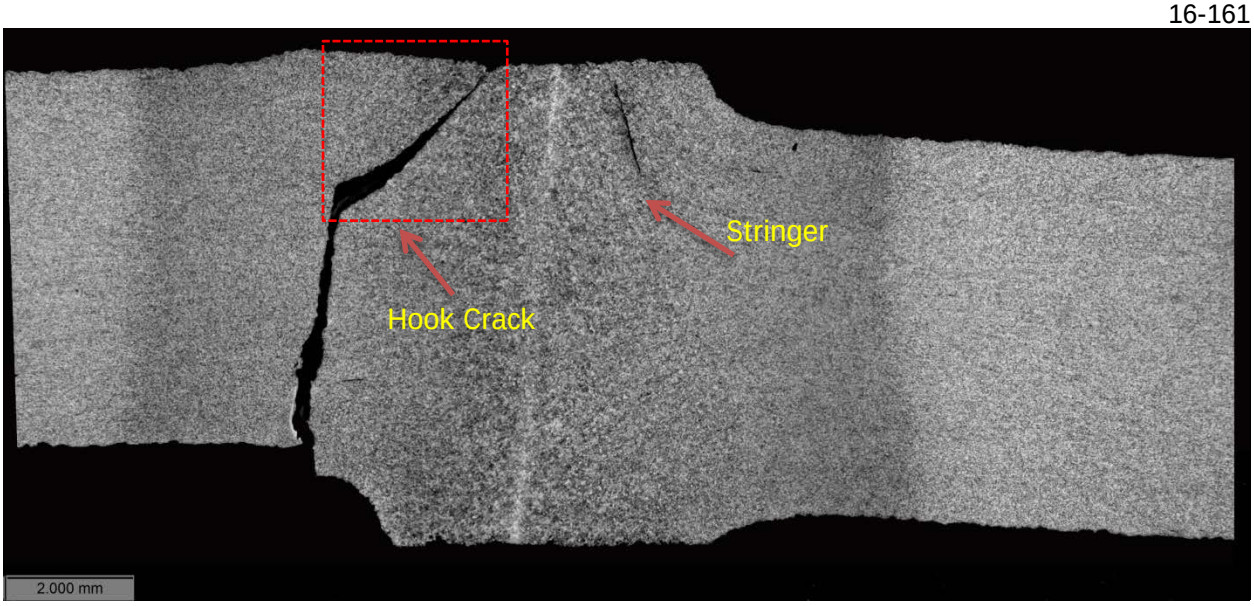

Figure 94. SWA #19, metallographic image 12.5X

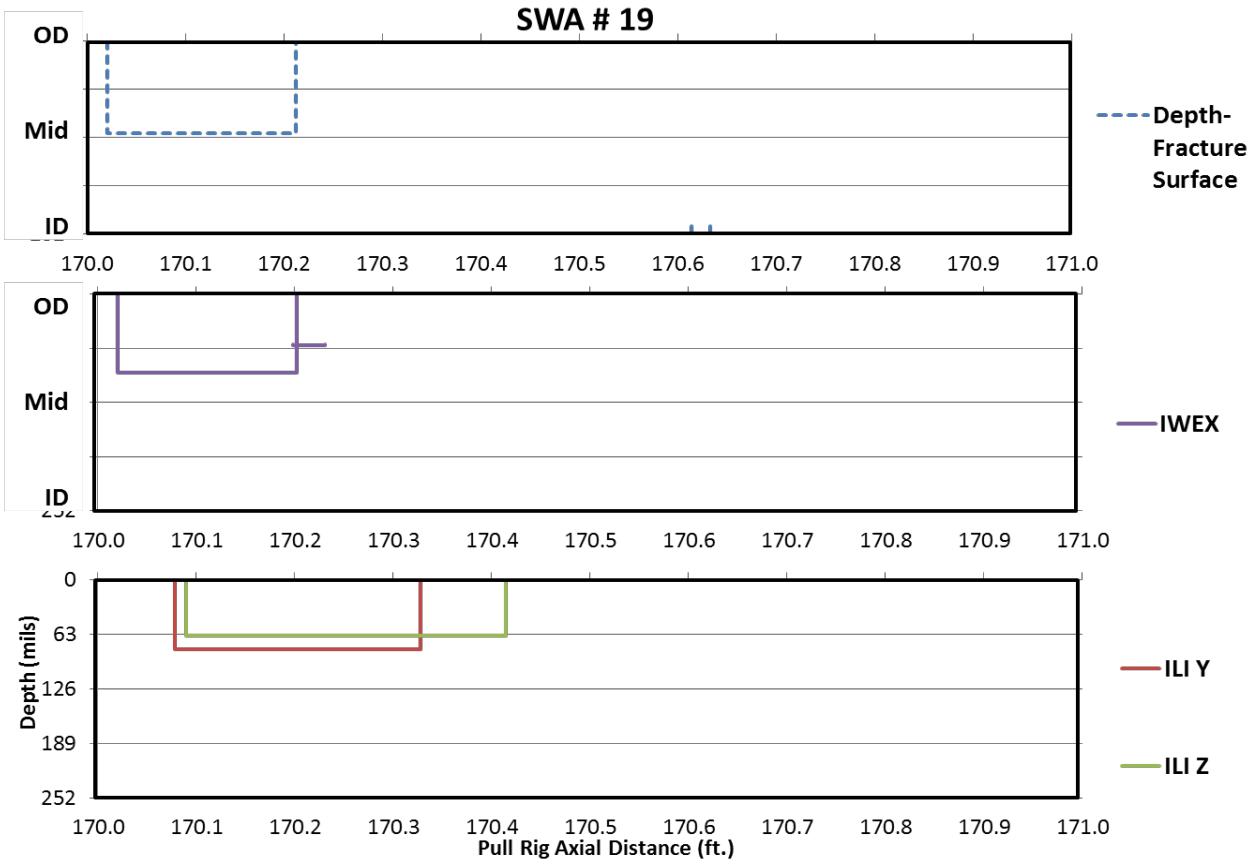

Figure 95. Depth profile and inspection results of SWA #19

Appendix B

Material Testing Results of Phase II Pipe

Kiefner and Associates
4480 Bridgeway Avenue, Suite D
Columbus, Ohio 43219
T 614 888 8220
F 614 888 7323
www.kiefner.com

April 13, 2016

Jennifer O'Brian
Mechanical Engineer/Research Scientist
Battelle
505 King Ave.
Columbus, OH 43201

Project Number: 0533-1601 Final
Re: Metallurgical Testing of Two 12-in OD Pipe Samples

Dear Ms. O'Brian:

On January 21, 2016 Kiefner and Associates, Inc. (Kiefner) received two 12-inch outer diameter (OD) pipe samples from Battelle for the purpose of performing the following tests and examinations: visual inspection and documentation, full-scale transverse tensile testing[i] of pipe material, chemical analysis[ii] of pipe material, Charpy V-notch (CVN) impact testing[iii] of the pipe base metal and longitudinal seam weld, and longitudinal seam weld metallographic analysis[iv]. The pipe samples were designated 16-33 and 16-37 prior to their arrival at Kiefner and are shown in the condition in which they were received in Figure 1 and Figure 2.

A summary of the results of our examination are presented in the following tables and figures. The full test results are presented in the appendix with the exception of the CVN results of which only the raw data was requested by Battelle.

Yours sincerely,

Devin Braun
Engineer I

Approved by

Carolyn Kolovich
Vice President, Pipeline

DB:tb

Table 1. Transverse tensile test results

	16-33 (T1)	16-37 (T2)
Yield Strength, psi (0.005 EUL Method)	48,100	52,300
Tensile Strength, psi	66,600	66,900
Elongation, % (2-in gage length)	32.5	28.4

Table 2. Chemistry analysis results

Element	16-33 (weight %)	16-37 (weight %)
Carbon	0.150	0.179
Manganese	0.669	0.602
Phosphorus	0.006	0.008
Sulfur	0.019	0.021
Silicon	0.016	0.008
Copper	0.048	0.064
Tin	0.006	0.007
Nickel	0.034	0.037
Chromium	0.026	0.029
Molybdenum	0.005	0.008
Aluminum	0.001	0.001
Vanadium	0.000	0.000
Niobium	0.001	0.001
Zirconium	0.001	0.001
Titanium	0.001	0.001
Boron	0.0001	0.0001
Calcium	0.0004	0.0003
Cobalt	0.002	0.002
CE_{IIW}	0.273	0.293

Table 3. Sample 16-33 pipe body CVN results

Specimen ID	Test Temperature	Bar Size, in		Impact, ft-lb		Lateral Expansion	Shear Area
	Degrees F	Width	Height	Measured	Full Size	mils	
1B-2	170	0.394	0.228	22.0	38.0	40	100%
1B-7	130	0.394	0.228	23.0	39.7	40	95%
1B-9	100	0.394	0.228	20.0	34.5	34	90%
1B-10	71	0.394	0.228	12.0	20.7	20	40%
1B-8	50	0.394	0.228	7.0	12.1	6	10%
1B-6	-5	0.394	0.228	3.0	5.2	0	0%
1B-5	-20	0.394	0.228	1.0	1.7	0	0%
1B-3	25	0.394	0.228	3.5	6.0	3	5%
1B-4	60	0.394	0.228	8.0	13.8	14	30%
1B-1	85	0.394	0.228	10.0	17.3	22	60%

Table 4. Sample 16-33 longitudinal seam weld HAZ CVN results

Specimen ID	Test Temperature	Bar Size, in		Impact, ft-lb		Lateral Expansion	Shear Area
	Degrees F	Width	Height	Measured	Full Size	mils	
1Z-9	170	0.394	0.217	20.0	36.3	35	95%
1Z-10	130	0.394	0.217	12.0	21.8	20	50%
1Z-3	100	0.394	0.217	11.0	19.9	20	50%
1Z-2	71	0.394	0.217	8.0	14.5	5	5%
1Z-8	50	0.394	0.217	3.0	5.4	5	0%
1Z-7	-5	0.394	0.217	3.0	5.4	3	0%
1Z-1	60	0.394	0.217	3.0	5.4	2	5%
1Z-4	85	0.394	0.217	4.5	8.2	6	10%
1Z-5	115	0.394	0.217	17.5	31.7	26	90%
1Z-6	150	0.394	0.217	18.0	32.6	33	100%

Table 5. Sample 16-33 longitudinal seam weld bondline CVN results

Specimen ID	Test Temperature	Bar Size, in		Impact, ft-lb		Lateral Expansion	Shear Area
	Degrees F	Width	Height	Measured	Full Size	mils	
1S-1	170	0.394	0.216	16.0	29.1	30	100%
1S-5	130	0.394	0.216	18.0	32.8	23	95%
1S-8	100	0.394	0.216	13.0	23.7	26	90%
1S-3	71	0.394	0.216	18.0	32.8	16	95%
1S-10	60	0.394	0.216	8.0	14.6	8	30%
1S-2	50	0.394	0.216	5.0	9.1	5	10%
1S-4	-5	0.394	0.216	5.0	9.1	5	10%
1S-9	70	0.394	0.216	7.0	12.7	7	50%
1S-6	85	0.394	0.216	15.0	27.3	25	100%
1S-7	115	0.394	0.216	10.0	18.2	21	95%

Table 6. Sample 16-37 pipe body CVN results

Specimen ID	Test Temperature	Bar Size, in		Impact, ft-lb		Lateral Expansion	Shear Area
	Degrees F	Width	Height	Measured	Full Size	mils	
2B-7	190 F	0.394	0.229	22.0	37.8	40	100%
2B-1	170 F	0.394	0.229	22.0	37.8	40	100%
2B-10	130 F	0.394	0.229	20.0	34.4	37	95%
2B-8	100 F	0.394	0.229	13.0	22.3	19	50%
2B-5	71 F	0.394	0.229	8.0	13.7	9	15%
2B-3	50 F	0.394	0.229	4.0	6.9	5	5%
2B-9	20 F	0.394	0.229	4.0	6.9	6	0%
2B-6	0 F	0.394	0.229	2.0	3.4	0	0%
2B-2	60 F	0.394	0.229	5.0	8.6	8	10%
2B-4	85 F	0.394	0.229	7.5	12.9	14	25%

Table 7. Sample 16-37 longitudinal seam weld HAZ CVN results

Specimen ID	Test Temperature	Bar Size, in		Impact, ft-lb		Lateral Expansion	Shear Area
	Degrees F	Width	Height	Measured	Full Size	mils	
2Z-1	190	0.394	0.229	15.0	37.8	40	100%
2Z-2	170	0.394	0.229	14.0	37.8	40	100%
2Z-4	130	0.394	0.229	10.0	34.4	37	95%
2Z-3	100	0.394	0.229	8.0	22.3	19	50%
2Z-6	71	0.394	0.229	5.0	13.7	9	15%
2Z-8	50	0.394	0.229	6.0	6.9	5	5%
2Z-5	20	0.394	0.229	3.0	6.9	6	0%
2Z-10	0	0.394	0.229	2.0	3.4	0	0%
2Z-7	50	0.394	0.229	5.0	8.6	8	10%
2Z-9	150	0.394	0.229	14.0	12.9	14	25%

Table 8. Sample 16-37 longitudinal seam weld bondline CVN results

Specimen ID	Test Temperature	Bar Size, in		Impact, ft-lb		Lateral Expansion	Shear Area
	Degrees F	Width	Height	Measured	Full Size	mils	
2S-3	190	0.394	0.218	14.0	25.3	19	100%
2S-4	170	0.394	0.218	13.0	23.5	20	97%
2S-9	130	0.394	0.218	10.0	18.0	19	85%
2S-6	100	0.394	0.218	8.0	14.4	9	60%
2S-8	71	0.394	0.218	6.0	10.8	6	15%
2S-1	50	0.394	0.218	6.0	10.8	7	15%
2S-2	20	0.394	0.218	4.0	7.2	7	0%
2S-5	0	0.394	0.218	5.0	9.0	9	0%
2S-7	50	0.394	0.218	5.0	9.0	10	15%
2S-10	85	0.394	0.218	7.0	12.6	13	35%

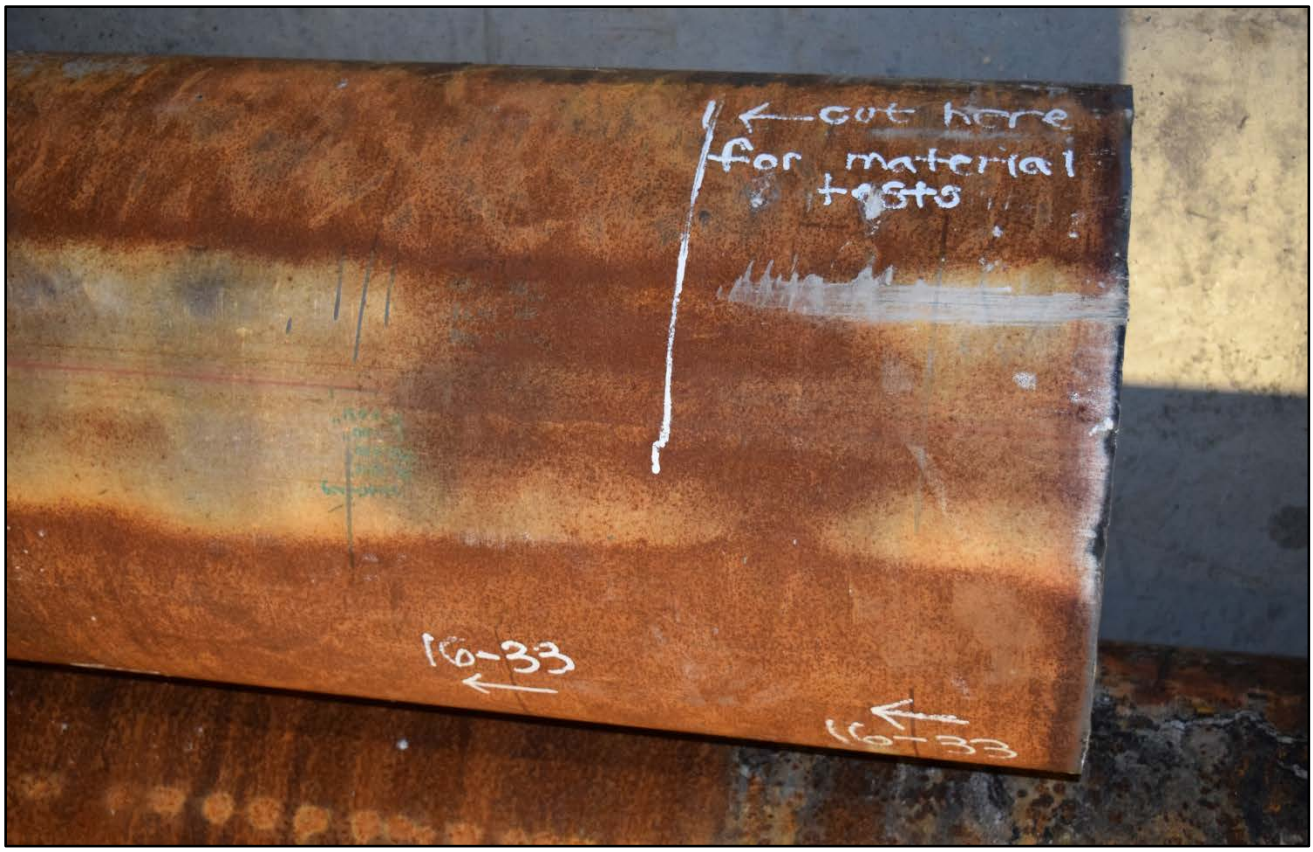

Figure 1. Sample 16-33 shown in the as-received condition

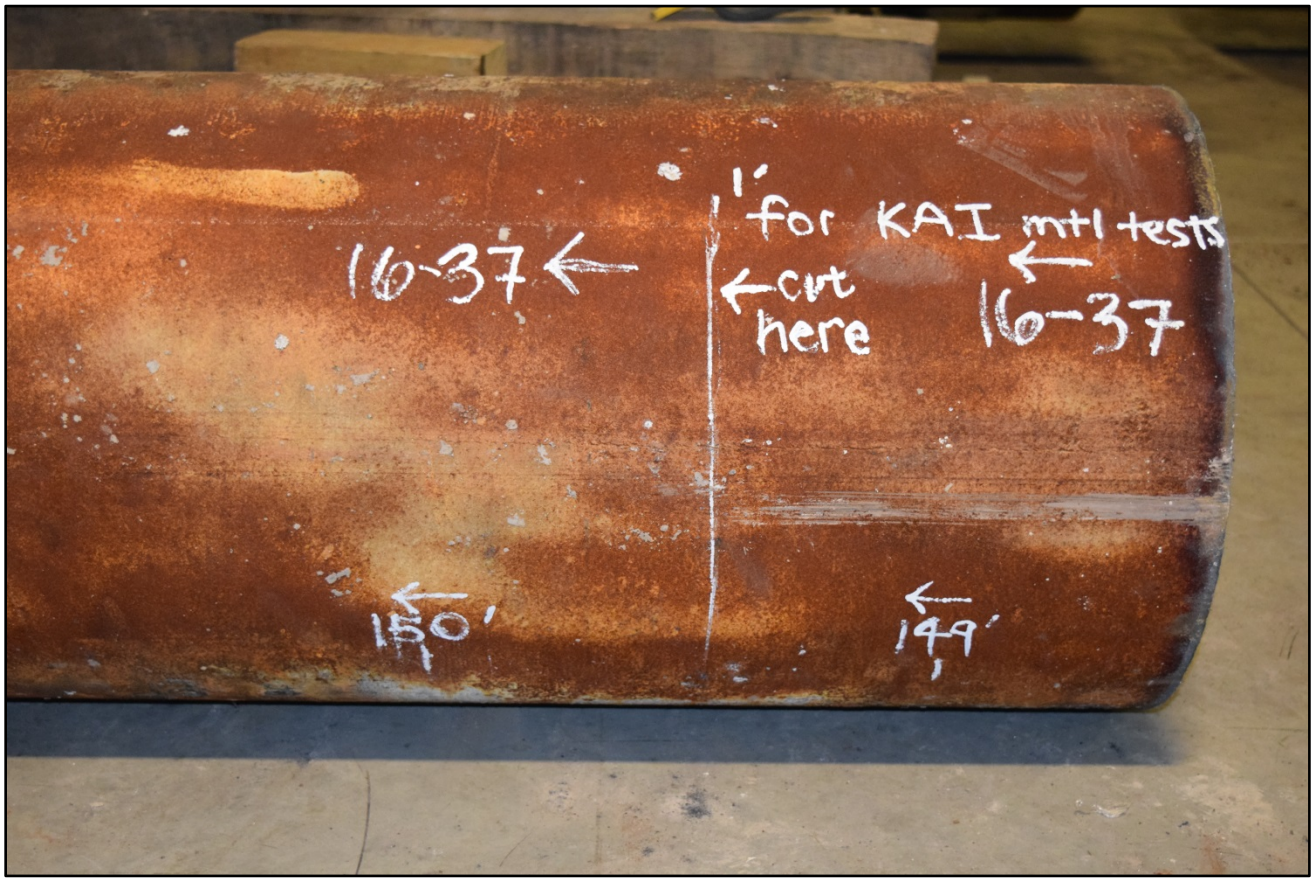

Figure 2. Sample 16-37 shown in the as-received condition

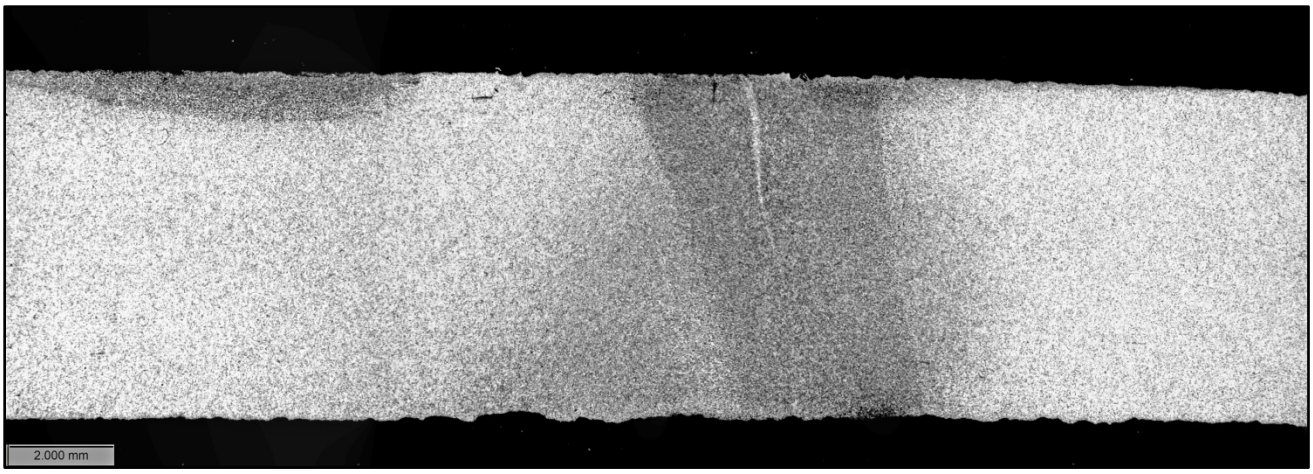

Figure 3. Sample 16-33 longitudinal seam weld metallographic cross section

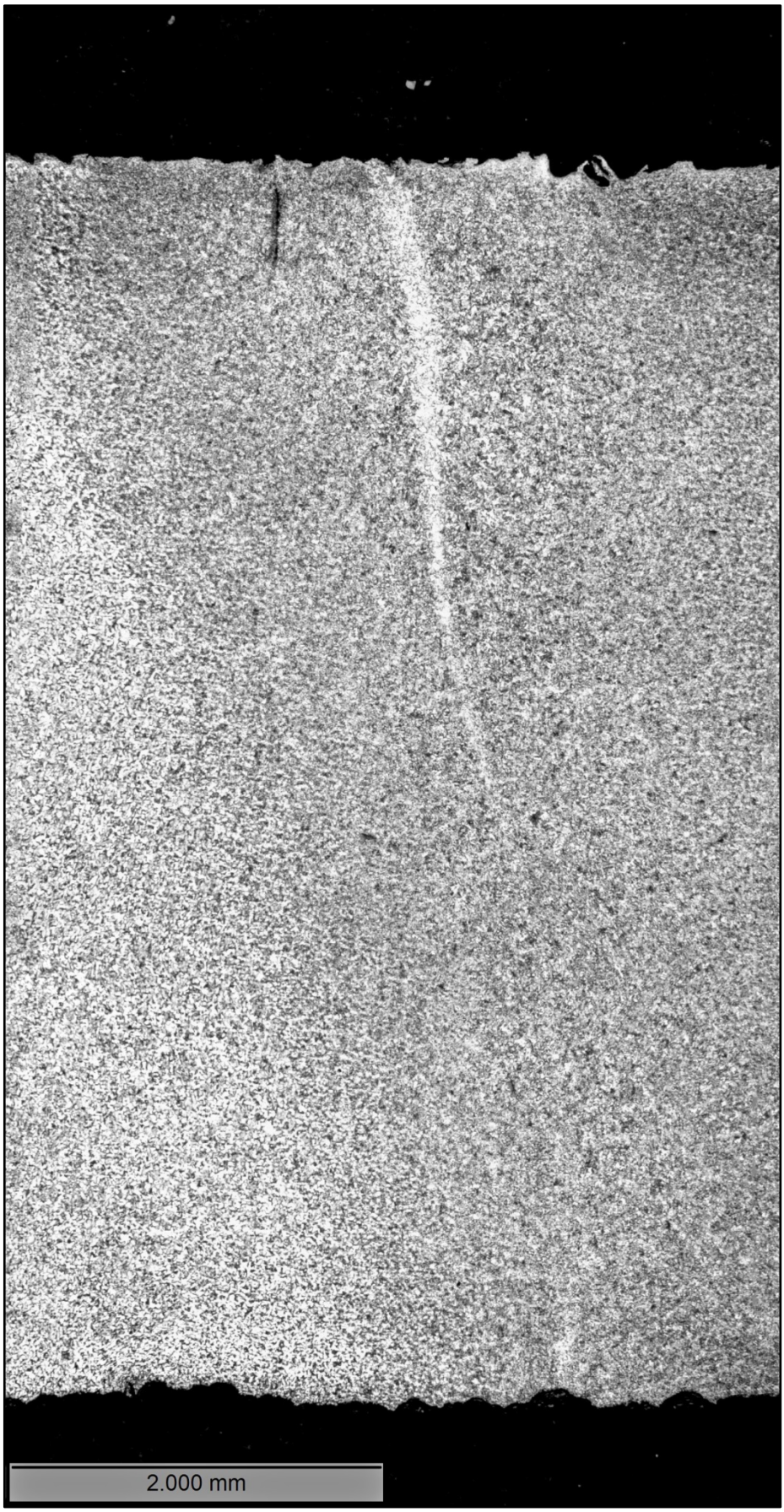

Figure 4. Detail of Sample 16-33 longitudinal seam weld bondline from Figure 3

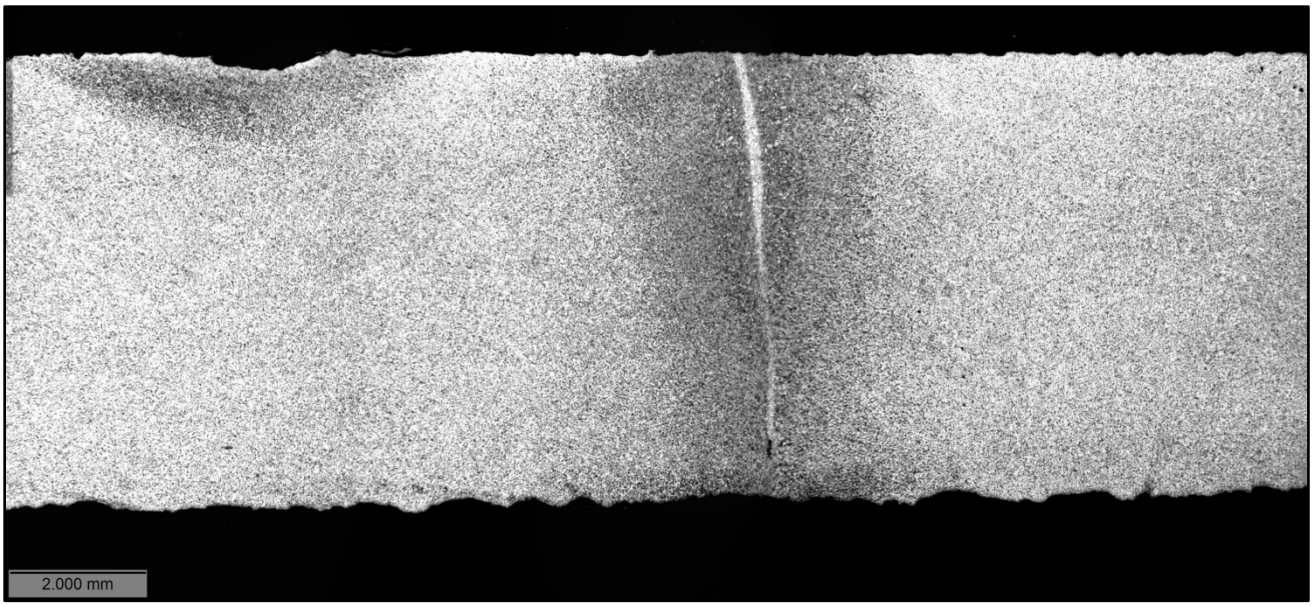

Figure 5. Sample 16-37 longitudinal seam weld metallographic cross section

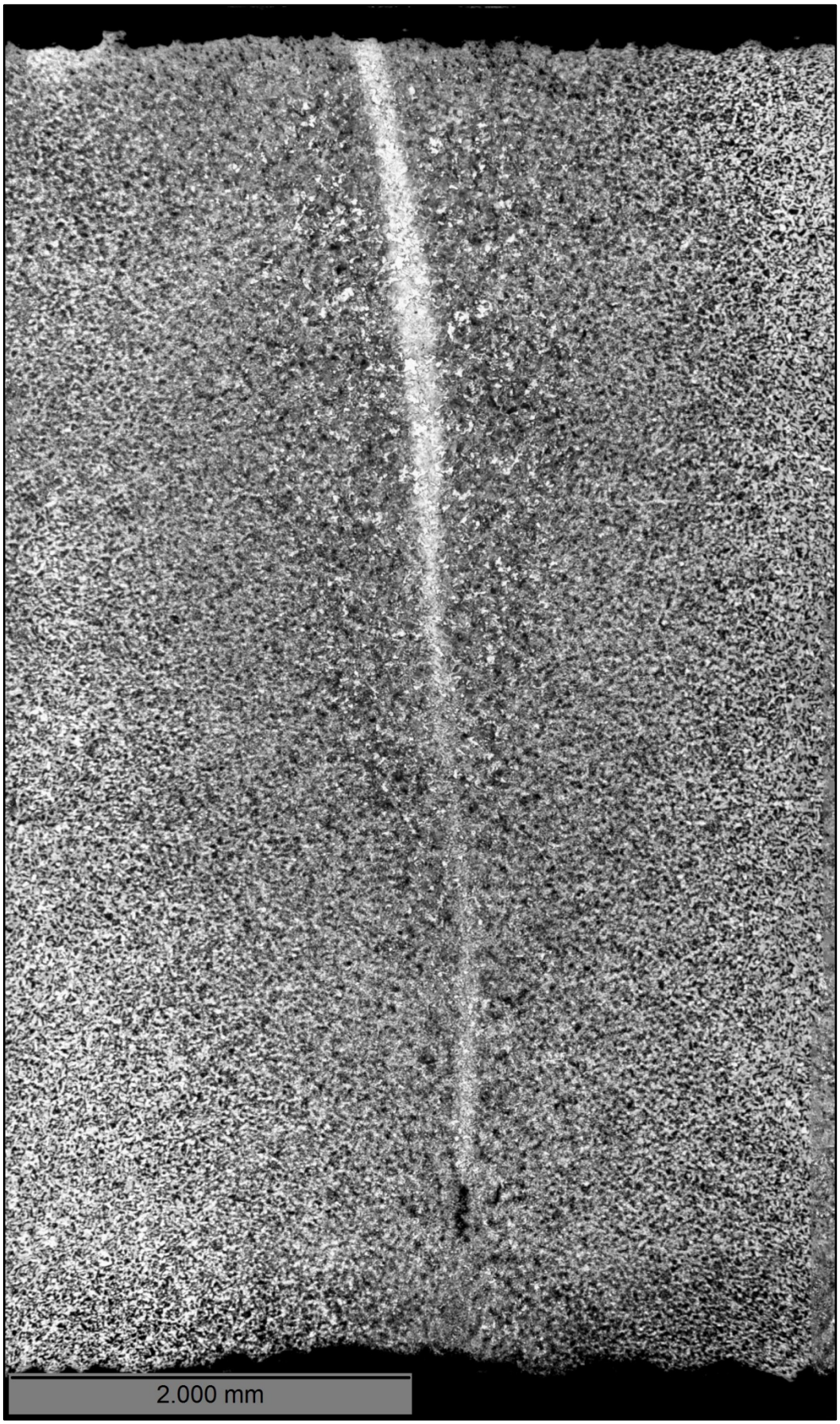

Figure 6. Detail of Sample 16-37 longitudinal seam weld bondline from Figure 5

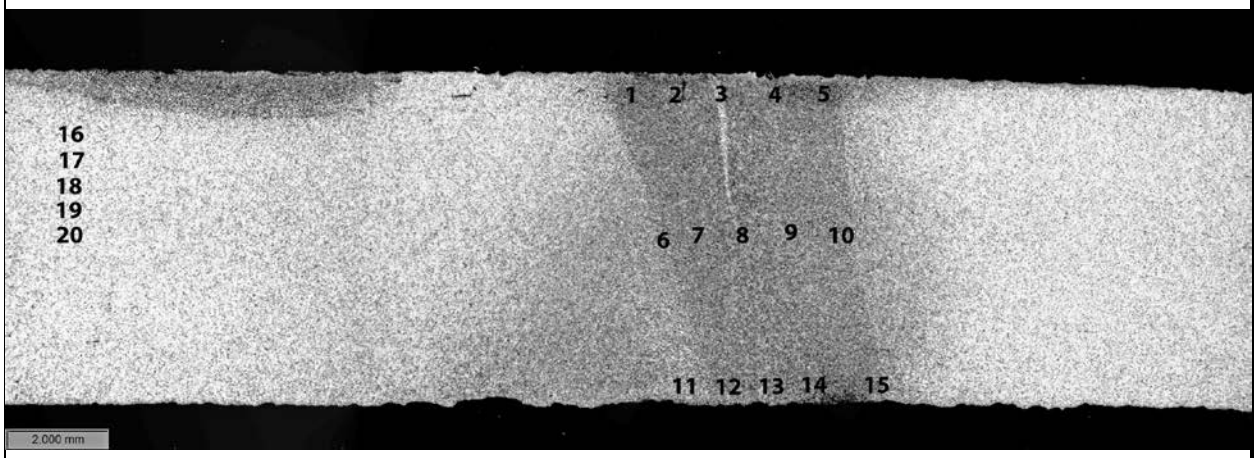

1	208.3	VHN	6	189.7	VHN	11	206.5	VHN	16	220.4	VHN
2	204.3	VHN	7	200.5	VHN	12	186.8	VHN	17	211.4	VHN
3	198.9	VHN	8	207.0	VHN	13	193.5	VHN	18	228.6	VHN
4	200.9	VHN	9	199.6	VHN	14	195.0	VHN	19	228.7	VHN
5	198.0	VHN	10	191.2	VHN	15	204.2	VHN	20	277.7	VHN

1	93.0	HRB	6	89.7	HRB	11	92.7	HRB	16	95.2	HRB
2	92.3	HRB	7	91.6	HRB	12	89.1	HRB	17	93.6	HRB
3	91.2	HRB	8	92.8	HRB	13	90.3	HRB	18	96.4	HRB
4	91.6	HRB	9	91.4	HRB	14	90.5	HRB	19	96.5	HRB
5	91.1	HRB	10	89.9	HRB	15	92.3	HRB	20	96.3	HRB

Figure 7. Microhardness locations and corresponding results for Sample 16-33 metallographic cross section

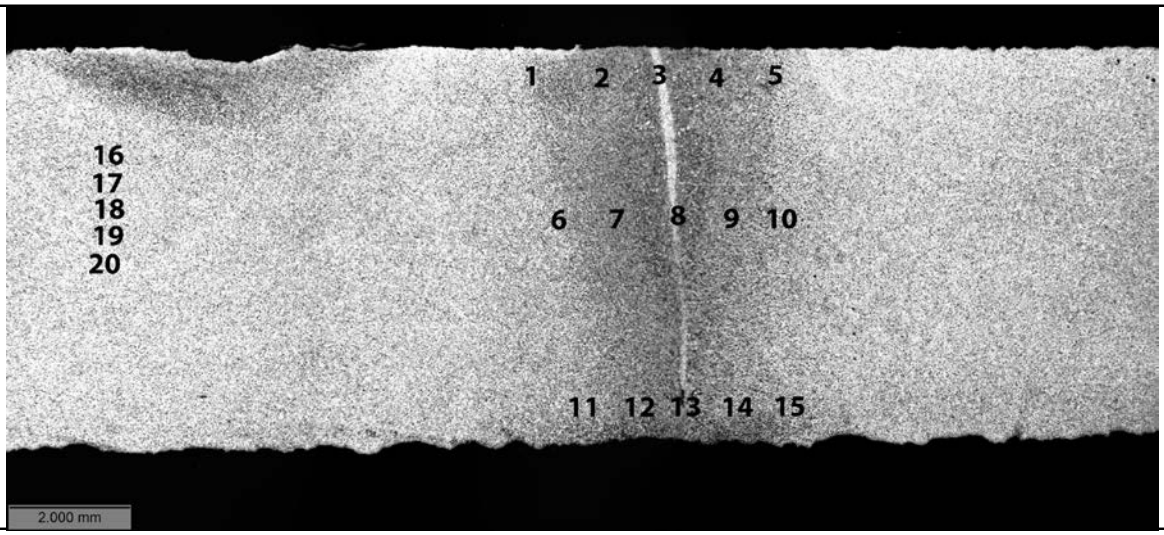

1	208.5	VHN	6	206.3	VHN	11	193.6	VHN	16	172.8	VHN
2	204.9	VHN	7	205.6	VHN	12	192.9	VHN	17	162.4	VHN
3	212.4	VHN	8	200.8	VHN	13	191.3	VHN	18	189.8	VHN
4	210.8	VHN	9	202.8	VHN	14	204.6	VHN	19	195.2	VHN
5	232.8	VHN	10	215.8	VHN	15	194.2	VHN	20	172.6	VHN

1	93.4	HRB	6	92.7	HRB	11	90.4	HRB	16	85.4	HRB
2	92.4	HRB	7	92.5	HRB	12	92.2	HRB	17	82.4	HRB
3	93.7	HRB	8	91.6	HRB	13	89.9	HRB	18	89.7	HRB
4	93.5	HRB	9	92.0	HRB	14	92.4	HRB	19	90.5	HRB
5	97.0	HRB	10	94.3	HRB	15	90.4	HRB	20	85.3	HRB

Figure 8. Microhardness locations and corresponding results for Sample 16-37 metallographic cross section

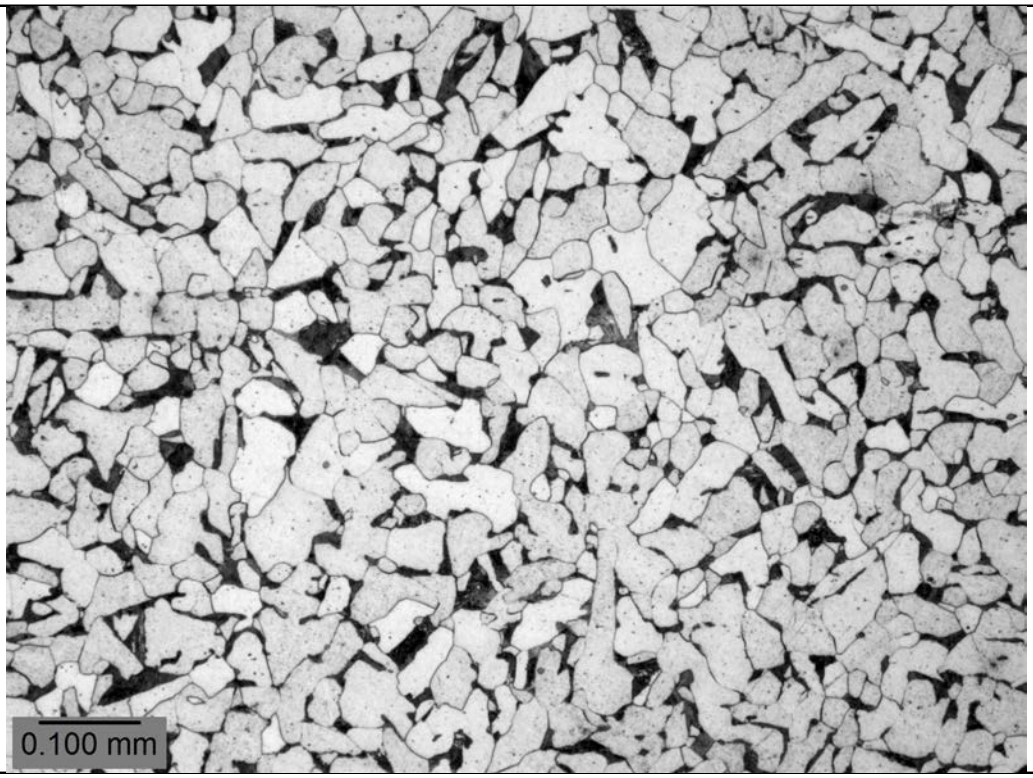

Average of 5 Measurements

Method:	Circles	Number:	N/A mm^2
Intercepts:	67.6	Mean Area:	N/A mm^2
Length:	1.6444 mm	Length:	N/A mm
Grain Size:	7.56		

Figure 9. Sample 16-33 grain structure and sizing

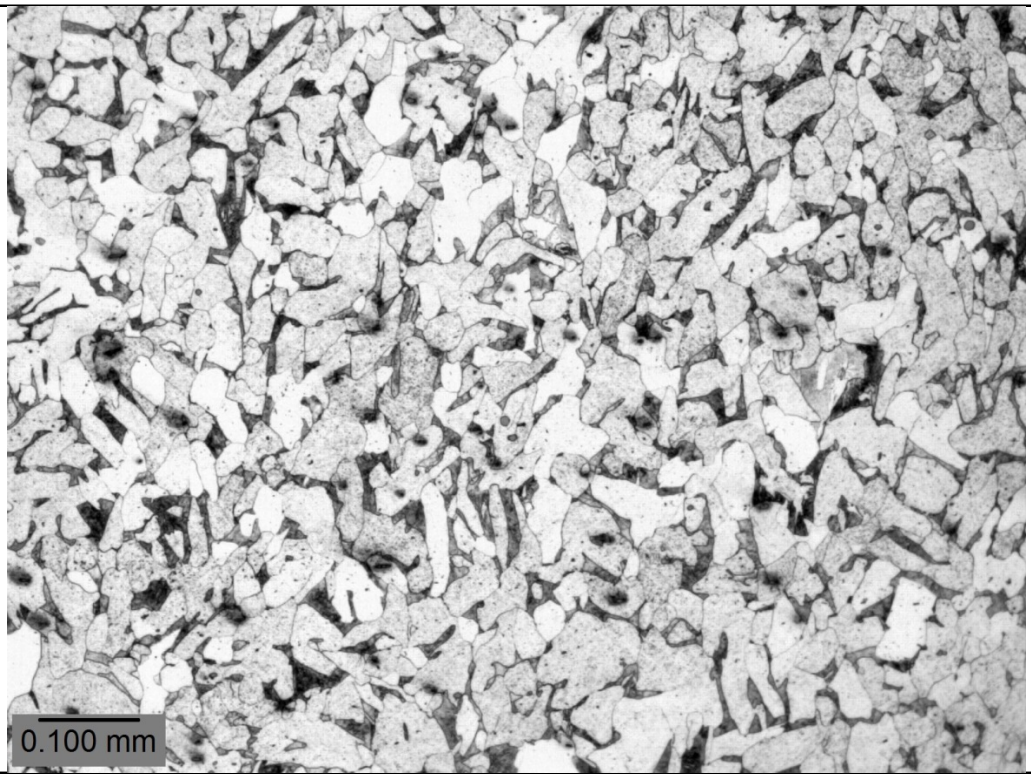

Average of 5 Measurements

Method:	Circles	Number:	N/A mm^2
Intercepts:	75	Mean Area:	N/A mm^2
Length:	377.5876 mm	Length:	N/A mm
Grain Size:	7.67		

Figure 10. Sample 16-37 grain structure and sizing

[i] Tensile testing was performed according to the most recent edition of ASTM E-8
[ii] Chemistry analysis was performed according to the most recent edition of ASTM A-751
[iii] Charpy V-Notch testing was performed according to the most recent edition of ASTM E-23
[iv] Metallographic cross sections were performed according to the most recent edition of ASTM E-3; microhardness testing was performed according to the most recent edition of ASTM E-384; grain size analysis was performed according to the most recent edition of ASTM E-112

DISCLAIMER

This document presents findings and/or recommendations based on engineering services performed by employees of Kiefner and Associates, Inc. The work addressed herein has been performed according to the authors' knowledge, information, and belief in accordance with commonly accepted procedures consistent with applicable standards of practice, and is not a guaranty or warranty, either expressed or implied.

The analysis and conclusions provided in this report are for the sole use and benefit of the Client. No information or representations contained herein are for the use or benefit of any party other than the party contracting with Kiefner. The scope of use of the information presented herein is limited to the facts as presented and examined, as outlined within the body of this document. No additional representations are made as to matters not specifically addressed within this report. Any additional facts or circumstances in existence but not described or considered within this report may change the analysis, outcomes and representations made in this report.

APPENDIX

1250 Arthur E. Adams Drive, Columbus, OH 43221

We Manufacture Innovation

Customer:	ApplusRTD	Project Number:	15795CSL
Contact:	Devin Braun	EWI Contact:	Rich Minshall
Address:	4480 Bridgeway Ave.	Phone:	614-688-5285
	Columbus	Email:	rminshall@ewi.org
	OH 43219		
Customer Sample ID:	15795-1 0533-1601	Specification:	N/A
LIMS Sample ID:	15795-1	Material Type:	Carbon Steel
Heat/Lot Number:	N/A		

Rectangular Tensile Test, ASTM E8

Initial Loading Rate (IPM): .1

Final Loading Rate (IPM): .1

Test Temp (C): 23

Test Date: 03/16/2016

Released By: Steve O'Mara

Specimen ID (N/A)	Original Width (in)	Original Thickness (in)	Orig GL (in)	UTS (psi)	0.5% Yield Stress (EUL) (psi)	Elongation (%)	ROA (%)	Failure Location (N/A)	Condition (N/A)
0533-1601-T1	1.501 38.1 (mm)	0.232 5.9 (mm)	2.008 51.0 (mm)	66600 459 (MPa)	48100 332 (MPa)	32.5	49.7	Within Gage Length	As Received
0533-1601-T2	1.501 38.1 (mm)	0.219 5.6 (mm)	2.011 51.1 (mm)	66900 461 (MPa)	52300 361 (MPa)	28.4	52.1	Within Gage Length	As Received

Notes:

Printed On: 3/16/2016 2:44:25 PM

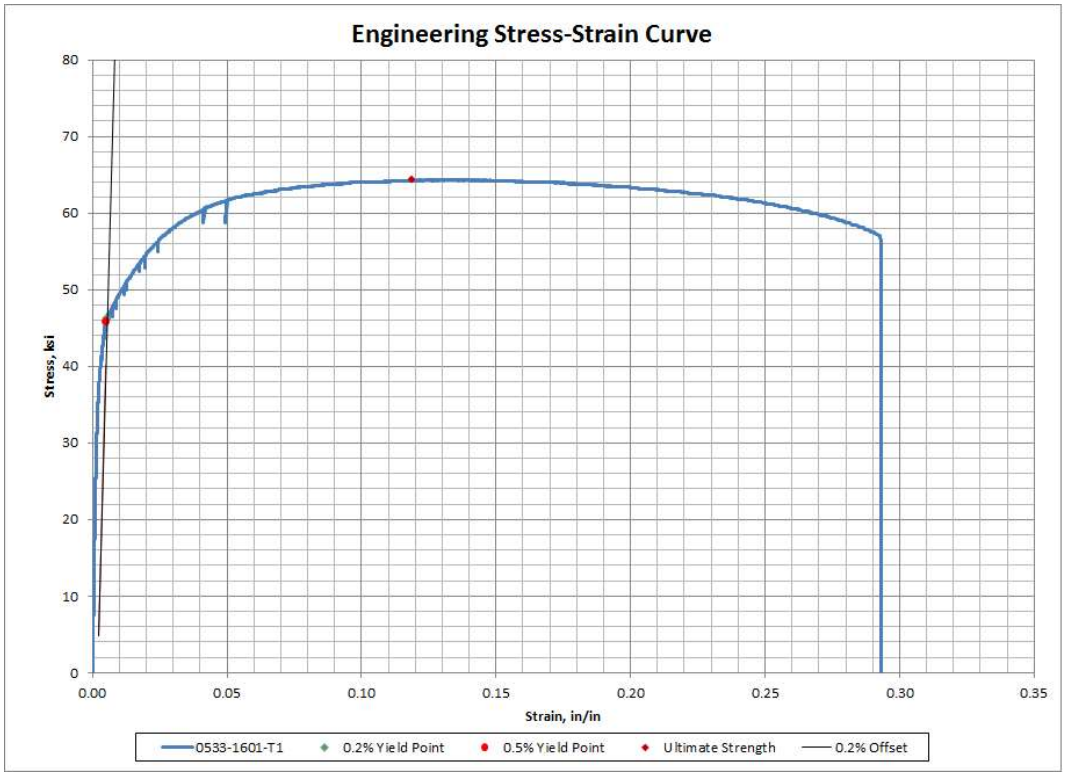

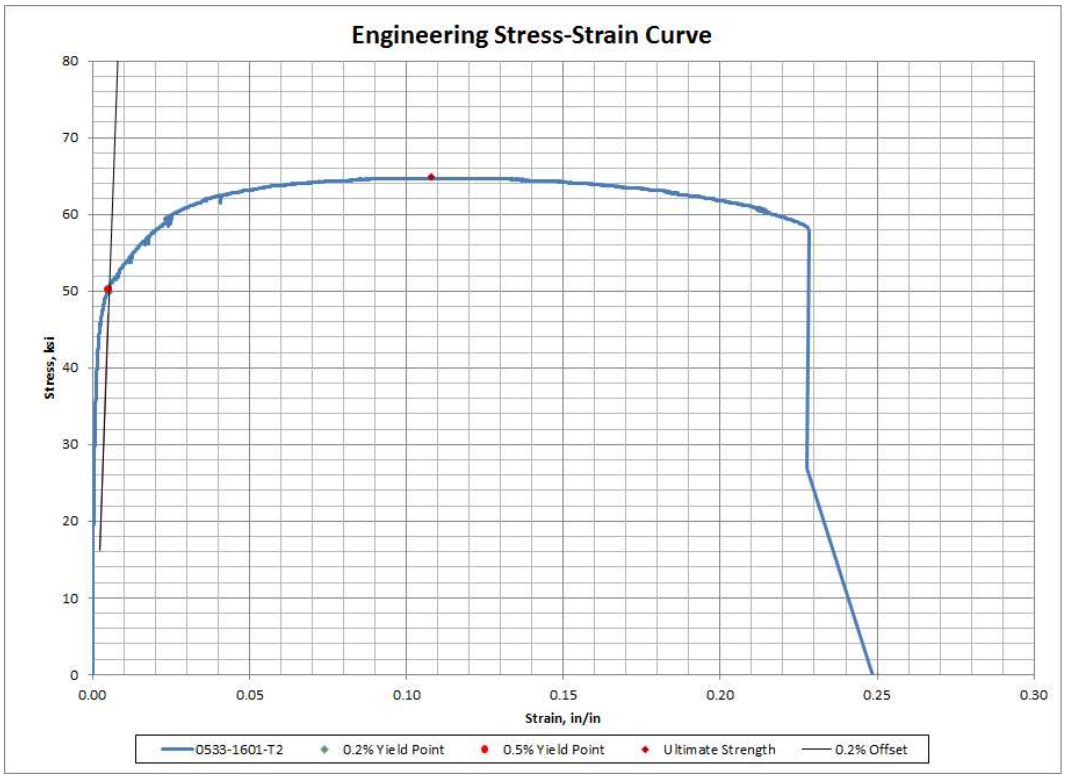

Printed On: 3/16/2016 2:44:25 PM